

แผ่นเงินระดับนาโนเมตรสังเคราะห์โดยใช้ไฮโดรเจนเปอร์ออกไซด์เป็นสารควบคุมรูปร่าง



นายบรรจงศักดิ์ ล้ำเหลือ

จุฬาลงกรณ์มหาวิทยาลัย

CHULALONGKORN UNIVERSITY

วิทยานิพนธ์นี้เป็นส่วนหนึ่งของการศึกษาตามหลักสูตรปริญญาวิทยาศาสตรมหาบัณฑิต

สาขาวิชาเคมี ภาควิชาเคมี

คณะวิทยาศาสตร์ จุฬาลงกรณ์มหาวิทยาลัย

ปีการศึกษา 2556

ลิขสิทธิ์ของจุฬาลงกรณ์มหาวิทยาลัย

บทคัดย่อและแฟ้มข้อมูลฉบับเต็มของวิทยานิพนธ์ตั้งแต่ปีการศึกษา 2554 ที่ให้บริการในคลังปัญญาจุฬาฯ (CUIR)

เป็นแฟ้มข้อมูลของนิสิตเจ้าของวิทยานิพนธ์ ที่ส่งผ่านทางบัณฑิตวิทยาลัย

The abstract and full text of theses from the academic year 2011 in Chulalongkorn University Intellectual Repository (CUIR) are the thesis authors' files submitted through the University Graduate School.

SILVER NANOSHEETS SYNTHESIZED BY USING HYDROGENPEROXIDE AS SHAPE  
CONTROLLING AGENT



Mr. Banjongsak Lamlua

จุฬาลงกรณ์มหาวิทยาลัย

CHULALONGKORN UNIVERSITY

A Thesis Submitted in Partial Fulfillment of the Requirements  
for the Degree of Master of Science Program in Chemistry

Department of Chemistry

Faculty of Science

Chulalongkorn University

Academic Year 2013

Copyright of Chulalongkorn University

Thesis Title	SILVER NANOSHEETS SYNTHESIZED BY USING HYDROGENPEROXIDE AS SHAPE CONTROLLING AGENT
By	Mr. Banjongsak Lamlua
Field of Study	Chemistry
Thesis Advisor	Associate Professor Sanong Ekgasit, Ph.D.
Thesis Co-Advisor	Associate Professor Chuchaat Thammacharoen

---

Accepted by the Faculty of Science, Chulalongkorn University in Partial Fulfillment of the Requirements for the Master's Degree

.....Dean of the Faculty of Science  
(Professor Supot Hannongbua, Dr.rer.nat.)

#### THESIS COMMITTEE

.....Chairman  
(Assistant Professor Preecha Lertpratchya, Ph.D.)

.....Thesis Advisor  
(Associate Professor Sanong Ekgasit, Ph.D.)

.....Thesis Co-Advisor  
(Associate Professor Chuchaat Thammacharoen)

.....Examiner  
(Kanet Wongravee, Ph.D.)

.....Examiner  
(Boonrat Lohwongwatana, Ph.D.)

.....External Examiner  
(Associate Professor Chinapong Kritayakornupong, Dr.rer.nat.)

บรรจจศักดิ์ ล้าเหลือ : แผ่นเงินระดับนาโนเมตรสังเคราะห์โดยใช้ไฮโดรเจนเปอร์ออกไซด์เป็นสารควบคุมรูปร่าง. (SILVER NANOSHEETS SYNTHESIZED BY USING HYDROGENPEROXIDE AS SHAPE CONTROLLING AGENT) อ.ที่ปรึกษาวิทยานิพนธ์หลัก: รศ. ดร.สนอง เอกสิทธิ์, อ.ที่ปรึกษาวิทยานิพนธ์ร่วม: รศ. ชูชาติ ธรรมเจริญ, 93 หน้า.

งานวิจัยนี้ได้พัฒนาวิธีการสังเคราะห์อนุภาคระดับนาโนเมตรของเงินแบบแผ่นด้วยวิธีใหม่ที่ง่าย รวดเร็ว ควบคุมขนาดได้อย่างแม่นยำ ไม่สร้างของเสียทำให้เป็นมิตรต่อสิ่งแวดล้อม สำหรับกรรมวิธีการสังเคราะห์ ไฮโดรเจนเปอร์ออกไซด์ทำหน้าที่เป็นทั้งตัวรีดิวซ์และออกซิไดซ์ ด้วยคุณสมบัติสองหน้าที่ของไฮโดรเจนเปอร์ออกไซด์ ทำให้ไฮโดรเจนเปอร์ออกไซด์สามารถเปลี่ยนอนุพันธ์ของเงิน เช่น เงินไอออน เงินออกไซด์ และอนุภาคของโลหะเงินระดับนาโนเมตร ไปเป็นอนุภาคระดับนาโนเมตรของเงินแบบแผ่นได้ จากการค้นพบช่วงความเข้มข้นของไฮโดรเจนเปอร์ออกไซด์ที่เหมาะสม ทำให้สามารถสังเคราะห์อนุภาคระดับนาโนเมตรแบบแผ่นของเงินที่สามารถควบคุมคุณสมบัติเชิงแสงได้ตามต้องการภายในเวลาเพียง 2 นาที อนุภาคระดับนาโนเมตรของเงินแบบแผ่นที่มีขนาดใหญ่กว่า 400 นาโนเมตรมีลักษณะเป็นคอลลอยด์สีขาวสะท้อนแสงได้ดี สามารถสังเคราะห์ขึ้นได้ภายใต้ภาวะความเป็นด่างโดยไม่ต้องใช้สารช่วยเสถียร อนุภาคระดับนาโนเมตรของเงินแบบแผ่นที่เตรียมได้จากกระบวนการนี้มีเสถียรภาพสูง ดังนั้นจึงสามารถเก็บผลิตภัณฑ์ไว้ใช้ในระยะเวลาอันยาวนานได้ กรรมวิธีการผลิตยังสามารถใช้ในการผลิตอนุภาคเงินปริมาณมากได้

จุฬาลงกรณ์มหาวิทยาลัย  
CHULALONGKORN UNIVERSITY

ภาควิชา เคมี

สาขาวิชา เคมี

ปีการศึกษา 2556

ลายมือชื่อนิสิต .....

ลายมือชื่อ อ.ที่ปรึกษาวิทยานิพนธ์หลัก .....

ลายมือชื่อ อ.ที่ปรึกษาวิทยานิพนธ์ร่วม .....

# # 5472010923 : MAJOR CHEMISTRY

KEYWORDS: SILVER OXIDE / HYDROGEN PEROXIDE / SELECTIVE ETCHING / SHAPE TRANSFORMATION / SILVER/ NANOPLATES / SILVER NANOSHEETS

BANJONGSAK LAMLUA: SILVER NANOSHEETS SYNTHESIZED BY USING HYDROGENPEROXIDE AS SHAPE CONTROLLING AGENT. ADVISOR: ASSOC. PROF. SANONG EKGASIT, Ph.D., CO-ADVISOR: ASSOC. PROF. CHUCHAAT THAMMACHAROEN, 93 pp.

In this research, silver nanoplates were fabricated by a novel method which is simple, fast, size controllable, waste free, and environmentally friendly. For synthesis procedure, hydrogen peroxide functions as both reducing and oxidizing agent. Due to the dual functions of hydrogen peroxide, it can transform various types of silver derivatives such as silver ion, silver oxide, and silver nanoparticles to silver nanoplates. According to the discovery of optimal hydrogen peroxide concentrations, this method can synthesize silver nanoplates with controlled the optical property in 2 minutes. For silver nanoplates with the lateral size greater than 400 nm having shiny white reflection, it is found that the nanoplates can be synthesized under alkaline condition without any addition of stabilizer. The as-prepared silver nanoplates from this method are highly stable. Therefore, the product can be kept for long term use. This method can be scale up for mass production.



Department: Chemistry

Field of Study: Chemistry

Academic Year: 2013

Student's Signature .....

Advisor's Signature .....

Co-Advisor's Signature .....

## ACKNOWLEDGEMENTS

I would like to wholeheartedly express my gratitude to Associate Professor Dr. Sanong Ekgasit and Associate Professor Chuchaat Thammacharoen for provide the useful suggestions, training and teaching the theoretical background and technical skills during my research as well as presentation skills.

I would like to thank Assistant Professor Dr. Preecha Lertpratchya, Associate Professor Dr. Chinapong Kritayakornupong, Dr. Boonrat Lohwongwatana, and Dr. Kanet Wongravee for usefully substantial suggestions as the thesis committee.

I also give a big thanks to my colleagues and organization: Sensor Research Unit, Department of Chemistry, Faculty of Science, Chulalongkorn University, and all good friends for the suggestions and spiritual supports throughout this research.

I would also especially like to thank the partial financial supports in my research: The Office of the National Research Council of Thailand (NRCT), Center of Innovative Nanotechnology Chulalongkorn University (CIN-CU), National Center of Excellence for Petroleum, Petrochemicals and Advanced Materials (CE PPAM).

Whatever shortcomings in the thesis remain, they are the sole responsibility of the author

Above all, I am profoundly grateful to my parents and endearing family for all their loves, understanding, support, and encouragement during the whole period of my study.

## CONTENTS

	Page
THAI ABSTRACT .....	iv
ENGLISH ABSTRACT .....	v
ACKNOWLEDGEMENTS .....	vi
CONTENTS .....	vii
LIST OF FIGURES .....	x
LIST OF SCHEMATIC .....	xx
LIST OF ABBREVIATIONS .....	xxi
CHAPTER I .....	1
INTRODUCTION .....	1
1.1 SILVER NANOPATES: PROPERTIES AND FABRICATION TECHNIQUES .....	1
1.2 THE OBJECTIVES OF THIS RESEARCH .....	4
1.3 SCOPES OF THIS RESEARCH .....	4
1.4 THE EXPECTED ACHIEVEMENT OF THIS RESEARCH .....	5
CHAPTER II .....	6
THEORY AND BACKGROUND .....	6
2.1 LOCALIZED SURFACE PLASMON RESONANCE (LSPR) OF SILVER NANOSTRUCTURE .....	6
2.2 APPLICATIONS OF SILVER NANOPATES .....	9
2.2.1 SURFACE ENHANCED RAMAN SCATTERING (SERS) .....	10
2.2.2 CHEMICAL AND BIOLOGICAL SENSORS .....	13
2.2.3 BUILDING BLOCKS FOR FABRICATION OF OTHER METALS .....	15
2.2.4 ANTIBACTERIAL APPLICATION .....	16
2.3 SHAPE CONTROLLED SYNTHESIS OF METAL NANOCRYSTALS .....	17
2.3.1 THERMODYNAMIC CONTROL .....	18
2.3.2 KINETICALLY CONTROL .....	19
2.3.3 OXIDATIVE ETCHING .....	21
2.4 SILVER NANOPATES FABRICATIONS .....	23

	Page
2.4.1 PHOTOCHEMICAL PROCESS .....	24
2.4.2 POLYOL PROCESS .....	29
2.4.3 RAPID THERMAL SYNTHESIS .....	31
2.4.4 SEED-MEDIATION PROCESS.....	34
2.4.5 ELECTROCHEMICAL PROCESS .....	37
2.4.6 HARD AND SOFT TEMPLATES TECHNIQUES .....	37
2.4.7 SONOCHEMICAL TECHNIQUES .....	38
2.5 REACTION OF HYDROGEN PEROXIDE AND SILVER .....	39
CHAPTER III .....	42
EXPERIMENTAL SECTION.....	42
3.1 CHEMICALS AND MATERIALS.....	42
3.2 FABRICATION OF SILVER NANOPATES FROM SILVER NANOSPHERES .....	42
3.2.1 OPTIMIZATION OF $[\text{NaBH}_4]/[\text{AgNO}_3]$ MOLAR RATIO .....	43
3.2.2 PREPARATION OF SILVER NANOSPHERES .....	43
3.2.3 SHAPE TRANSFORMATION OF SILVER NANOSPHERES TO SILVER NANOPATES.....	44
3.2.4 STRUCTURAL EVOLUTION OF SILVER NANOSPHERES TO SILVER NANOPATES UNDER DIFFERENT STABILIZATIONS .....	45
3.3 FABRICATION OF SILVER NANOPATES/NANOSHEETS FROM SILVER OXIDE .....	46
3.4 IN-SITU SYNTHESIS OF SILVER NANOPATES/NANOSHEETS WITHOUT STABILIZATION.....	47
3.5 CHARACTERIZATIONS .....	47
3.5.1 UV-VISIBLE SPECTROSCOPY.....	47
3.5.2 SCANNING ELECTRON MICROSCOPY.....	48
3.5.3 TRANSMISSION ELECTRON MICROSCOPY .....	48
3.5.4 X-RAY DIFFERATION TECHNIQUE .....	48
CHAPTER IV .....	49
RESULTS AND DISCUSSION.....	49



	Page
4.1 OPTIMIZATION OF APPROPRIATE $[\text{NaBH}_4]/[\text{AgNO}_3]$ MOLAR RATIO .....	49
4.2 FABRICATION OF SILVER NANOPATES BY USING NON-STABILIZED SILVER NANOSPHERES .....	50
4.3 FABRICATION OF SILVER NANOPATES BY USING POLYVINYL- .....	52
PYRROLIDONE (PVP) STABILIZED SILVER NANOSPHERES.....	52
4.4 FABRICATION OF SILVER NANOPATES BY USING TRISODIUM CITRATE (TSC) STABILIZED SILVER NANOSPHERES .....	60
4.5 FABRICATION OF SILVER NANOPATES BY USING PVP- COMBINED TSC- STABILIZED SILVER NANOSPHERES .....	61
4.6 STRUCTURAL EVOLUTION OF SILVER NANOSPHERES TO SILVER NANOPATES UNDER DIFFERENT STABILIZATIONS .....	62
4.7 FABRICATION OF SILVER NANOPATES/NANOSHEETS FROM SILVER OXIDE .....	64
4.8 IN-SITU SYNTHESIS OF SILVER NANOPATES/NANOSHEETS WITHOUT STABILIZATION.....	75
4.9 OXIDATION OF METALLIC SILVER AND REDUCTION OF SILVER ION BY HYDROGEN PEROXIDE.....	78
4.10 PROPOSED MECHANISM OF SILVER NANOPATES FORMATION .....	83
CHAPTER V .....	86
CONCLUSIONS .....	86
REFERENCES .....	87
VITA.....	93

## LIST OF FIGURES

Figure	Page
2.1 Schematic diagram of plasmon oscillation for a metallic nanosphere, showing the displacement of the negatively charged conduction electron cloud relative with the metallic nuclei.....	6
2.2 The calculated optical coefficients of 50 nm Ag nanosphere.....	8
2.3 Extinction coefficients calculated by DDA method of 100 nm edge length triangular Ag prisms with snips of 0, 10, and 20 nm. The inset shows the shape of a snipped prism. The prism thickness is 16 nm. Results are based on DDA calculations with a 2nm cubic grid. For snip = 0, 68 704 dipoles are used in the calculation.....	9
2.4 SERS spectra of 1 $\mu$ M adenine molecules on the surface of (1) larger and (2) smaller petals of flower-liked Ag nanoplates.....	11
2.5 Comparison of SERS spectra taken from single 1,4-BDT coated Ag nanospheres (55 nm in diameter) deposited on Ag nanoplates with different edge lengths (A) and thicknesses (B), respectively. (A) The Ag nanospheres were deposited on (1) Si wafer, and on Ag nanoplates with edge lengths of (2) 0.5, (3) 1, and (4) 2 mm. (B) The Ag nanospheres were deposited on Ag nanoplates with thicknesses of (5) 18, (6) 50, and (7) 100 nm. Note that the SERS signals in (A) and (B) are on different scales.....	12
2.6 Darkfield microscopic micrographs of pancreatic cancer cells after incubation with (A) no nanoplates, (B) PEGylated nano-plates, and (C) a-EGFR conjugated nanoplates. All scale bars are 20 $\mu$ m.....	14

Figure	Page
2.7 (A) Color change of colloidal Ag nanoplates after reacts with $\text{Cl}^-$ and (B) corresponding UV-visible spectra of silver nanoplates indicate the ability for sensing $\text{Cl}^-$ in aqueous solution.....	17
2.8 TEM images of (A) initial silver nanoprisms, (B) samples at 45 min with gold deposition on the prism stages and (C) samples from stage 2 with some small pinholes, (D) samples with partially refilled pinholes after 120 min (stage 3), (E) samples at 200 min with full gold shells (stage 4), and (F) a typical final gold-coated nanoprism (the inset is the cross-sectional view with a scale bar of 10 nm).....	15
2.9 Dose-response of <i>E. coli</i> exposed to various air-exposed AgNPs. EC50 increases with the increasing particle size, suggesting size-dependent toxicity. This is an indirect effect associated with $\text{Ag}^+$ release (smaller AgNPs release more $\text{Ag}^+$ and are more toxic).....	17
2.10 (A) Deposition pictures of blue colloidal Ag nanoplates on cotton fiber, (B, C) SEM images of Ag nanoplates coated on cotton fiber.....	17
2.11 (A) Schematic diagram of a plate-like seed with a random hexagonal close-packed (rhcp) structure. (B and C) HRTEM images taken from the side face of Ag nanoplates.....	21
2.12 (A and B) High-resolution TEM (HRTEM) images of a decahedral Ag nanocrystal.....	22

Figure	Page	
2.13	The polyol synthesis of Ag nanocrystals in which $\text{AgNO}_3$ serve as Ag precursor and PVP as capping agent. The reaction was conducted under air and 0.06 mM NaCl was added. Reaction times: (A, B) 10 min and (C, D) 44 h. (A, C) Photo picture of the reaction solution, in which the yellow color indicates the presence of Ag nanocrystals. (B, D) TEM images of the Ag nanocrystals produced at each time.....	23
2.14	TEM images (reverse print) mapping the morphology changes (A) before irradiation and after (B) 40, (C) 55, and (D) 70 hours of 40-watt fluorescence irradiation. Except for the inset in (A), the scale bar is 200 nm for all four images.....	25
2.15	TEM images showing the conversion of silver nanosphere to hexagonal nanoplates: (A) before irradiation and after (B) 3.5, (C) 8, and (d) 10 hour of irradiation. Inset: Enlarged photos are showing triangular (E) and hexagonal (F) silver nanoplates stacks.....	26
2.16	(A) Evolution of extinction spectra of silver nanoplates under heat treatment for various periods, 0, 30, 73, 125, 169, and 205 s. (B) Extinction spectra of 205 s heated silver nanoplates before and after light irradiation for 90, 210, and 270 min. TEM images of (C) the initial silver nanoprisms, and the silver obtained nanoplates after heat treatment for (D) 73, e) 125, and (F) 205 s, (G) silver nanoprisms transformed from silver nanodisks under light irradiation, and (H) silver nanoplates from initial silver nanoprisms after light irradiation....	28

Figure	Page
2.17 TEM images of Ag nanoprisms with average edge lengths of (A) 24 nm, (B) 36 nm, (C) 52 nm, (D) 72 nm, (E) 92 nm, and (F) 120 nm synthesize by utilizing 0.2 g, 0.4 g, 0.5 g, 0.8 g, 1.1 g, and 1.5 g of PVP, respectively.....	29
2.18 (A) UV-spectrum, and (B) TEM images of Ag nanoprisms synthesized by using ethylene glycol monoethyl ether as reducing agent.....	30
2.19 Schematic of Ag nanoparticles conversion to nanoprisms with NaBH <sub>4</sub> and H <sub>2</sub> O <sub>2</sub> . The inset picture is set of colloidal Ag nanoprisms with NaBH <sub>4</sub> concentrations of 0.30, 0.50, 0.67, and 0.80 mM, respectively	31
2.20 (A) UV-visible spectra of colloidal Ag nanoprisms synthesized by using 20 mM of H <sub>2</sub> O <sub>2</sub> with various NaBH <sub>4</sub> concentrations of I) 0.30, II) 0.50, III) 0.67, and IV) 0.80 mM, respectively. (B) TEM image of Ag nanoprisms sample IV.....	32
2.21 (A) UV-visible spectra of silver nanoparticles synthesized by different conditions; (B, D) TEM images of products, which were synthesized in the presence of (B) PVP only, (C) PVP and H <sub>2</sub> O <sub>2</sub> , and (D) PVP, citrate, and H <sub>2</sub> O <sub>2</sub> together. The inset in (D) shows a TEM image in which Ag nanoplates stand vertically upon their edges.....	33
2.22 (A) UV-visible-NIR spectra of Ag cubes and bipyramids mixture and prisms, (B) TEM image of cubes and bipyramids, and (C) TEM image of prism obtained after transformation process time of 30 minutes.....	34

Figure	Page
2.23 TEM image of the flat-lay purified truncated triangular Ag nanoplates growth in CTAB micelles.....	35
2.24 TEM images of truncated triangular Ag nanoplates synthesized under micelles of CTAB when increasing the volume of 3.5 nM original Ag nanoseeds from (A) 30, (B) 60, (C) 125, and (D) 250 $\mu\text{L}$ , respectively.....	35
2.25 (A) TEM and (B-F) SEM images of triangular Ag nanoplates synthesized by different of cycle growth; (A) after removal of PVP by centrifuging and washing to larger Ag nanoplates after (B) one, (C) two, (D) four, (E) five, and (F) seven cycles of seeded growth.....	36
2.26 SEM images of Ag nanostructures fabricated on (A, B) an n-type GaAs wafer and (C) a p-type GaAs wafer obtained from reactions of the wafers with a 2 M aqueous $\text{AgNO}_3$ for 3 minutes in the dark at room temperature.....	37
2.27 TEM image of Ag nanodisks including with polystyrene after aging for 1 month.....	38
2.28 TEM images of the Ag nanoplates prepared under different ultrasonic irradiation intensities: (A) $55 \text{ W/cm}^2$ , (B) $65 \text{ W/cm}^2$ .....	39
3.1 Systematic color change after an addition of $\text{H}_2\text{O}_2$ in to PVP stabilized AgNPs colloid ( $R = 65$ ) indicates shape transformation of AgNPs to AgNPLs.....	44

Figure	Page	
3.2	Fade-off of yellow colloidal AgNPs after an addition of H <sub>2</sub> O <sub>2</sub> in to TSC stabilized AgNPs colloid (R = 65) indicates oxidatively dissolved of AgNPs.....	45
3.3	Preparation of PVP stabilized Ag <sub>2</sub> O.....	46
4.1	(A) UV-visible spectra of PVP-AgNPs synthesized by different molar ratio of [NaBH <sub>4</sub> ]/[AgNO <sub>3</sub> ]. (B) Plotted of [NaBH <sub>4</sub> ]/[AgNO <sub>3</sub> ] molar ratio against the maximum extinction at 404 nm.....	49
4.2	(A) Colloidal products of AgNPs/AgNPLs synthesized by using a non-stabilized AgNPs as a silver source under different molar ratio of [H <sub>2</sub> O <sub>2</sub> ]/[AgNO <sub>3</sub> ]. (B) Corresponding UV-visible spectra of the as-synthesized AgNPs/AgNPLs of (A).....	50
4.3	SEM micrographs of AgNPLs synthesized by using nAgNPs as a silver source under [H <sub>2</sub> O <sub>2</sub> ]/[AgNO <sub>3</sub> ] molar ratio of (A and B) 65 and (C and D) 80.....	51
4.4	(A) Colloidal products of AgNPs/AgNPLs synthesized by using a PVP stabilized AgNPs as a silver source under different molar ratio of [H <sub>2</sub> O <sub>2</sub> ]/[AgNO <sub>3</sub> ]. (B) Corresponding UV-visible spectra of the as synthesized AgNPs/AgNPLs of (A).....	53
4.5	UV-visible spectra show the over oxidatively dissolution of PVP-AgNPs when the molar ratio of R = 500 is employed.....	54
4.6	UV-visible spectra of PVP-stabilized colloid of AgNPs (A) before and (B) after an addition of H <sub>2</sub> O <sub>2</sub> with a molar ratio R of 65. The colloids	

Figure	Page
were stabilized by 0, 1.4, 2.8, 5.6, 11, 22, 45, 90, and 180 mM PVP.....	55
4.7 UV-visible spectra of AgNPLs colloids obtained after a H <sub>2</sub> O <sub>2</sub> -induced shape transformation of AgNPs (0.232 mM) with various PVP concentrations: (A) 0.9 mM, (B) 2.7 mM, (C) 6.3 mM, and (D) 9.0 mM. The AgNPs colloids were transformed by H <sub>2</sub> O <sub>2</sub> with molar ratios R of 10, 20, 30, 50, and 65. The black lines are spectra of the original colloids of AgNPs.....	57
4.8 TEM images of (A) AgNPs and AgNPLs of colloids shown in Figure 4.7C with the molar ratio R of (B) 30, (C) 40, (D) 53, (E) 65, and (F) 80. The scale bars indicate 50 nm (A, B) and 100 nm (C-F).....	59
4.9 (A) XRD pattern of AgNPLs prepared from the shape transformation of AgNPs and (B) SAED pattern of a selected AgNPLs on a TEM grid.....	60
4.10 (A) Colloidal products of AgNPs/AgNPLs synthesized by using a TSC-stabilized AgNPs as a silver source under different molar ratio of [H <sub>2</sub> O <sub>2</sub> ]/[AgNO <sub>3</sub> ]. (B) Corresponding UV-visible spectra of the as synthesized AgNPs/AgNPLs of (A).....	61
4.11 (A) Colloidal products of AgNPs/AgNPLs synthesized by using a TSC combined PVP-stabilized AgNPs as a silver source under different molar ratio of [H <sub>2</sub> O <sub>2</sub> ]/[AgNO <sub>3</sub> ]. (B) Corresponding UV-visible spectra of the as synthesized AgNPs/AgNPLs of (A).....	62
4.12 Real-time UV-visible spectral evolution after an addition of H <sub>2</sub> O <sub>2</sub> into (A) non-stabilized, (B) PVP-stabilized, (C) TSC-stabilized, and (D) TSC/PVP-stabilized colloid of AgNPs. The spectra were recorded for a	



- period of 2 min with a 10 s intervals. The experimental conditions are  $[AgNO_3] = 0.116$  mM,  $[H_2O_2] = 2.94$  mM,  $[PVP] = 2.72$  mM,  $[TSC] = 0.05$  mM. The black lines are spectra of the original colloids of AgNPs 63
- 4.13 UV-visible spectra and SEM micrographs of (A) 4.5 mM PVP stabilized  $Ag_2O$  (PVP- $Ag_2O$ ) of pH8, and (B-E) AgNPs synthesized by using PVP- $Ag_2O$  of (A) as a silver source, initial concentration of  $H_2O_2$  equal to 0.0979 M, and vary molar ratios  $[H_2O_2]/[AgNO_3]$  in the range of 0.08-1 66
- 4.14 UV-visible spectra and SEM micrographs of (A) 4.5 mM PVP stabilized  $Ag_2O$  (PVP- $Ag_2O$ ) of pH8, and (B-E) AgNPs synthesized by using PVP- $Ag_2O$  of (A) as a silver source, initial concentration of  $H_2O_2$  equal to 0.979 M, and vary molar ratios of  $[H_2O_2]/[AgNO_3]$  in the range of 2-10 68
- 4.15 UV-visible spectra and SEM micrographs of (A) 4.5 mM PVP stabilized  $Ag_2O$  (PVP- $Ag_2O$ ) of pH8, and (B-E) AgNPs synthesized by using PVP- $Ag_2O$  of (A) as a silver source, initial concentration of  $H_2O_2$  equal to 9.79 M, and vary molar ratios of  $[H_2O_2]/[AgNO_3]$  in the range of 20-100..... 70
- 4.16 UV-visible spectra and SEM micrographs of AgNPs synthesized by using PVP- $Ag_2O$  of pH8 ( $[AgNO_3] = 9.28$  mM) as a silver source. Using of initial  $H_2O_2$  concentration of 0.979 M,  $[H_2O_2]/[AgNO_3]$  molar ratio of 10. (A-F) varying of PVP contents in the range of 0-27.0 mM..... 73
- 4.17 UV-visible spectra and SEM micrographs of AgNPs synthesized by using PVP- $Ag_2O$  of pH8 ( $[AgNO_3] = 9.28$  mM) as a silver source. Using of initial  $H_2O_2$  concentration of 0.979 M,  $[H_2O_2]/[AgNO_3]$  molar ratio of 10. (A-F) varying of PVP contents in the range of 36.0-81.0 mM..... 74

Figure	Page
4.18 SEM micrographs of Ag nanoplates/nanosheets synthesized by in-situ method using 2.3 mM [AgNO <sub>3</sub> ], 3.3 mM [NaBH <sub>4</sub> ], and [H <sub>2</sub> O <sub>2</sub> ] of (A) 0, (B) 0.26, (C) 0.28, (D) 0.33, (E) 0.35, and (F) 0.53 M, respectively.....	76
4.19 SEM micrographs of Ag nanoplates/nanosheets synthesized by in-situ method using 0.35 M [H <sub>2</sub> O <sub>2</sub> ], 3.3 mM [NaBH <sub>4</sub> ], and [AgNO <sub>3</sub> ] of (A) 0.6, (B) 1.4, (C) 2.3, (D) 2.5, (E) 2.8, and (F) 3.2 mM, respectively.....	76
4.20 SEM micrographs of Ag nanoplates/nanosheets synthesized by in-situ method using 0.35 M [H <sub>2</sub> O <sub>2</sub> ], 2.3 mM [AgNO <sub>3</sub> ], and [NaBH <sub>4</sub> ] of (A) 2.3, (B) 2.6, (C) 3.3, (D) 3.7, (E) 4.1, and (F) 4.3 mM, respectively.....	77
4.21 Equipotential points where $E_{\text{cell}}(\text{Ox}) = E_{\text{cell}}(\text{Red})$ as a function of [Ag <sup>+</sup> ].....	80
4.22 $E_{\text{cell}}(\text{Ox})$ (A), $E_{\text{cell}}(\text{Red})$ (B), and $\Delta E_{\text{cell}}$ (D) as a function of [Ag <sup>+</sup> ] at pH 2, 4, 7, and 8. The R molar ratio was fixed at 40. $E_{\text{cell}}(\text{Ox})$ and $E_{\text{cell}}(\text{Red})$ at pH 7 are compared in (C).....	80
4.23 $E_{\text{cell}}(\text{Ox})$ (A), $E_{\text{cell}}(\text{Red})$ (B), and $\Delta E_{\text{cell}}$ (D) as a function of pH at 1, 50, and 100 $\mu\text{M}$ Ag <sup>+</sup> . The R molar ratio was fixed at 40. $E_{\text{cell}}(\text{Ox})$ and $E_{\text{cell}}(\text{Red})$ at 100 $\mu\text{M}$ Ag <sup>+</sup> are compared in (C).....	81
4.24 $E_{\text{cell}}(\text{Ox})$ (A), $E_{\text{cell}}(\text{Red})$ (B), and $\Delta E_{\text{cell}}$ (D) as a function of R at 1, 50, and 100 $\mu\text{M}$ Ag <sup>+</sup> . pH was fixed at 7. $E_{\text{cell}}(\text{Ox})$ and $E_{\text{cell}}(\text{Red})$ at 100 $\mu\text{M}$ Ag <sup>+</sup> are compared in (C).....	82

Figure	Page
4.25 $E_{\text{cell}}(\text{Ox})$ (A), $E_{\text{cell}}(\text{Red})$ (B), and $\Delta E_{\text{cell}}$ (D) as a function of R at pH 2, 4, 7, and 8. $[\text{Ag}^+]$ was fixed at $100 \mu\text{M}$ . $E_{\text{cell}}(\text{Ox})$ and $E_{\text{cell}}(\text{Red})$ at pH 7 are compared in (C).....	83



## LIST OF SCHEMATIC

Schematic	Page
4.1 Proposed mechanisms for the shape transformation of AgNPs to AgNPLs induced by H <sub>2</sub> O <sub>2</sub> ; (A) with PVP stabilization and (B) with TSC stabilization.....	85



## LIST OF ABBREVIATIONS

AgNPs	: Silver nanospheres
AgNPLs	: Silver nanoplates
AgNShs	: Silver nanosheets
SERS	: Surface enhanced Raman scattering
nm	: Nanometer
AgNO <sub>3</sub>	: Silver nitrate
H <sub>2</sub> O <sub>2</sub>	: Hydrogen peroxide
PVP	: Polyvinylpyrrolidone
TSC	: Trisodium citrate
NaOH	: Sodium hydroxide
Ag <sub>2</sub> O	: Silver oxide
NaBH <sub>4</sub>	: Sodium borohydride
XRD	: X-ray diffraction
SAED	: Selected area electron diffraction
TEM	: Transmission electron microscopy
μL	: Microlite (volume)
ppm	: Parts per million (concentration, mg/L)
M	: Molar (concentration, mol/L)
mM	: milli Molar (concentration, mmol/L)
μM	: micro Molar (concentration, μmol/L)
SEM	: Scanning electron microscopy
UV-vis	: UV-visible
NIR	: Near infrared region
DPR	: dipole plasmon resonance
iDPR	: in-plane dipole plasmon resonance
opDPR	: out-of-plane dipole plasmon resonance
ipDPR	: in-plane dipole plasmon resonance

## CHAPTER I

### INTRODUCTION

#### 1.1 SILVER NANOPlates: PROPERTIES AND FABRICATION TECHNIQUES

More than ten years ago, two-dimensional silver nanoplates such as nanoprisms and nanosheets of various sizes and shapes (triangular, truncated triangular, hexagonal, and round disk) have gained substantial interests due to their size- and shape-dependent optical properties [1, 2]. The optical activity of the silver nanoplates could be selectively tuned across the visible region into near-infrared (NIR) region by dictating the degree of anisotropy [2, 3]. Silver nanoplates of specific optical properties exhibit great potentials in various applications such as surface-enhanced Raman scattering [4], chemical and biological sensors [5, 6], catalysts [7, 8], surface-enhanced fluorescence [9], building blocks for complex nanophotonic devices and circuits [10]. Many synthetic methods were developed for the fabrication of silver nanoplates including photochemical processes [11-15], hard and soft template processes [16], rapid thermal chemical reductions [17-19], electrochemical techniques [20], and sonochemical methods [21]. Owing to the demanding for nanomaterials with specific properties for preferring applications, developments of novel techniques for creating nanostructures with desired morphologies and functionalities are constantly required.

Recently, efficient seed mediated approaches for preparation of anisotropic silver nanoplates and nanosheets were developed [22-30]. These thermal methods utilize the shape selective oxidative etching of  $H_2O_2$  to discriminately dissolve unstable seeds while preserving those with stacking faults. The nanoplates were then grown from the survival seeds under a suitable environment consisting of additional metal ions, reducing agents, and surface capping agents. Anisotropic seeds with planar twinned defects and/or stacking faults, whose preparation protocol was pioneered by Mirkin's group [17, 26], generated at the early stage are prime pivotal for the engineering of the anisotropic nanoplates. The most famous reagent for silver nanoplates fabrication that sometime was given as irreplaceable agent is trisodium citrate (TSC) [11-15, 17, 26]. The roles of trisodium citrate (TSC) were demonstrated by many research groups, as reducing agent, stabilizer, complexing agent and surface blocking agent [31-33]. Normally, trisodium citrate (TSC) was proven as an essential ingredient, although replaceable by many di- and tricarboxylate compounds with two nearest carboxylate groups separated by two or three carbon atoms [19, 25], for the development and growth of nanoplates. TSC facilitates the lateral growth of anisotropic nanoplates by preferentially binding onto the flat Ag {111} facets, thus preventing a further deposition of Ag atoms on this facet [19, 25, 34-37].

Polyvinylpyrrolidone (PVP) is generally employed as a secondary ligand promotes the formation of uniform nanoplates by preventing the aggregation of nanoparticles. Although it can be replaced by other reagents that containing with hydroxyl groups (i.e., ethylene glycol, polyethylene glycol, and polyvinyl alcohol), PVP plays a crucial role on the evolution of nanoplates by preferentially binding onto the Ag{100} facets [19, 35]. A successive lateral and vertical growth of silver nanoplates is capable of increasing the edge length for more than 100 times and increasing plate thickness for nearly 40 times of the original seeds using TSC and PVP [35]. The high efficiency synthesis protocols of silver nanoplates above still maintain some drawbacks endowed with many required chemical reagents, a long time reaction, complicated routes, and difficulty to modify the nanoplates surface. Therefore, the scale up production of silver nanoplates for widely applications is still impossible.

This work, we have successfully pioneered the fast and simple novel method of silver nanoplate fabrication with precisely tuned optical property across visible region into NIR region. In our synthetic protocols, three types of silver source: silver ion ( $\text{Ag}^+$ ), silver nanospheres (AgNPs) and silver oxide ( $\text{Ag}_2\text{O}$ ) were applied as a silver reservoir. The hydrogen peroxide ( $\text{H}_2\text{O}_2$ ) was employed as a shape transformation agent. The shape transformation process was performed by using a



solution of low  $\text{H}_2\text{O}_2$  concentration in order to minimize the oxidizing power while maintaining reducing capability. The highly stable silver nanoplates (AgNPLs)/ silver nanosheets (AgNShs) colloid could be obtained within 2 minutes by simply adding  $\text{H}_2\text{O}_2$  into the original AgNPs and  $\text{Ag}_2\text{O}$  colloid. The cyclic oxidation/reduction of  $\text{Ag}/\text{Ag}^+$  driven by the oxidative etching and weak reducing power of  $\text{H}_2\text{O}_2$  enabled the nanoplates growth without any requirement of additional metal ions.

## 1.2 THE OBJECTIVES OF THIS RESEARCH

- 1.2.1 To develop a novel method for synthesizing of silver nanosheets/nanoplates without stabilization by using sodium borohydride ( $\text{NaBH}_4$ ) as a reducing agent and hydrogen peroxide ( $\text{H}_2\text{O}_2$ ) as a shape controlling agent.
- 1.2.2 To develop a novel method to synthesize silver nanosheets by utilizing  $\text{H}_2\text{O}_2$  as a reducing and shape controlling agent.
- 1.2.3 To design synthetic strategies to control the optical property of as-synthesized silver nanoplates.

## 1.3 SCOPES OF THIS RESEARCH

- 1.3.1 Synthesize the high concentration and high stability silver nanoplates colloid by utilizing the dual function of  $\text{H}_2\text{O}_2$ .
- 1.3.2 Investigate the role of all chemical components ( $[\text{H}_2\text{O}_2]$ ,  $[\text{AgNO}_3]$ ,  $[\text{PVP}]$ , and  $[\text{TSC}]$ ) on the formation silver nanoplates.

1.3.3 Propose the mechanism of structural evolution of silver nanoplates.

#### 1.4 THE EXPECTED ACHIEVEMENT OF THIS RESEARCH

Achieve a new method to synthesize silver nanoplates/nanosheets including the contexts of fast, simple, high scale, environmentally friendly, low cost, and particle size tunable across the visible region in to the NIR region.



## CHAPTER II

### THEORY AND BACKGROUND

#### 2.1 LOCALIZED SURFACE PLASMON RESONANCE (LSPR) OF SILVER NANOSTRUCTURE

When metallic substances such as Au, Ag, and Cu are reduced into a small volume with nanometer-size dimensions, the interaction between light (electromagnetic wave) and conductive electrons on their surface will occur strongly. Under the certain excitation frequency, the time-varying electric field associated with light exerts a force on the negatively charged electron cloud in the conduction band of those metals, and drives their electrons to oscillate (up and down) collectively [2, 3, 23, 38-40]. This collective oscillation is in resonance with incident light, leading to a strong oscillation of the surface electrons. Figure 2.1 illustrates this phenomenon caused by metallic nanospheres [3]. This phenomenon is called “localized surface plasmon resonance (LSPR).

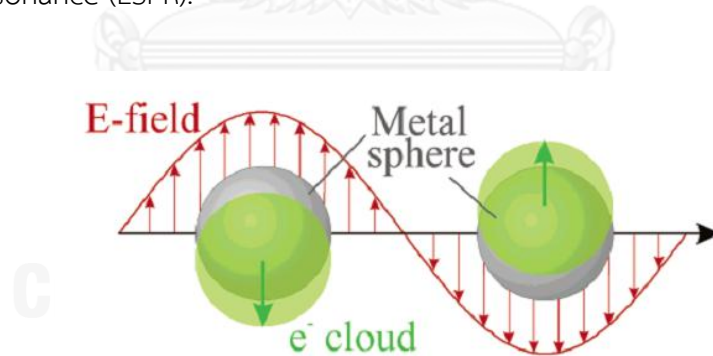


**Figure 2.1** Schematic diagram of plasmon oscillation for a metallic nanosphere, showing the displacement of the negatively charged conduction electron cloud relative with the metallic nuclei [3].

In order to understand the fundamentals of LSPR, detailed study on Mie's theory have been made. In the early 20<sup>th</sup> century, Gustav Mie developed an analytical solution of Maxwell's equations to describe the scattering and absorption of light by spherical particles [23]. For relatively small particles ( $d \leq \lambda$ ), Mie scattering corresponds with the more familiar Rayleigh scattering. Finding the scattered fields produced by a plane wave incident on a smooth conducting sphere results in the following total scattering, extinction, and absorption cross-sections [41]:

$$\sigma_{sca} = \frac{2\pi}{|k|^2} \sum_{L=1}^{\infty} (2L + 1) (|a_L|^2 + |b_L|^2) \quad (2.1)$$

$$\sigma_{ext} = \frac{2\pi}{|k|^2} \sum_{L=1}^{\infty} (2L + 1) [Re(a_L + b_L)] \quad (2.2)$$

$$\sigma_{abs} = \sigma_{ext} - \sigma_{sca} \quad (2.3)$$

Where  $k$  is the incoming wave vector and  $L$  is integers representing the dipole, quadrupole, and higher multipoles of the scattering. In the above expressions,  $a_L$  and  $b_L$  are the calculated parameters from the Riccati-Bessel functions. From the mathematical calculation, Sosa *et al.* demonstrated the absorption, extinction, and scattering coefficient of 50 nm Ag nanosphere (Figure 2.2). At around 320 nm in spectra, all coefficients have a local minimum that corresponds to the wavelength at which the dielectric function of silver, both real and imaginary parts, almost vanishes [42].

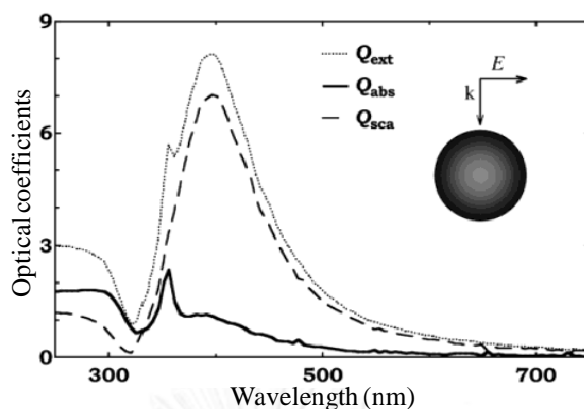


**Figure 2.2** The calculated optical coefficients of 50 nm Ag nanosphere [42].

This feature of the spectra is inherent to the material properties and is independent of the particle morphology. Below 320 nm, the absorption is mainly caused by the intra-band electronic transitions of silver. Therefore, this is also independent with the Ag nanoparticle shape and size, which sometimes are called the characteristic of Ag nanoparticles.

For the two-dimensional Ag nanostructures, especially triangular nanoprisms, the context of LSPR has been completely assigned [3, 40, 42]. Figure 2.3 shows the extinction spectra calculated by discrete dipole approximation (DDA) method for 100 nm triangular Ag nanoplates. The results show that there are three peaks, which are assigned to different plasmon oscillation modes. A long wavelength peak at 770 nm (black line, here referring to the complete 100 nm triangular shape) corresponding to in-plane dipole plasmon resonance. A weaker peak at 460 nm, and a small sharp peak at 335 nm are attributed to in-plane and out-of-plane quadrupole oscillations, respectively. Moreover, the out-of-plane quadrupole oscillation around 330-340 nm is also well-known as a characteristic of plate-like nanostructure of Ag. In addition, the red and green lines are resulted from 5 and 10 nm snipping triangular

shape. The results show that Ag nanoprism is very sensitive to edge snipping. The 20-nm snipped prism gives a peak that is blue-shifted around 100 nm compared with the perfect prism. On the other hand, the other peaks are more weakly sensitive to snipping.

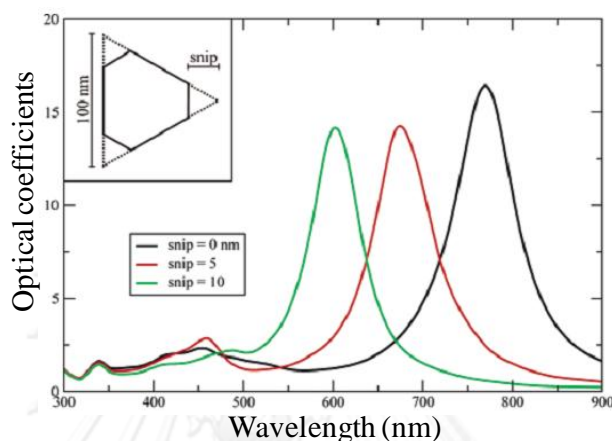


**Figure 2.3** Extinction coefficients calculated by DDA method of 100 nm edge length triangular Ag prisms with snips of 0, 10, and 20 nm. The inset shows the shape of a snipped prism. The prism thickness is 16 nm. Results are based on DDA calculations with a 2 nm cubic grid. For snip = 0, 68, 704 dipoles are used in the calculation [3].

## 2.2 APPLICATIONS OF SILVER NANOPlates

According to their unique shape- and size-dependent optical properties, such two-dimensional silver nanoplates have gained intensive interests since at least one decade ago. Silver nanoplates which possess specific optical properties exhibit great potentials in various applications such as surface enhanced Raman scattering (SERS) substrates [4], chemical and biological sensors [5, 6], catalysts [7, 8], surface enhanced fluorescence substrates [9], building blocks for complex nanophotonic

devices and circuits [10], as well as antibacterial agents [43-48]. The detailed information of silver nanoplates applications is described in the following section.

### 2.2.1 SURFACE ENHANCED RAMAN SCATTERING (SERS)

The well-known specific application of silver nanocrystals is SERS. Many research groups have been dedicated in the enhancement of Raman scattering for a long time. Due to the possession in controllable optical property of such two dimensional silver nanostructures by manipulating the degree of anisotropy, the arbitrary of this enhancement across the visible into the NIR region is eligible [1, 2]. The aggregated silver nanoplates can be served as a more effective SERS substrates for 2-aminothiophol (2-ATP) [49]. The aggregated phenomena can make coupling each other of silver nanoplates, which increase the electromagnetic field resulting in SERS enhancement. The enhance factor (EF) is proposed by:

$$EF = (I_{SERS}/C_{SERS})/(I_{normal}/C_{bulk}) \quad (2.4)$$

Where  $C_{bulk}$  is the concentration of the molecules in the bulk samples,  $C_{SERS}$  is the concentration of the adsorbed molecules on the silver surface.  $I_{normal}$  and  $I_{SERS}$  are the intensity of a certain vibration in normal and SERS Raman spectra, respectively.

Likewise, the SERS activity of flower-liked Ag nanoplates in the determination of R6G molecule using 514-nm excitation laser could obtain about five times than that obtained from Ag nanospheres [50]. In addition, DNA base adenine is also applied as a target molecule by functionalized 0.1  $\mu$ M adenine onto two types of flower-liked Ag nanoplates with larger and smaller petals. The results show two

prominent Raman peaks at 730 and 1305  $\text{cm}^{-1}$  (Figure 2.4) attributed to purine ring breathing and CN stretching mode, respectively. The higher degree of anisotropy flower-like Ag nanoplates, larger petal one shows a higher enhancement factor in SERS as indicated by the peak at 730  $\text{cm}^{-1}$  is 1.6 time stronger than that from smaller petal structures. From this evidence, it implies the possibility to use flower-like Ag nanoplates for directly detect nucleotide-based molecule including adenine that is able to observe DNA sequencing rapidly.

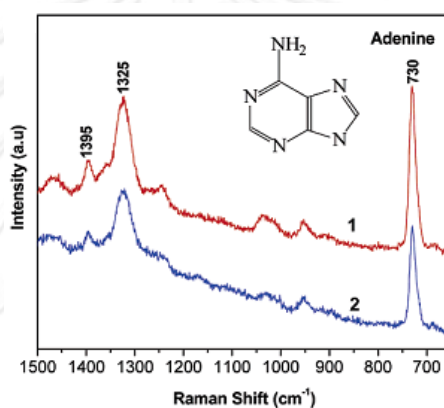


**Figure 2.4** SERS spectra of 1  $\mu\text{M}$  adenine molecules on the surface of (1) larger and (2) smaller petals of flower-like Ag nanoplates [50].

Recently, understanding about the enhancement factor of SERS which strongly depends on silver nanoplate thickness further than lateral sizes is revealed [35]. The SERS spectra of 1,4-benzenedithiol (1, 4-BDT) functionalized with 55 nm silver nanospheres deposited on silver nanoplates using 514 nm excitation laser were recorded. Moreover, the effects of edge length and thickness of silver nanoplates were investigated.



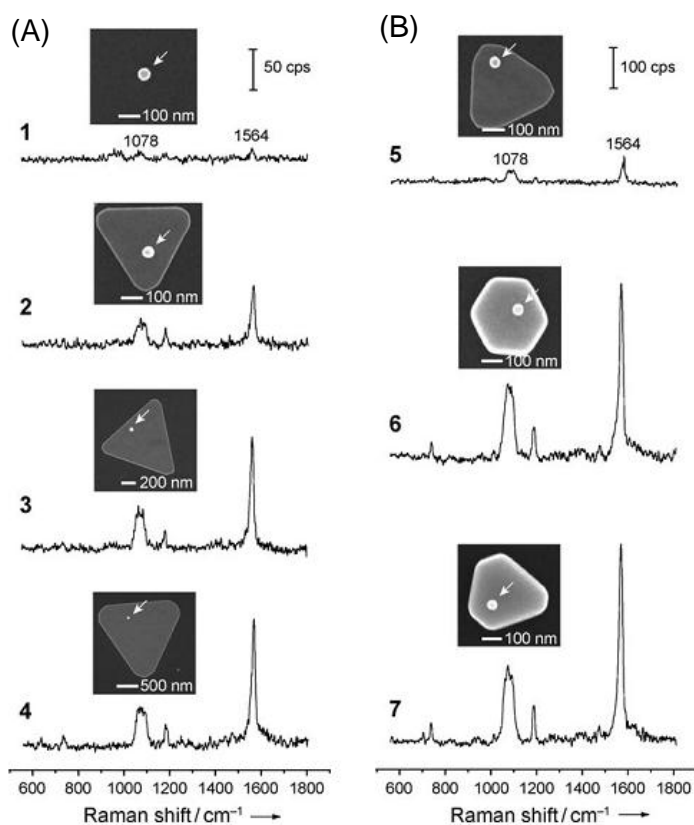


**Figure 2.5** Comparison of SERS spectra taken from single 1,4-BDT coated Ag nanospheres (55 nm in diameter) deposited on Ag nanoplates with different edge lengths (A) and thicknesses (B), respectively. (A) The Ag nanospheres were deposited on (1) Si wafer, and on Ag nanoplates with edge lengths of (2) 0.5, (3) 1, and (4) 2 mm. (B) The Ag nanospheres were deposited on Ag nanoplates with thicknesses of (5) 18, (6) 50, and (7) 100 nm. Note that the SERS signals in (A) and (B) are on different scales [35].

The characteristic peaks for 1,4-BDT express at 1078 and 1564 cm<sup>-1</sup>. As shown in Figure 2.5A., for the parameter of edge length, the peak at 1564 cm<sup>-1</sup> collected from Ag nanoplates with edge length of 0.5 μm (curve 2) is about five times greater than that on the silicon wafer (curve 1). However, this peak collected

from Ag nanoplates with edge length of 1 and 2  $\mu\text{m}$  is only 2 times greater than that of 0.5  $\mu\text{m}$ . Therefore, the effect of different silver nanospheres deposition regions is not significant. On the other hand, when Ag nanoplates with 0.4  $\mu\text{m}$  edge length and different thickness were investigated, as shown in Figure 2.5B, the  $1564\text{ cm}^{-1}$  peaks collected from Ag nanospheres deposited on 55- and 100-nm-thick Ag nanoplates (curve 6 and 7) are almost similar. They were stronger than that on 18-nm-thick Ag nanoplates (curve 5) for six times. These results clearly indicate that SERS enhancement factors for Ag nanospheres actually have a strong dependence on the thickness of the Ag nanoplate substrate.

### 2.2.2 CHEMICAL AND BIOLOGICAL SENSORS

Likewise the above surface-enhanced Raman scattering (SERS), the remarkable Ag nanoplate application is molecular detection. Recently, both chemical and biological molecules are also demonstrated.

For the biomolecular detection, protein and DNA are revealed [51, 52]. Due to the preferential binding with some biological molecules of crystal structure defects of Ag nanoplates, twinned defect and/or stacking fault, allows researcher to perform the predictive environmental toxicology [51]. Furthermore, for medical application, Ag nanoplates are also used as a host of biomedical imaging and sensing [52]. A modified surface of Ag nanoplates with targeting and passivating molecules, such as antibodies and PEG, is able to target the pancreatic cancer cell. As shown in Figure 2.6, these *in vitro* results demonstrate the potential of a-EGFR conjugated nanoplates to molecularly bond with pancreatic cancer cells.

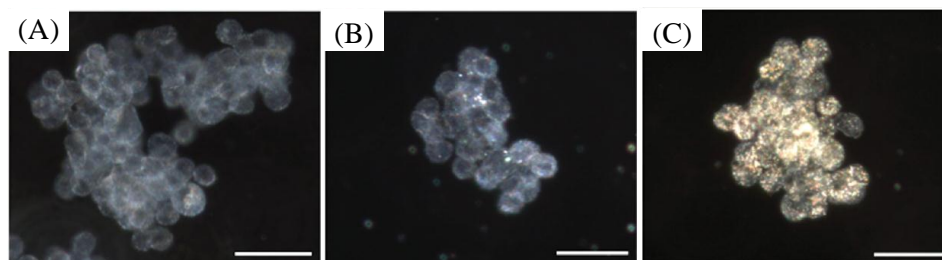


**Figure 2.6** Darkfield microscopic micrographs of pancreatic cancer cells after incubation with (A) no nanoplates, (B) PEGylated nanoplates, and (C) a-EGFR conjugated nanoplates. All scale bars are 20  $\mu\text{m}$  [52].

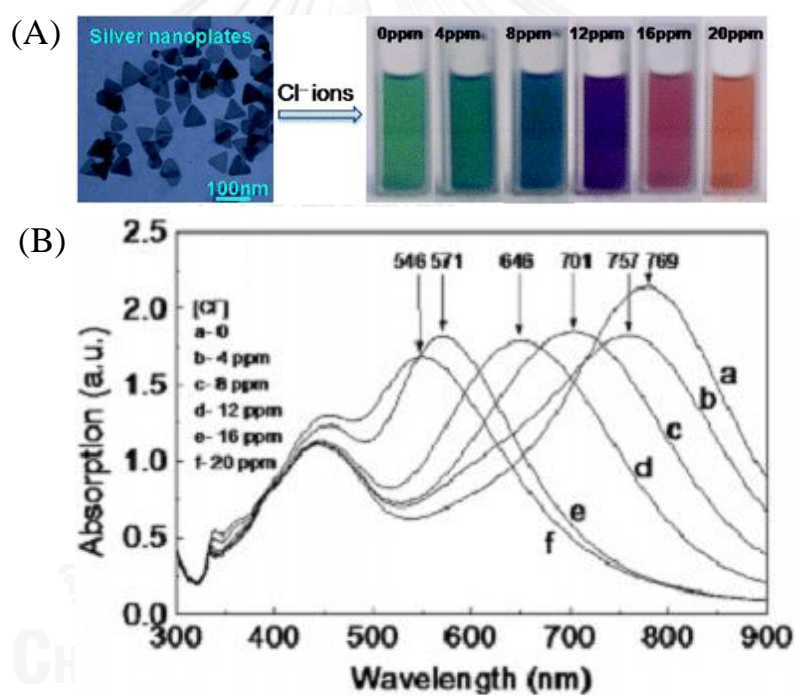


**Figure 2.7** (A) Color change of colloidal Ag nanoplates after reacts with  $\text{Cl}^-$  and (B) corresponding UV-visible spectra of silver nanoplates indicate the ability for sensing  $\text{Cl}^-$  in aqueous solution [53].

Similarly, chemicals such as organic molecules, inorganic cations, and halide anions are successfully detected by plate like nanostructures of Ag metal [53].

Ag nanoplates with edge length of 70 nm and 2 nm thickness in aqueous solution can be utilized as a sensor of halide anions. By observing a shift in surface plasmon resonance, the colloidal silver nanoplates shows a high sensitivity on the order of  $1 \times 10^{-6}$  M in detecting halides in water at room temperature (Figure 2.7 shows an example in the case of  $\text{Cl}^-$ ).

### 2.2.3 BUILDING BLOCKS FOR FABRICATION OF OTHER METALS

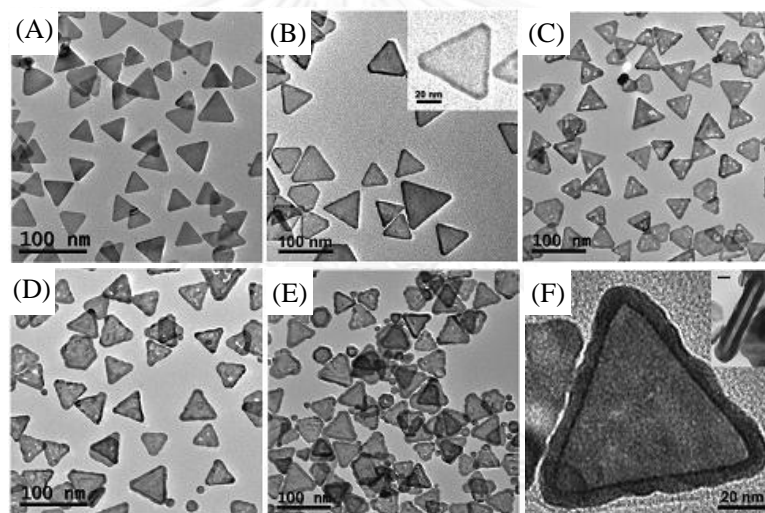


**Figure 2.8** TEM images of (A) initial silver nanoprisms, (B) samples at 45 min with gold deposition on the prism stages and (C) samples from stage 2 with some small pinholes, (D) samples with partially refilled pinholes after 120 min (stage 3), (E) samples at 200 min with full gold shells (stage 4), and (F) a typical final gold-coated nanoprism (the inset is the cross-sectional view with a scale bar of 10 nm) [54].

Stability of Ag nanostructures is an important problem in wildly applications. In order to solve this limitation, nanostructures of other inert metals

such as Au, Pd, and Pt are fabricated [10, 54, 55]. Especially Au metal, many researchers have been explored their methods for controlling morphology of Au nanocrystals. Galvanic replacement reaction is also performed to generate Au nanostructure by using nanocrystals of metallic Ag as a template [54]. Figure 2.8 illustrates the perfect of Au-coated Ag nanoprisms synthesized by slow galvanic reaction of  $\text{HAuCl}_4$  with Ag nanoprisms templates in the solution of  $\text{NH}_2\text{OH}$  within 200 minutes.

#### 2.2.4 ANTIBACTERIAL APPLICATION

Recently, the most widely commercialized application of Ag nanoparticles is antimicrobial application [43-46]. An increase in Ag nanoparticles application in consumer products are easily observed, including household antiseptic sprays and antimicrobial coatings for medical devices [43-45, 47]. The activity of various shapes and sizes of Ag nanocrystals in antibacterial application have been already revealed [48]. The results indicate that, previous understanding crystal morphology of Ag nanoparticles known to effect bacteria toxicity are indirect effectors, but strongly depending on rate of  $\text{Ag}^+$  releasing (Figure 2.9). The formerly understood that smaller Ag nanoparticles play more effects on antibacterial activity; indeed,  $\text{Ag}^+$  is the main effect. In the case of Ag nanoplates, due to the designable of colloidal color, and the high aspect ratio lead to good adhesion, a wildly use in antiseptic coating for various types of materials are eligible [47]. Figure 2.10 shows the coating of Ag nanoplates on cotton fiber.

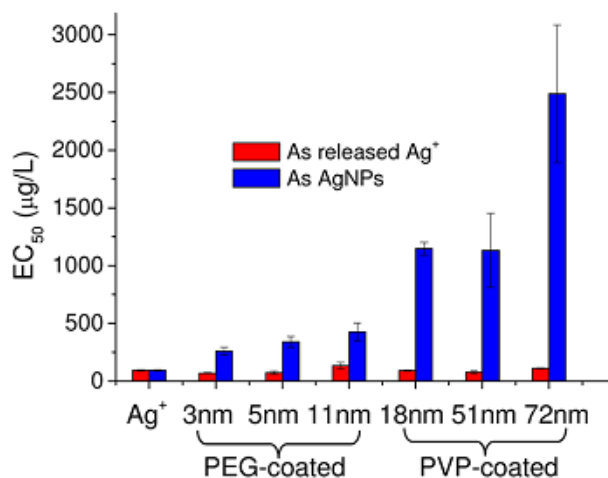


**Figure 2.9** Dose–response of *E. coli* exposed to various air-exposed AgNPs. EC<sub>50</sub> increases with the increasing particle size, suggesting size-dependent toxicity. This is an indirect effect associated with Ag<sup>+</sup> release (smaller AgNPs release more Ag<sup>+</sup> and are more toxic) [48].

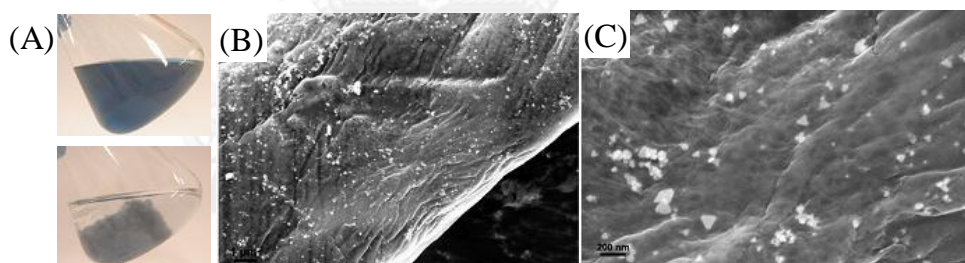


**Figure 2.10** (A) Deposition pictures of blue colloidal Ag nanoplates on cotton fiber, (B, C) SEM images of Ag nanoplates coated on cotton fiber [47].

### 2.3 SHAPE CONTROLLED SYNTHESIS OF METAL NANOCRYSTALS

Noble metal nanostructures especially Ag and Au have gained a great interest due to their morphology dependent the optical properties. More than ten years ago, many research groups have been focusing on the manipulated parameters in order to perform a nucleation and growth for specific shape and size

nanostructure. Although, most nanocrystals synthetic protocols reveal an application of only simple chemicals which can be seen in chemistry books, but behind the very simple chemistry the nucleation and growth mechanism still extremely complicated. The understanding in nanocrystals growth mechanism is very important for the further controlled synthesis. Many approaches have been proven for their reproducible and controllable on the shape control synthesis. In fact, scientists have just begun to understand the complex physics that lead to the formation of nanocrystals with specific shapes.

### 2.3.1 THERMODYNAMIC CONTROL

Under thermodynamic control reaction, the most stable product was produced. To estimate the most stable product, the single-crystal seeds generation could be considered by using the context of Wulff's theorem [56, 57], which tries to decrease the total interfacial free energy of a system under a limited volume. The interfacial free energy,  $\gamma$  can be assigned as the required energy for making a unit area of "new" surface [Eq. (2.5)] where  $G$  is the free energy and  $A$  is the surface area.

$$\gamma = \left( \frac{\partial G}{\partial A} \right)_{n_i, T, P} \quad (2.5)$$

For a freshly formed seed, crystal symmetry is broken by missing bonds at the surface, causing the surface atoms to be attracted toward the interior. In order to pull the surface atoms back to their initial positions, a restoring force is required. By using the ideal surface model, the interfacial free energy is given by Equation (2.6) where  $N_b$  is the number of broken bonds,  $\epsilon$  is the bond strength, and  $\rho_a$  is the density of surface atoms [58, 59].

$$\gamma = \frac{1}{2} N_b \epsilon \rho_a \quad (2.6)$$

In case of fcc metal structure with a lattice constant of  $a$ , the estimation of surface energies of crystallographic facets that normally cover the nanocrystals can be given by:  $\gamma_{\{100\}} = 4(\epsilon/a^2)$ ,  $\gamma_{\{110\}} = 4.24(\epsilon/a^2)$ , and  $\gamma_{\{111\}} = 3.36(\epsilon/a^2)$ . Therefore, the comparison of interfacial free energies can be rearranged by  $\gamma_{\{111\}} < \gamma_{\{100\}} < \gamma_{\{110\}}$ . This sequence suggests that a single-crystal seed should be octahedral or tetrahedral shape in order to maximize the exhibition of  $\{111\}$  facets which is the best approach to minimize the total surface energy. Both octahedral and tetrahedral shape, have larger surface areas than a cube at the same volume. In consequence, single-crystal seeds are expected to survive as truncated octahedrons (or Wulff polyhedrons) covered by a mixing of  $\{111\}$  and  $\{100\}$  facets. This quasi-spherical shape has the smallest surface area to minimize the total interfacial free energy.

### 2.3.2 KINETICALLY CONTROL

When multiply twinned seeds are relatively small, in order to minimize the total free energy, the extra strain energy caused by twinning plane could be compensated by maximizing the surface coverage with  $\{111\}$  facets [60]. If these seeds growth rapidly, however, theoretical study points out that the  $\{111\}$  facets low surface energy notable conserve the excessive strain energy for a long time, culminating in their transformation to be the single crystals [60-62]. This understanding indicates the necessity of multiply twinned seeds confinement to be relatively small sizes in order to increase their yields. In practical, this condition can be achieved by maintaining the atomic generation rates consistency sufficiently low.



When the creation rate of metal atoms is slow, multiply twinned seeds will beats over single-crystal once because they can be existed at small sizes for a long period. Under the same reduction kinetics, singly twinned seeds may also appear, although in lower quantities than the multiply twinned ones due to the higher energy of {100} facets. In summary, it is possible to control the population of seeds containing with different numbers of twin defects by varying the reduction or decomposition rate of a precursor, which is the main concept of kinetic control. When the decomposition or reduction becomes sufficiently slow, the atoms tend to form nuclei and seeds by random hexagonal close packing (rhcp), including with the stacking faults [63]. This synthetic pathway has been known as “kinetically controlled” and the seed generally takes morphologies without from those by thermodynamics favored. For example, incorporation of stacking faults and/ or twin planes can result in the formation of a plate-like seed (Figure 2.11A). Entirely different from the polyhedral seeds, a plate-like seed is enveloped by {111} facets at both the top and bottom surfaces, comprising of stacking faults and/or twin defects along the vertical direction (Figures 2.11B and C). Owing to a relatively large surface area as compared with a polyhedral seed at the same volume and the lattice strain energy caused by defects, the total free energy of a plate-like seed is extremely high nevertheless its coverage with {111} planes. Therefore, formation of plate-like seeds can never be favored in conditions of thermodynamics controlled. To obtain plate-like seeds in system, both nucleation and growth must avoid from a thermodynamically controlled route. In practice, strategies to achieve the kinetically controlled reaction can be done by many methods: 1) keep slowing down of precursor decomposition or reduction [64, 65], 2) utilization the weak reducing agent [66], 3) integrating the reduction to an

oxidation process concertedly [67], or 4) exploitation of the Ostwald ripening process [68, 69].

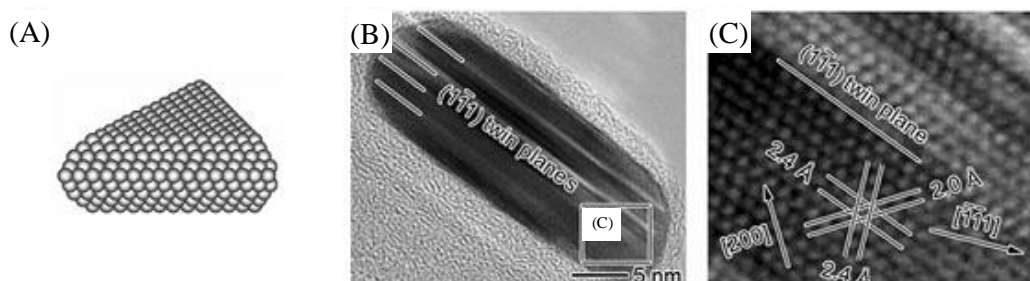


**Figure 2.11** (A) Schematic diagram of a plate-like seed with a random hexagonal close-packed (rhcp) structure. (B and C) HRTEM images taken from the side face of Ag nanoplates [64].

### 2.3.3 OXIDATIVE ETCHING

Etching environments are the key role once for nanocrystals structure formation, due to their powerfully manipulate the distribution of single-crystal versus twinned seeds, which zero-valent metal atoms are oxidized back to ions [70]. Normally, the nanostructures synthetic processes were conducted in air, so  $O_2$  is present in the solution throughout the entire reaction process. If a ligand for the metal ion precursor is also present in the same solution, a combination of the ligand and  $O_2$  can result in a powerful etchant for both the nuclei and seeds. As shown in Figures 2.12, the defect zones in twinned seeds take a much higher in energy compare with the single-crystal regions and thus are most unstable to an oxidative environment, with their atoms will being attacked by the etchant, oxidized, and dissolved into the solution. In contrast, single-crystal seeds are more capable of resistance to oxidative etching as an absent of twin boundary defects on the surface. By utilization of this selectivity, the quantity of different seed types in the system can

be operated controllably. For example, in the polyol synthesis of Ag nanocrystals, all twinned seeds can be removed completely from the solution by adding a small amount of  $\text{Cl}^-$  to the reaction (Figure 2.13) [70].

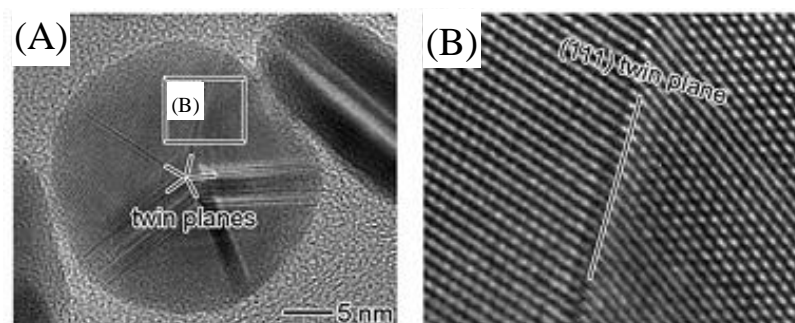


**Figure 2.12** (A and B) High-resolution TEM (HRTEM) images of a decahedral Ag nanocrystal [64].

Oxidative etching has already been validated for several of noble metals, including Ag, Pd, and Rh. [70]. From these researches, both  $\text{O}_2$  and a ligand are required for the observation of oxidative etching. For example, when a polyol synthetic procedure for Ag nanocrystals is conducted under the presence of argon, the multiply twinned seeds at the early stage of reaction. Also, if without an addition of  $\text{Cl}^-$ , multiply twinned seeds will be formed quickly and growth as a quasi-spherical particles. Only if both  $\text{O}_2$  and  $\text{Cl}^-$  are applied, the reaction will produce a high yield of single-crystal seeds.

Based on the same mechanism as mention above, multiply twinned seeds can be reserved by: 1) bubbling some inert gas through reaction in order to remove  $\text{O}_2$  [71], 2) utilization of an appropriate capping agents (e.g., citrate) for blocking oxygen adsorption on the seeds [72], or 3) suppressing the power of

oxidative etching by expelled oxygen in the system by using a redox pair (e.g.,  $\text{Fe}^{\text{III/II}}$  or  $\text{Cu}^{\text{II/I}}$  salts) [63, 64].

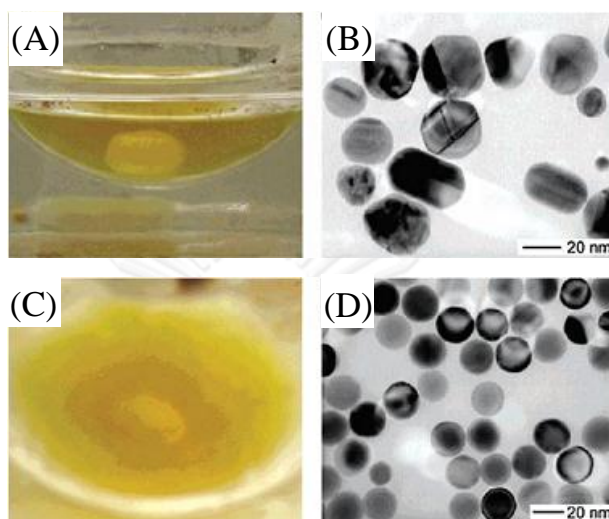


**Figure 2.13** The polyol synthesis of Ag nanocrystals in which  $\text{AgNO}_3$  serve as Ag precursor and PVP as capping agent. The reaction was conducted under air and 0.06 mM NaCl was added. Reaction times: (A, B) 10 min and (C, D) 44 h. (A, C) Photo picture of the reaction solution, in which the yellow color indicates the presence of Ag nanocrystals. (B, D) TEM images of the Ag nanocrystals produced at each time [70].

#### 2.4 SILVER NANOPATES FABRICATIONS

In the case of silver, the preparation of two dimensional silver nanostructure, in order to achieve this objective, many efforts to switch thermodynamically to be kinetically control reaction were demonstrated. The examples of kinetically control reaction strategy including with exploitation of mild reducing agents (i.e., PVP, ascorbic acid, or glycylglycine) [66] and complexing the  $\text{Ag}^+$  precursor with some strongly co-ordination polymer such as polyacrylamide (PAM) in

order to reduce the reduction rate [64]. Whereby, in the past decade, many methods for silver nanoplates fabrication were developed. Among of them, the solution-based techniques have gain a greatly famous, due to their controllable, simple, and high yield of obtained silver nanoplates. The solution based silver nanoplates preparation techniques could be classified into many groups depending on strategies and applied chemical reagents as further descriptions in the following sections.

#### 2.4.1 PHOTOCHEMICAL PROCESS

Light irradiation induced shape transformation of silver nanospheres to be silver nanoplates is the first strategy of kinetically control reaction. Many research groups have demonstrated their efficiency of silver nanoplates preparation by using some assistant chemicals for silver nanoplates growth under light irradiation [11-14]. This first stage of this frontier is an idea of Mirkin s' research groups [11]. They have pioneered the most important window for light irradiation technique. The original silver nanospheres were prepared by using  $\text{AgNO}_3$  precursor as a Ag source, Trisodium citrate (TSC) as a capping and reducing agent,  $\text{NaBH}_4$  as a reducing agent, and Bis(p-sulfonatophenyl) phenylphosphine dihydrate dipotassium salt (BSPP) as stabilizer. The obtained original Ag nanospheres were then irradiated by 40-watt fluorescence light. By the time dependent transmission electron microscopy (TEM) observation, the results show that original Ag nanospheres with diameter around 8.0 nm were transformed into prismatic structures that existence as a two dimensional triangles (Figure 2.14). Both edge length and population of Ag nanoprisms increase with function of time concomitant with a decreasing of spherical Ag nanoparticles population. Clarify that, from this technique, Ag nanoprisms develop from the original spherical nanoparticles.

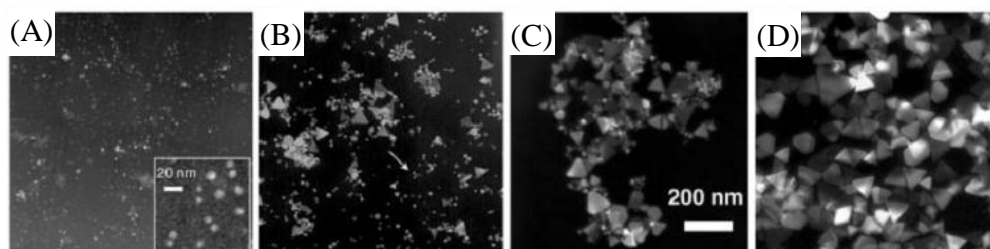


**Figure 2.14** TEM images (reverse print) mapping the morphology changes (A) before irradiation and after (B) 40, (C) 55, and (D) 70 hours of 40-watt fluorescence irradiation. Except for the inset in (A), the scale bar is 200 nm for all four images [11].

Following by, An *et.al* have successfully prepared hexagonal Ag nanoplates from triangular Ag nanoprisms [13]. In the synthesis protocol, they prepared the initial Ag nanoseeds by drop  $\text{NaBH}_4$  into the mixture aqueous solution of  $\text{AgNO}_3$  and TSC solution. Then, the obtained yellow colloidal of Ag nanospheres was irradiated by 70-watt Sodium lamp. The shape transformation from spheres into plates was visually observed by a series of color change from yellow to green, purple, and pink when taken irradiation time increase from 3.5, 8, and 10 hours, respectively. TEM images indicated that under light irradiation, original Ag nanospheres (Figure 2.15A) will be firstly transformed to be triangular nanoprisms (Figure 2.15B), subsequence by the formation of hexagonal Ag nanoplates (Figure 2.15C and D) after increasing the irradiation time.

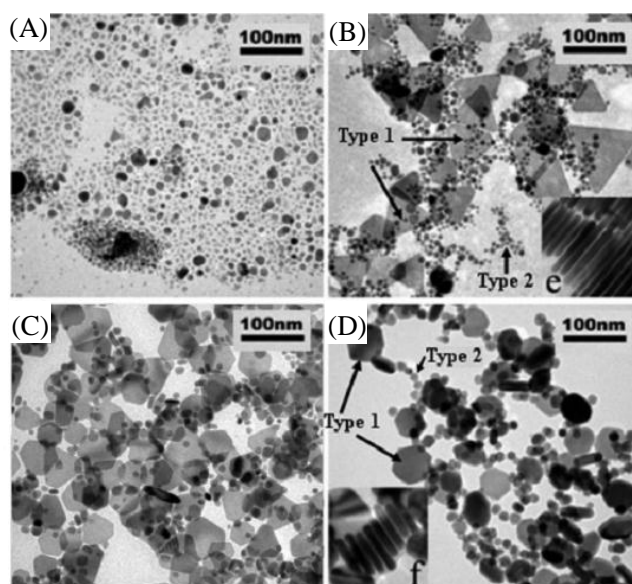
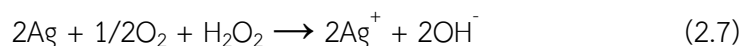


**Figure 2.15** TEM images showing the conversion of silver nanosphere to hexagonal nanoplates: (A) before irradiation and after (B) 3.5, (C) 8, and (d) 10 hour of irradiation. Inset: Enlarged photos are showing triangular (E) and hexagonal (F) silver nanoplates stacks [13].

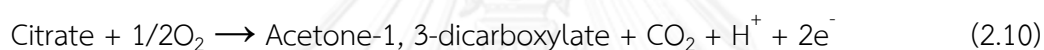
Up to date, the mechanism of Ag nanoplates preparation by photoinduced conversion process has been successfully clarified [14]. From this study,  $O_2$  is required for evolving oxidatively dissolved Ag nanospheres to be  $Ag^+$ , presumably caused the presence of Ostwald ripening process. From the quantification analysis of citrate during photoconversion process, due to the decreasing after light irradiation indicated consummation of this ligand, and the reaction rate is depend on citrate content. The mechanism is proposed base on these phenomena by combination the oxidative etching of the Ag nanoseeds and the subsequent photoreduction of aqueous  $Ag^+$ . Ag nanoseeds that absorb and scatter light weakly reduce  $O_2$  and lose  $Ag^+$  as follows:



Ag nanoprisms absorb and scatter more strongly oxidize citrate, reduce  $\text{Ag}^+$ , and gain Ag as follows:



The photo-oxidation of citrate by  $\text{O}_2$ , catalyzed by silver could be written in totally as follows:



From control experiments, this reaction does not occur when the system not include neither Ag nanoseede nor photoinduction. Similarly, with the same applied chemicals regent, Tang *et al.* revealed that Ag nanoplates synthetic system including with citrate undergoes both light irradiated photo-oxidation and heating method [11-15]. Under the same reaction system, both heating and light irradiation are applied in order to involve the shape conversion and reconstruction, respectively. Oxygen plays a pivotal role in shape evolution from Ag nanoprisms to be nanodisks. Confirmed by SPR spectra (Figure 2.16A), under thermal irradiation, the initial Ag nanoprisms are converted to smaller nanodisks indicated by a slightly blueshift of the in-plane dipole plasmon resonance after heat treatment. And TEM images (Figure 2.16C-H), 28 nm edge length and 5.5 nm in thick Ag nanoprisms can be transform to be nanodisks with edge length of 25, 23, and 19.6 nm concomitant



the increasing in thickness around 5.9, 7.1, and 7.2 nm after heating time for 73, 125, and 205 seconds, respectively.

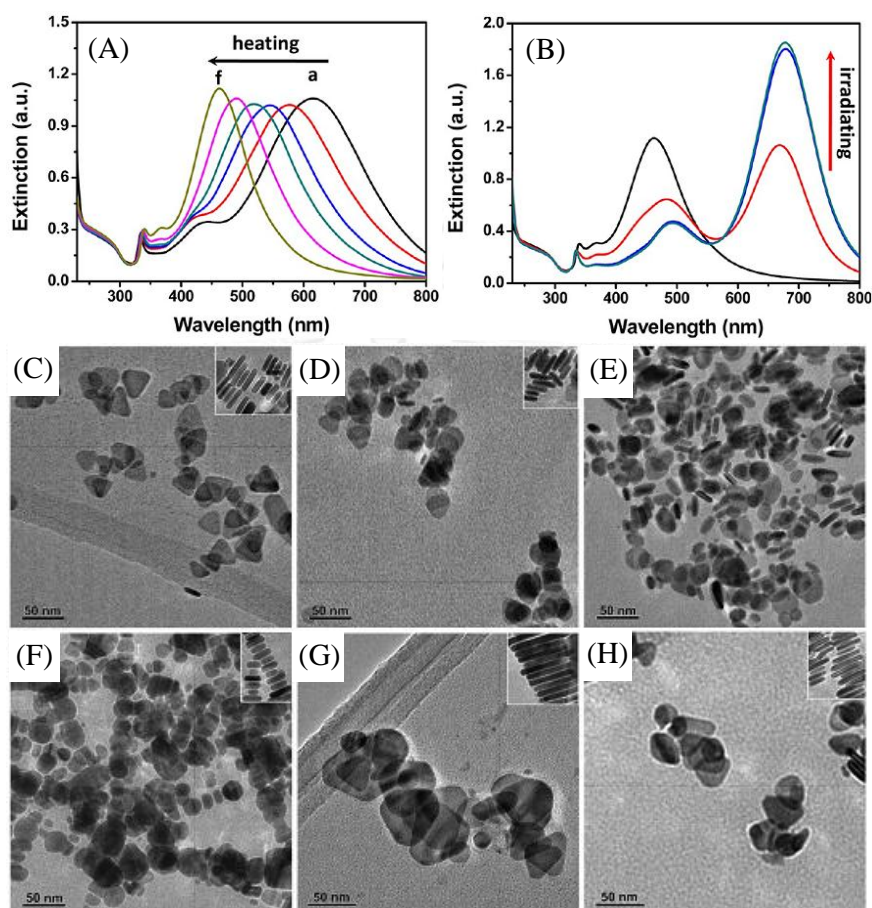


**Figure 2.16** (A) Evolution of extinction spectra of silver nanoplates under heat treatment for various periods, 0, 30, 73, 125, 169, and 205 s. (B) Extinction spectra of 205 s heated silver nanoplates before and after light irradiation for 90, 210, and 270 min. TEM images of (C) the initial silver nanoprisms, and the silver obtained nanoplates after heat treatment for (D) 73, e) 125, and (F) 205 s, (G) silver nanoprisms transformed from silver nanodisks under light irradiation, and (H) silver nanoplates from initial silver nanoprisms after light irradiation [15].

Surly, the thermal treatment influences the decreasing of aspect ratio (edge length/thickness) that reconfirm by a slightly redshift of the out-of-plane around 340 nm (Figure 2.16A). On the other hand, for the same reaction, subsequent by light irradiation capable of reconstruction of small Ag nanodisks back to larger nanoprisms with lateral size of 62.4 nm and thickness of 9.2 nm (Figure 2.16G) corresponding to SPR observation (Figure 2.16B). Citrate ions are needed for the photoinduced reconversion from Ag nanodisks back to nanoprisms.

#### 2.4.2 POLYOL PROCESS

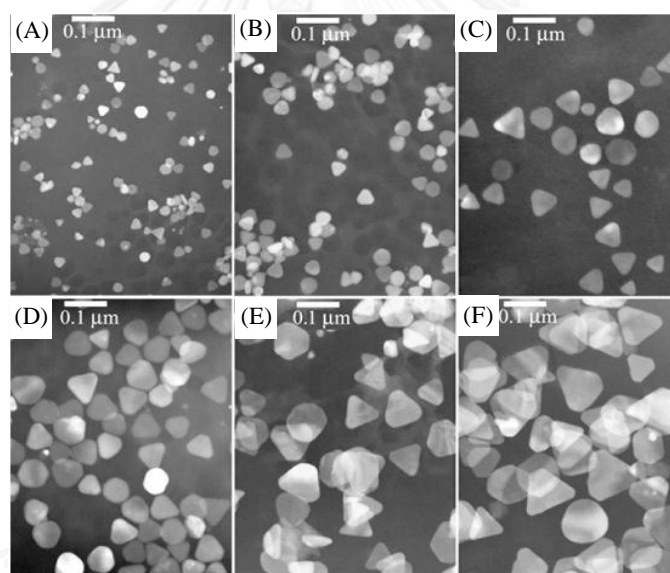


**Figure 2.17** TEM images of Ag nanoprisms with average edge lengths of (A) 24 nm, (B) 36 nm, (C) 52 nm, (D) 72 nm, (E) 92 nm, and (F) 120 nm synthesized by utilizing 0.2 g, 0.4 g, 0.5 g, 0.8 g, 1.1 g, and 1.5 g of PVP, respectively [73].

Polyol process is the name of metallic nanocrystals fabrication using organic hydroxyl as both solvent and reductant [73, 74]. Utilization the interface of

water/PVP/*n*-pentanol able to fabricate Ag nanoprisms with size dependent on PVP contents [73]. From this study, due to the preferential binding on (100) facets of PVP, it also promotes the self-assembly on those same facets, therefore larger edge length of Ag nanoprism can be obtained by increasing PVP concentration. Figure 2.17 shows the increasing of nanoprisms lateral size when the greater amount of PVP is applied.

The modified Polyol process [74], by replacing the normal reducing agent of this process, ethylene glycol with only one hydroxyl reducing group such as ethylene glycol monoalkyl ethers under the microwave assistant, The Ag nanodisks/nanoprisms can be also obtained as shown in Figure 2.18.

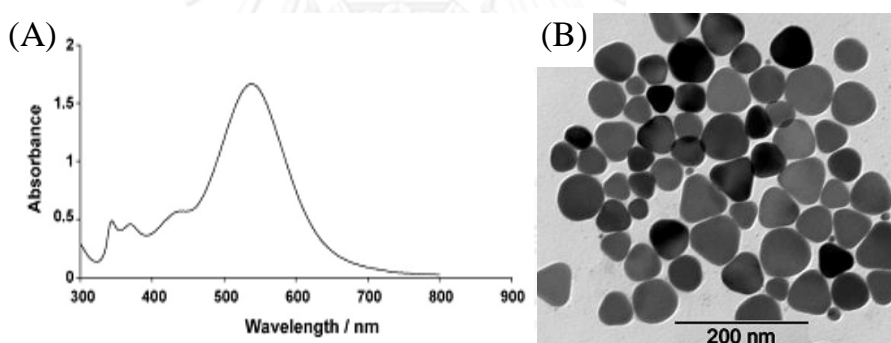


**Figure 2.18** (A) UV-spectrum, and (B) TEM images of Ag nanoprisms synthesized by using ethylene glycol monoethyl ether as reducing agent [74].

Although the high concentration of Ag nanoplates can be obtained by Polyol synthetic route, requirements of thermal treatment and complexing organic reductant still limit for large scale synthesizing and suitable for the widely application, respectively. Therefore, research and development in the contexts of fast and simple route for Ag nanoplates fabrication still challenge for nanoscientist.

### 2.4.3 RAPID THERMAL SYNTHESIS

Likewise, the photochemical technique, rapid thermal synthesizing of Ag nanoplates is pioneered by Mirkin's research group since 2005 [17]. This powerful technique is the first time informatively description of the necessary selectively etching in Ag nanoplates formation. Moreover, this is the first time for hydrogen peroxide ( $H_2O_2$ ) exploitation. By the simple chemical utilization (Figure 2.19), uniformly triangular Ag nanoprisms can be obtained within 30 minutes. Citrate is the pivotal agent for Ag nanoprisms formation. The size of triangular Ag nanoprisms can be selectively tune by adjusting concentrations of  $H_2O_2$  and  $NaBH_4$  reducing agent. Figure 2.20 illustrates the systematic red shift of the in-plane dipole resonance (increasing in nanoprisms edge length) of Ag nanoprisms by introduce the greater amount of  $H_2O_2$ .

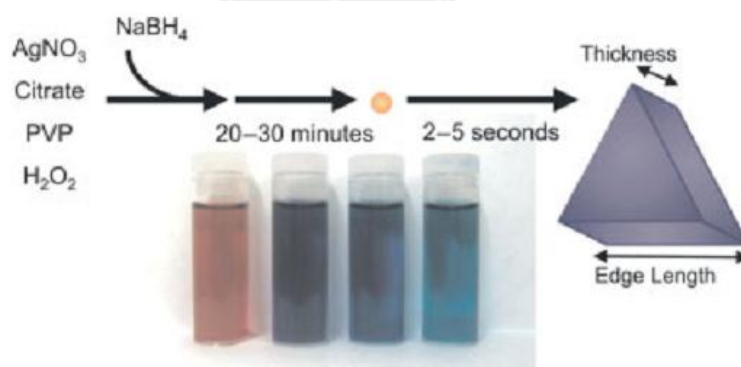


**Figure 2.19** Schematic diagram of Ag nanoparticles conversion to nanoprisms with  $NaBH_4$  and  $H_2O_2$ . The inset picture is set of colloidal Ag nanoprisms with  $NaBH_4$  concentrations of 0.30, 0.50, 0.67, and 0.80 mM, respectively [17].

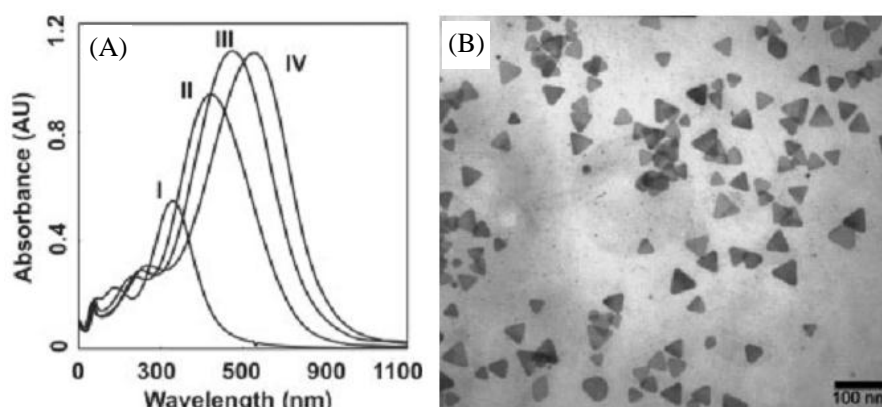


**Figure 2.20** (A) UV-visible spectra of colloidal Ag nanoprisms synthesized by using 20 mM of H<sub>2</sub>O<sub>2</sub> with various NaBH<sub>4</sub> concentrations of I) 0.30, II) 0.50, III) 0.67, and IV) 0.80 mM, respectively. (B) TEM image of Ag nanoprisms sample IV [17].

For various of Ag nanoplates preparation techniques, photochemical reduction [11-14], thermal etching [15], and rapid thermal process [17-19]. In order to gained a great yield of well define morphology of plate like Ag nanostructure, citrate is required as surface capping agent which it can preferentially binds on the (111) facets then promotes the evolution of Ag nanocrystals in the others (100) facets [22, 24-33]. By simulation techniques, citrates able to selectively binds on the (111) facets for four bonds prevail those of PVP or others reagents because of geometry mismatch [32]. Therefore, it is not exaggerate to give the citrates ion as a magic surface directing agent. Until, the systematic in detail study the role of many chemical reagents, which were conducted by Zhang *et al.* in 2011. This study indicated the function of selective binding on (111) facets of citrates can be completely replaced by many di- and tricarboxylate compounds whose two nearest carboxylate groups are separated with two or three carbon atoms. Most importantly,

$\text{H}_2\text{O}_2$  plays a pivotal role in determining the shape transformation into plates. The powerful oxidative property of  $\text{H}_2\text{O}_2$ , assists the preferential formation of silver nanoplates by inducing the generation of planar twinned defects and removing other less stable structures. Figure 2.21 illustrates the role of Citrate, PVP, and  $\text{H}_2\text{O}_2$  in the Ag nanoplates formation.

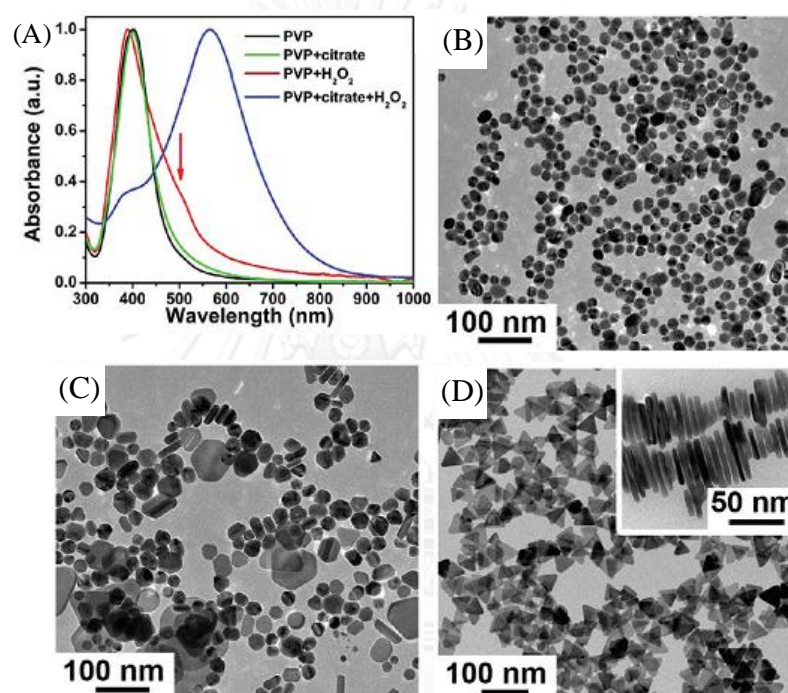


**Figure 2.21** (A) UV-visible spectra of silver nanoparticles synthesized by different conditions; (B, D) TEM images of products, which were synthesized in the presence of (B) PVP only, (C) PVP and  $\text{H}_2\text{O}_2$ , and (D) PVP, citrate, and  $\text{H}_2\text{O}_2$  together. The inset in (D) shows a TEM image in which Ag nanoplates stand vertically upon their edges [19].

Moreover, the power role of  $\text{H}_2\text{O}_2$  in Ag nanoplates fabrication was declared again by Tsuji *et al.* in 2012 [18]. By the powerfully oxidative of  $\text{H}_2\text{O}_2$ , the completely dissolve Ag nanocrystals in to  $\text{Ag}^+$  is eligible. Then, under the etching

environment, the dissolved  $\text{Ag}^+$  can be reduced and selective nucleation by  $\text{NaBH}_4$  and citrate back to plates like seeds, which will grow to be perfect triangular Ag nanoprisms. From this synthetic strategy, various Ag nanocrystals shape such as spheres, rod, bipyramid, and cube can be transformed to triangular Ag nanoprism completely. Figure 2.22 shows the ability to transform cube and bipyramid Ag nanostructure to be perfect triangular Ag nanoprisms.

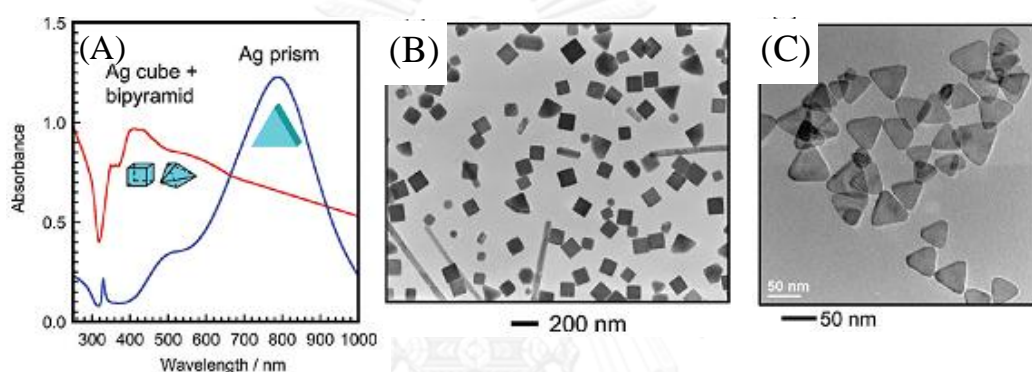


**Figure 2.22** (A) UV-visible-NIR spectra of Ag cubes and bipyramids mixture and prisms, (B) TEM image of cubes and bipyramids, and (C) TEM image of prism obtained after transformation process time of 30 minutes [18].

#### 2.4.4 SEED-MEDIATION PROCESS

Among those photochemical techniques and rapid thermal synthesis of Ag nanoplates as mention above, seed-mediated synthetic route is the most famous once, that was applied for a widely engineering of anisotropic nanostructures [22]. In practical, this technique combining with two steps, the original seed preparation and growth stage under a growth solution. Normally, surfactant and mild reducing agent are required for the morphology controlling. In the presence of micelles of CTAB and

$\text{NaBH}_4$  as reducing agent, 68 nm edge lengths and 24 nm thick of truncated triangular Ag nanoplates have been obtained, as shown in Figure 2.23.

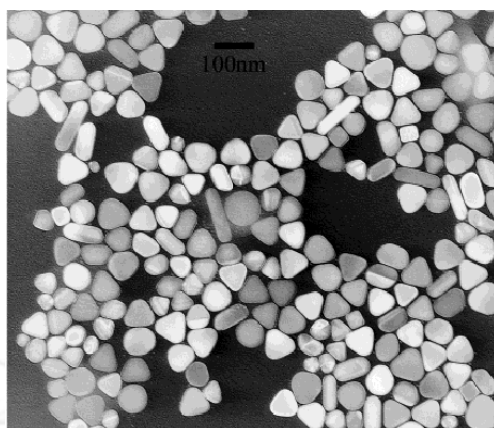


**Figure 2.23** TEM image of the flat-lay purified truncated triangular Ag nanoplates growth in CTAB micelles [22].

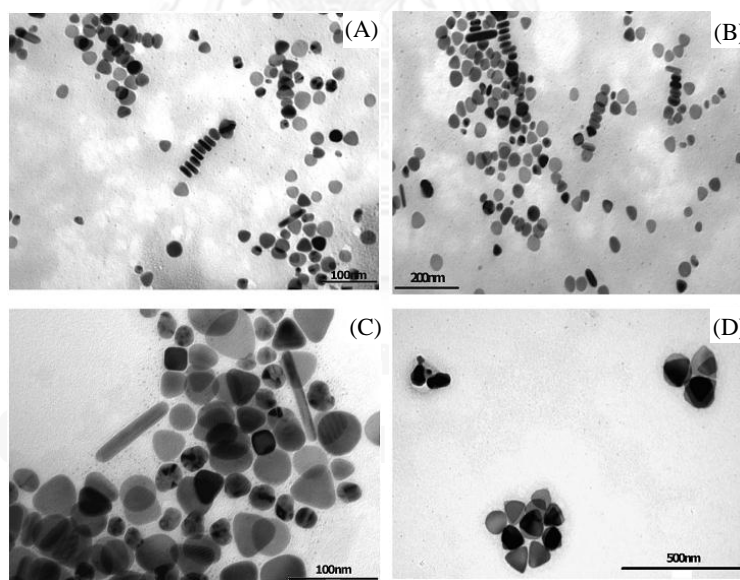


**Figure 2.24** TEM images of truncated triangular Ag nanoplates synthesized under micelles of CTAB when increasing the volume of 3.5 nM original Ag nanoseeds from (A) 30, (B) 60, (C) 125, and (D) 250  $\mu\text{L}$ , respectively [24].



Based upon this method, later, size of obtained Ag nanoplates can be controlled by adjusting some parameters, for example; concentration of original Ag seeds, surfactant, and reducing agent [24]. By increasing the amount of added original Ag nanoseeds, the larger of edge length of Ag nanoplates are formed, that can be observed by Figure 2.24.

Moreover, with this technique, Zhang *et al.* in 2010 [30] have been successfully prepared the uniform Ag nanoplates by replacing CTAB with citrate ion. In their synthetic route, citrates can retard the reaction rate and then promote the kinetically formation of uniform triangular Ag nanoplates. Figure 2.25 shows that the larger triangular Ag nanoplates were fabricated by increasing the cycle growth.

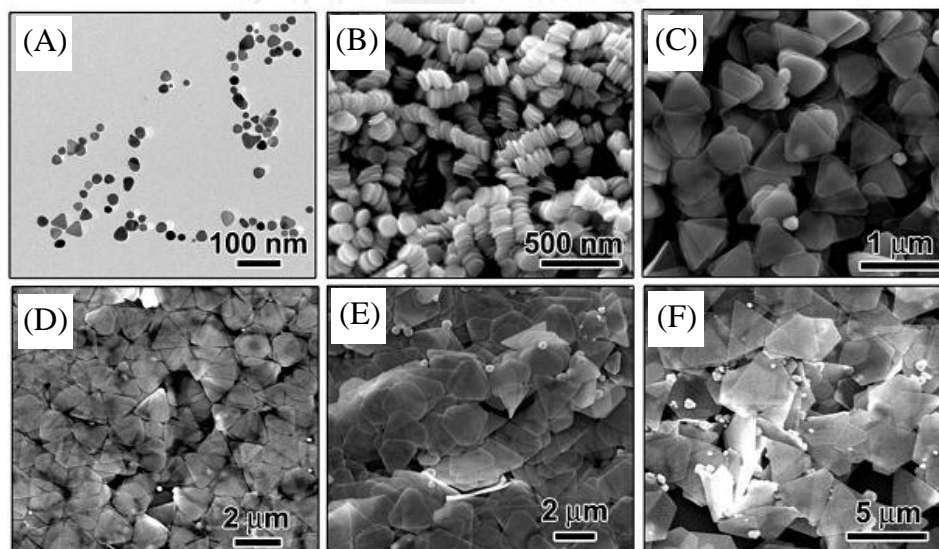


**Figure 2.25** (A) TEM and (B-F) SEM images of triangular Ag nanoplates synthesized by different cycle growth; (A) after removal of PVP by centrifuging and washing to larger Ag nanoplates after (B) one, (C) two, (D) four, (E) five, and (F) seven cycles of seeded growth [30].

#### 2.4.5 ELECTROCHEMICAL PROCESS

The galvanic reaction is also applied for Ag nanoplates fabrication. Sun *et al.* in 2010 have successfully engineered silver nanoplates on semiconductor wafers at room temperature through a simple galvanic reaction between an aqueous solution of  $\text{AgNO}_3$  and n-type GaAs [20]. From this work, only n-type GaAs as electrons source produce the uniform Ag nanoplates as shown in Figure 2.26A and B. The another p-type GaAs ( Figure 2.26C) not able to generate Ag nanoplates owing to its surface electrons are very strong reductant, therefore the quickly reducing  $\text{Ag}^+$  ions to Ag atoms is normally occurred, which are consequentially coalescence and growth into Ag nanocrystals.

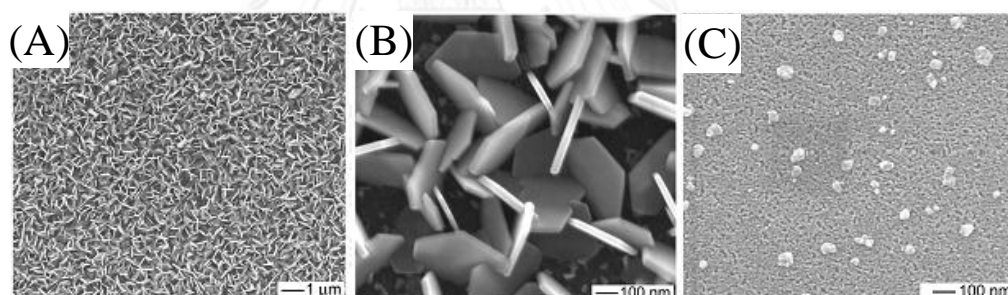


**Figure 2.26** SEM images of Ag nanostructures fabricated on (A, B) an n-type GaAs wafer and (C) a p-type GaAs wafer obtained from reactions of the wafers with a 2 M aqueous  $\text{AgNO}_3$  for 3 minutes in the dark at room temperature [20].

#### 2.4.6 HARD AND SOFT TEMPLATES TECHNIQUES

In order to gain the remarkable shape and size control ability of Ag nanoplates, hard and soft chemical templates are also applied for directing the crystal growth in the synthetic procedure. The carboxylate-functionalized polystyrene

spheres, CTAB, and many kinds of thiol can be served as a template for Ag nanoplates fabrication.

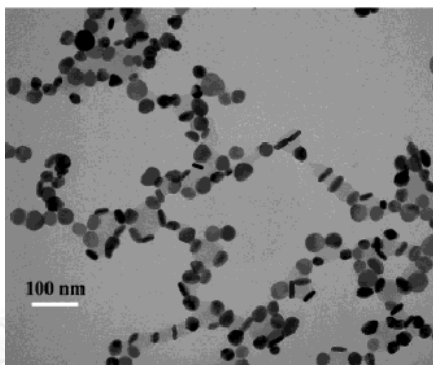


**Figure 2.27** TEM image of Ag nanodisks including with polystyrene after aging for 1 month [16].

With polystyrene spheres, using DMF as both solvent and reducing agent [16] able to produce 90 % of Ag nanodisks with average diameter of 36 nm and of thickness 9 nm (Figure 2.27). Although the capable of precisely morphology controlling, due to difficulty of template removal is limitation for widely application.

#### 2.4.7 SONOCHEMICAL TECHNIQUES

For the intention for minimizing time of reaction, ultra sonic irradiation wave is alternatively assistant techniques using for accelerate the rate of Ag nanoplates formation [21]. Ultrasonic-assisted Ostwald ripening under *N,N*-dimethylformamide solution with the presence of poly(vinylpyrrolidone), selectively crystal growth on different planes engineered plate-like nanostructure of Ag. The increasing of ultrasonic intensity from 55 to 65  $\text{w}/\text{cm}^2$  induced Ag nanoplates growth in average edge length of 120 to 150 nm, respectively (Figure 2.28.).

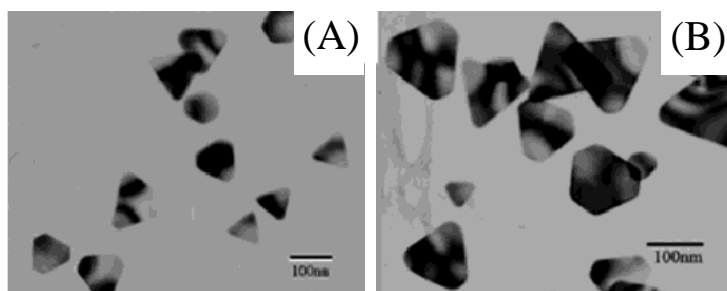


**Figure 2.28** TEM images of the Ag nanoplates prepared under different ultrasonic irradiation intensities: (A)  $55 \text{ W/cm}^2$ , (B)  $65 \text{ W/cm}^2$  [21].

In summary, from all reviews of various techniques for Ag nanoplates fabrication, although the precisely shape and size controllable can be obtained by many techniques, due to the complicate in practically, the requirements of many chemical reagents, low capacity of Ag concentrations, and long period needed of synthetic procedure are the essence drawback of these above techniques. The limitations of applicable in commercial scale caused the wildly utilizations still impossible. Therefore, the further development under the aims of rapid and simple as well as high scale capacity is extremely required. Herein, this research will explored the magic synthetic partway for Ag nanoplates preparation, with high optical property control under simple chemistry but powerfully manipulate the arbitrary color of Ag nanoplates colloid.

## 2.5 REACTION OF HYDROGEN PEROXIDE AND SILVER

Generally,  $\text{H}_2\text{O}_2$  is well known to autocatalytically decompose on the metallic surface such as Pt, Pd, and Ag [68-70]. Interestingly, in the case of silver while oxidatively dissolve silver metal, silver nanoparticles, and silver alloys are informatively described [18, 19, 30], the current operation deliberately uses  $\text{H}_2\text{O}_2$  of

low concentration in order to suppress above activities is still challenge way for chemist that we have given this strategy as a main concept of this work. Behind the strongly oxidative nature of  $\text{H}_2\text{O}_2$ , the weakly reducing capability is also presence. As given below, the standard redox potentials of  $\text{H}_2\text{O}_2$  are known to strongly dependent on pH of the solution [75]. For the reduction potential of Ag and  $\text{H}_2\text{O}_2$  under an acidic condition:



According to Eqs. 2.14 and 2.15, the positive values of the net standard redox potentials indicate that both reactions in a relatively mild acidic medium possible occur. However, the oxidative dissolution is more favored as the potential is more positive. Therefore, the understanding in fundamental electrochemistry is the essence window for exploitation of dual functionalities of  $\text{H}_2\text{O}_2$ .

From the Nernst's equations, the cell potentials at various concentrations of  $\text{Ag}^+$  and  $\text{H}^+$  can be expressed by:

$$E_{\text{cell}}(\text{Ox}) = 0.964 - \frac{RT}{nF} \ln \frac{[\text{Ag}^+]^2}{[\text{H}^+]^2[\text{H}_2\text{O}_2]} = 0.964 - \frac{RT}{nF} \ln \frac{[\text{Ag}^+]}{[\text{H}^+]^2 R} \quad (2.16)$$

$$E_{\text{cell}}(\text{Red}) = 0.104 - \frac{RT}{nF} \ln \frac{[\text{H}^+]^2 p(\text{O}_2)}{[\text{Ag}^+]^2 [\text{H}_2\text{O}_2]} = 0.104 - \frac{RT}{nF} \ln \frac{[\text{H}^+]^2}{[\text{Ag}^+]^3 R} \quad (2.17)$$

$$\Delta E_{\text{cell}} = E_{\text{cell}}(\text{Ox}) - E_{\text{cell}}(\text{Red}) \quad (2.18)$$

The molar ratio  $R$  is defined as  $[\text{H}_2\text{O}_2]:[\text{Ag}^+]$ . The pressure of oxygen gas evolved during the reaction is neglected and set equal to 1 atm. The difference between the oxidation and reduction cell potentials is defined as  $\Delta E_{\text{cell}}$ . Unless stated otherwise, the temperature used for the calculation is constrained at 28 °C. This research, we will thoroughly calculate the reduction potential under the variation of  $\text{H}_2\text{O}_2$  and  $\text{Ag}^+$  concentrations or pH dependent. Then, indicate/confirm the possibility of the dual functions, concerted oxidation/reduction of  $\text{H}_2\text{O}_2$  under catalytic performance of Ag nanocrystals that will be described in the results and discussion section.

## CHAPTER III

### EXPERIMENTAL SECTION

#### 3.1 CHEMICALS AND MATERIALS

Polyvinylpyrrolidone-K30 (PVP,  $(C_6H_9NO)_n$  with average molecular weight of 40,000,  $\geq 99.0\%$ ), trisodium citrate ( $Na_3C_6H_5O_7$ , TSC,  $\geq 99.0\%$ ), sodium borohydride ( $NaBH_4$ , 98.0%), hydrogen peroxide ( $H_2O_2$ , 33.3% w/v or 9.79 M), sodium hydroxide ( $NaOH$ , 99.0%), and silver nitrate ( $AgNO_3$ ,  $\geq 99.0\%$ ) were purchased from Merck®. All chemicals were analytical grade and were used as received without additional purification. De-ionized water was used as a solvent for all synthetic routes.

#### 3.2 FABRICATION OF SILVER NANOPATES FROM SILVER NANOSPHERES

In order to prepare Ag nanoplates with precisely controllable optical properties, silver nanospheres (AgNPs) were firstly synthesized using conventional  $NaBH_4$  reducing agent. To prevent aggregation of AgNPs, PVP and TSC capping agents were also employed in this step. After that, the as-synthesized AgNPs were transformed to silver nanoplates (AgNPLs) using  $H_2O_2$ . In our procedure,  $H_2O_2$  acts as both oxidizing agent and reducing agent. To precisely utilize dual function of  $H_2O_2$ , the colloid of AgNPs should be cleaned without any other oxidizing/reducing agent.

Therefore, the synthesis of AgNPs using  $NaBH_4$  as reducing agent must be optimized.  $Ag^+$  and  $NaBH_4$  must not remain in the AgNPs colloid because  $H_2O_2$  can be decomposed by these two species, and then the transformation of AgNPs to AgNPLs can be inhibited.

### 3.2.1 OPTIMIZATION OF $[\text{NaBH}_4]/[\text{AgNO}_3]$ MOLAR RATIO

The sufficient mole ratio of  $[\text{NaBH}_4]/[\text{AgNO}_3]$  was investigated by direct reduction of  $\text{AgNO}_3$  using  $\text{NaBH}_4$ . This investigation was done in the cuvette cell. Experimentally, 2 mL of 0.116 mM  $\text{AgNO}_3$  stabilized with 0.45 mM of PVP-K30 was reduced by stepwise addition 5.3  $\mu\text{L}$  of 6.87 mM  $\text{NaBH}_4$ . The reduction ability of  $\text{NaBH}_4$  was monitored by UV-visible spectroscopy. The 400-nm characteristic extinction of AgNPs was post-recorded for every  $\text{NaBH}_4$  addition. Finally, the appropriate mole ratio of  $[\text{NaBH}_4]/[\text{AgNO}_3]$  was then explored by plotting the intensity at extinction maxima (around 400 nm) against the  $\text{NaBH}_4$  concentration.

### 3.2.2 PREPARATION OF SILVER NANOSPHERES

The optimal  $[\text{NaBH}_4]/[\text{AgNO}_3]$  molar ratio of 1.414 was obtained from the procedure in 3.2.1. This ratio was applied for all AgNP preparations. In this research, four types of AgNPs colloid synthesized by a  $\text{NaBH}_4$ -reduction were: (A) non-stabilized, (B) 5.6 mM PVP-stabilized, (C) 0.1 mM TSC-stabilized, and (D) 5.6 and 0.1 mM of PVP/TSC-stabilized AgNPs. Briefly, a solution of  $\text{AgNO}_3$  (0.232 mM, 200 mL), with and without an addition of TSC and/or PVP was mixed under a vigorous stir for 15 minutes. Then, 973  $\mu\text{L}$  of 68.7 mM  $\text{NaBH}_4$  was added in to this solution to reduce and generate AgNPs. The yellow colloids of as-synthesized AgNPs were aged for 1 h in order to ensure a complete decomposition of  $\text{NaBH}_4$  before the shape transformation process.



### 3.2.3 SHAPE TRANSFORMATION OF SILVER NANOSPHERES TO SILVER NANOPLATES

The shape transformation of AgNSs to AgNPLs was simply accomplished by adding an exactly pre-determined volume of  $\text{H}_2\text{O}_2$  solution (979 mM, 0 – 379  $\mu\text{L}$ ) into a 20 mL of original AgNP colloid under a vigorous stir. A desired mole ratio of  $[\text{H}_2\text{O}_2]/[\text{AgNO}_3]$ , defined as R, was achieved by adjusting the volume of  $\text{H}_2\text{O}_2$  solution.

For the PVP stabilized AgNP system with mole ratio (R) of 65, after an addition of  $\text{H}_2\text{O}_2$ , series of color changes from yellow to red, pink, purple, blue, and magenta was visually observed (Figure 3.1). The color change indicates the decomposition of AgNSs with a concomitant formation and growth of AgNPLs. The reaction was spontaneous and completed within 2 minutes.



**Figure 3.1** Systematic color change after an addition of  $\text{H}_2\text{O}_2$  in to PVP stabilized AgNPs colloid (R = 65) indicates shape transformation of AgNPs to AgNPLs.

For the TSC stabilized system, after an injection of  $\text{H}_2\text{O}_2$  in to original AgNPs colloid, a fade-off of yellow color of AgNPs was observed (Figure 3.2). This phenomenon indicates the oxidatively dissolution of AgNPs.

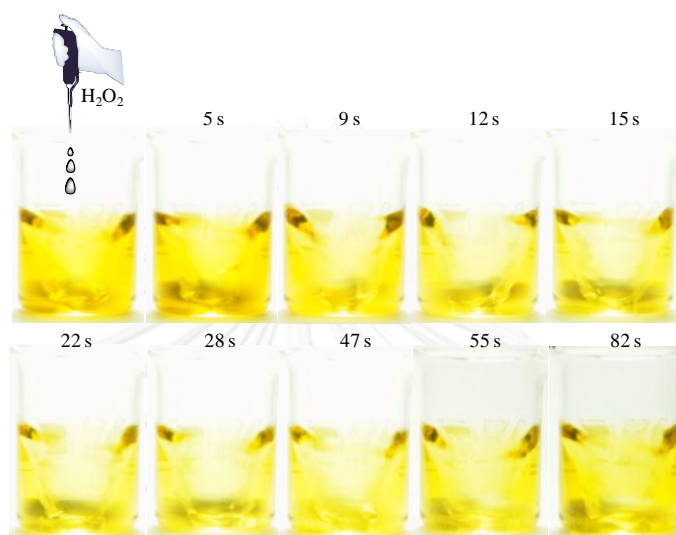


**Figure 3.2** Fade-off of yellow colloidal AgNPs after an addition of  $\text{H}_2\text{O}_2$  in to TSC stabilized AgNPs colloid ( $R = 65$ ) indicates oxidatively dissolved of AgNPs.

### 3.2.4 STRUCTURAL EVOLUTION OF SILVER NANOSPHERES TO SILVER NANOPLATES UNDER DIFFERENT STABILIZATIONS

In order to understand the mechanism of shape transformation of AgNPs to AgNPLs under different stabilizations, time dependent of surface plasmon resonance changes were observed. This experimental section, all reactions were done in the cuvette cell. Firstly, the 2.00 mL of 0.116 mM of AgNPs with 0.45 mM PVP stabilization was introduced in the cuvette cell, and then the original spectrum of AgNPs was recorded. Subsequently, the 62  $\mu\text{L}$  of 0.097 M  $\text{H}_2\text{O}_2$  was rapidly injected in to the original AgNPs colloid, and follow closely by shaking and measurement of the

extinction spectrum within 10 s. The changes of surface plasmon resonance were recorded every 10 s intervals.

### 3.3 FABRICATION OF SILVER NANOPlates/NANOSHEETS FROM SILVER OXIDE

Silver oxide ( $\text{Ag}_2\text{O}$ ) was also used as a silver source to produce AgNPLs/AgNSHs. Firstly,  $\text{Ag}_2\text{O}$  was prepared by mixing 2.00 mL of 927 mM  $\text{AgNO}_3$ , 195.5 mL of DI water, and 2.00 mL of 450 mM PVP-K30 under a vigorous stir. Then,  $\text{Ag}_2\text{O}$  was generated by pH adjustment. This study, we have focusing on the utilization of pH8  $\text{Ag}_2\text{O}$  colloid. To produce the pH8 of PVP stabilized  $\text{Ag}_2\text{O}$  colloid, 0.5 mL of 0.5 M NaOH was introduced into the initial pH4 of PVP stabilized  $\text{AgNO}_3$  solution. As shown in Figure 3.3, after an addition of NaOH, the milky yellow of PVP stabilized  $\text{Ag}_2\text{O}$  colloid was obtained.

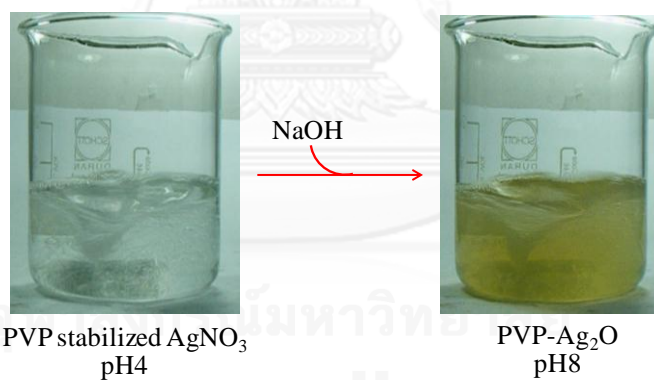


**Figure 3.3** Preparation of PVP stabilized  $\text{Ag}_2\text{O}$ .

For the AgNPLs/AgNSHs fabrication step, 20 mL of PVP stabilized  $\text{Ag}_2\text{O}$  colloid was stirred vigorously. Then, exactly pre-determined volume of  $\text{H}_2\text{O}_2$  solution was rapidly injected in to this colloid. The volume of used  $\text{H}_2\text{O}_2$  was calculated by molar ratio of  $[\text{H}_2\text{O}_2]/[\text{AgNO}_3]$ , defined as R. We have investigated the effect of both mole ratio of  $[\text{H}_2\text{O}_2]/[\text{Ag}_2\text{O}]$  and PVP contents systemically.

### 3.4 IN-SITU SYNTHESIS OF SILVER NANOPlates/NANOSHEETS WITHOUT STABILIZATION

In this study, naked silver nanoplates/nanosheets were also synthesized by in-situ method. The 6.6 mM NaBH<sub>4</sub> solution was prepared by dissolving 0.025 g of NaBH<sub>4</sub> in 100 mL of DI water. Then 10 mL of this solution was diluted and adjusted volume to 20 mL with DI water to make a 3.3 mM NaBH<sub>4</sub> (Fraction I). Fraction II solution of 2.3 mM AgNO<sub>3</sub> and 0.35 M H<sub>2</sub>O<sub>2</sub> was prepared by mixing of 50 μL of 927 mM AgNO<sub>3</sub> (100,000 ppm) and 700 μL of 9.79 M H<sub>2</sub>O<sub>2</sub> (33.3 % wt/v), then adjusted volume to 20 mL by DI water. Both of Fraction I and II were stirred vigorously for 5 minutes. Then rapidly added Fraction II into Fraction I and stirred for 2 minutes, silver nanoplates/nanosheets were fabricated. The effects of AgNO<sub>3</sub>, H<sub>2</sub>O<sub>2</sub>, and NaBH<sub>4</sub> concentrations on Ag nanoplates/nanosheets formation were investigated.

### 3.5 CHARACTERIZATIONS

The characteristics of as-synthesized AgNPs, AgNPLs, AgNPSHs, and Ag<sub>2</sub>O were investigated by various following techniques.

#### 3.5.1 UV-VISIBLE SPECTROSCOPY

All UV-visible spectra were recorded using portable UV-visible spectrometer (Ocean Optics, Inc. –USB2000) with a light source of Deuterium lamp (Mikropack. –DH2000). All colloid samples were prepared at 0.116 mM (10 ppm) of [Ag] samples. The quartz cuvette was pre-treated by concentrated nitric acid (HNO<sub>3</sub>), and then rinsed by de-ionized water before operation. The de-ionized water was also used as reference throughout all experiments.

### 3.5.2 SCANNING ELECTRON MICROSCOPY

Scanning electron microscopy (SEM) micrographs were taken using JELO 6500A (analytical electron microscope) at 5-30 kV under high vacuum mode, using a secondary electron imaging (SEI) detector. To prepared SEM samples, AgNPLs, AgNShs, and Ag<sub>2</sub>O were cleaned up by centrifugation for at least three times. These precipitated samples were transferred to carbon tape which was deposited on aluminum stub.

### 3.5.3 TRANSMISSION ELECTRON MICROSCOPY

For TEM samples preparation, the as-synthesized AgNPLs colloids were dropped directly on carbon coated Formvar grid. After drying samples overnight, TEM images were collected by operating Hitachi/S-4800 transmission electron microscope at 100 kV.

### 3.5.4 X-RAY DIFFERATION TECHNIQUE

Concentrated and cleaned AgNPLs/AgNPLs were dropped on glass sample holder. Then, the XRD pattern was collected using a Rigaku D/MAX-2200 instrument (Cu K $\alpha$ 1 radiation) at 50 kV and 250 mA with a range of 30-90 degree by step scanning with a 0.02 step size.

## CHAPTER IV

### RESULTS AND DISCUSSION

#### 4.1 OPTIMIZATION OF APPROPRIATE $[\text{NaBH}_4]/[\text{AgNO}_3]$ MOLAR RATIO

Since, the aim of this research is to exploit the concerted oxidation/reduction of  $\text{H}_2\text{O}_2$ . Therefore, the well-cleaned system without contamination of others reductant or oxidant is required. The conventional reduction system, the appropriate molar ratio of  $[\text{NaBH}_4]/[\text{AgNO}_3]$  was examined to ensure that  $\text{NaBH}_4$  is not remain in the original colloid, and muffled to the growth mechanism.

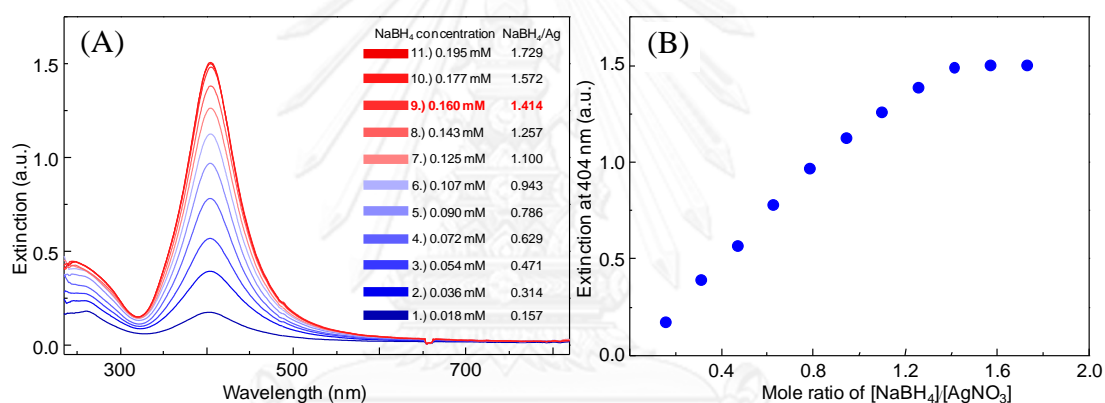


**Figure 4.1** (A) UV-visible spectra of PVP-AgNPs synthesized by different molar ratio of  $[\text{NaBH}_4]/[\text{AgNO}_3]$ . (B) Plotted of  $[\text{NaBH}_4]/[\text{AgNO}_3]$  molar ratio against the maximum extinction at 404 nm.

Practically,  $\text{Ag}^+$  ion from  $\text{AgNO}_3$  was reduced by  $\text{NaBH}_4$  directly with PVP stabilization. The amount of AgNPs was investigated by recording the maximum extinction at 404 nm. Figure 4.1 shows the surface plasmon resonance of PVP-AgNPs colloid in various concentration of  $\text{NaBH}_4$  (different molar ratio of  $[\text{NaBH}_4]/[\text{AgNO}_3]$ ). When the concentration of  $\text{NaBH}_4$  increased from 0.018 mM to 0.160 mM, the maximum extinction at 404 nm dramatically rose linearly. Until the

concentration of  $\text{NaBH}_4$  increased continuously from 0.160 mM to 0.195 mM, the maximum extinction at 404 nm was still unchanged. Therefore, the appropriate  $\text{NaBH}_4$  concentration in this study was 0.160 mM which corresponded to  $[\text{NaBH}_4]/[\text{AgNO}_3]$  molar ratio of 1.414. This sufficient molar ratio of  $[\text{NaBH}_4]/[\text{AgNO}_3]$  will be applied for all conventional  $\text{NaBH}_4$  reduction systems.

#### 4.2 FABRICATION OF SILVER NANOPLATES BY USING NON-STABILIZED SILVER NANOSPHERES

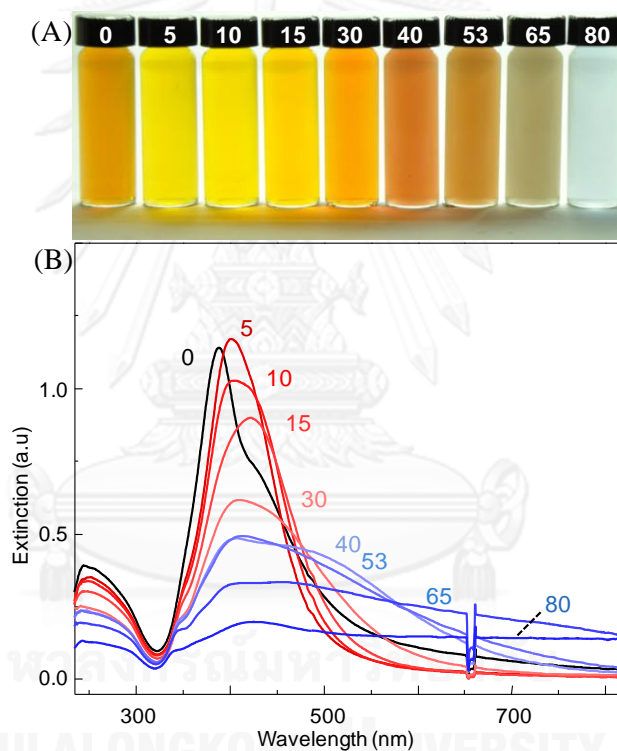


**Figure 4.2** (A) Colloidal products of AgNPs/AgNPLs synthesized by using a non-stabilized AgNPs as a silver source under different molar ratio of  $[\text{H}_2\text{O}_2]/[\text{AgNO}_3]$ . (B) Corresponding UV-visible spectra of the as-synthesized AgNPs/AgNPLs of (A).

The non-stabilized Ag nanoparticles is applied as a Ag source for shape transformation process. R value represents the molar ratios of  $[H_2O_2]/[AgNO_3]$ . Figure 4.2A illustrates the brownish yellow color due to the aggregation of original nAgNPs colloid ( $R=0$ ). This behavior of aggregated AgNPs is confirmed again by the corresponding of dipole plasmon resonance (DPR) at 395 nm with a shoulder at  $\sim 440$  nm (black line) as shown in Figure 4.2B.

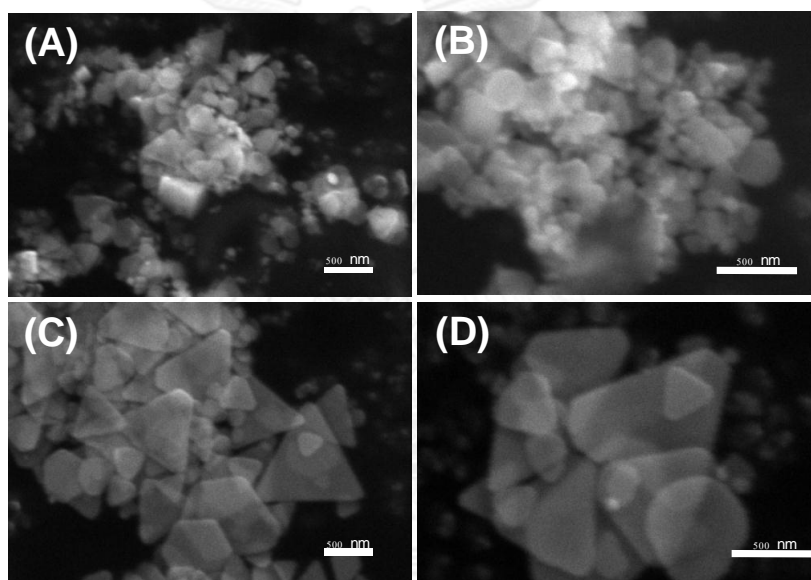


**Figure 4.3** SEM micrographs of AgNPs synthesized by using nAgNPs as a silver source under  $[H_2O_2]/[AgNO_3]$  molar ratio of (A and B) 65 and (C and D) 80.

After an addition of  $H_2O_2$  with a molar ratio R of 5, a slightly increase of the extinction with a redshift of the DPR together with a disappearance of the shoulder indicated a disintegration of the aggregated nAgNPs. When increasing the molar ratio R, the redshift of the in-plane dipole plasmon resonance (ipDPR) with a gradual development of the out-of-plane quadrupole plasmon resonance (opQPR) at



340 nm indicated a formation of plate-like nanostructures. The systematic decreased in the extinction at 400 nm indicated a dissolution of nAgNPs. With the molar ratio R of 80, the colloid contains with AgNPLs and large AgNPs as indicated by the UV-visible spectrum and SEM micrographs as shown in Figure 4.3. The systematic spectral changes and the development of nanoplates signify an evolution of nanostructures induced by the concerted oxidation/reduction of  $H_2O_2$ . However, due to an absence of a stabilizer, the structural change is heavily interfered by aggregation of newly formed nanoplates.

#### **4.3 FABRICATION OF SILVER NANOPLATES BY USING POLYVINYL-PYRROLIDONE (PVP) STABILIZED SILVER NANOSPHERES**

In the case of PVP-stabilized AgNPs, after an addition of  $H_2O_2$  in Figure 4.4A, a systematic color change of the colloid from yellow to orange, red, purple, blue, and magenta depending on the amount of added  $H_2O_2$  is observed. Figure 4.4B illustrates surface plasmon resonance spectra of correspondence colloidal AgNPLs. For Figure 4.4A, at the molar ratio R of 5, a ~10% decrease of plasmon extinction with a slight redshift of the DPR from 402 nm to 406 nm without any development of a new nanostructure indicated a dissolution of small AgNPs. With the molar ratio R of 10, a ~30% drop of the plasmon extinction with a development of shoulders at 340 and 500 nm signify an early formation of AgNPLs. As the molar ratio R is increased to 15, the orange colloid showed a 50% extinction drop of the 402 nm DPR with an appearance of the 500 nm ipDPR of AgNPLs. The extinction of the 500 nm ipDPR reached the maximum with a disappearance of the AgNPs as the molar ratio R became 30. The isosbestic point at 450 nm indicates that AgNPLs with the ipDPR at 500 nm are developed with the expense of the AgNPs.

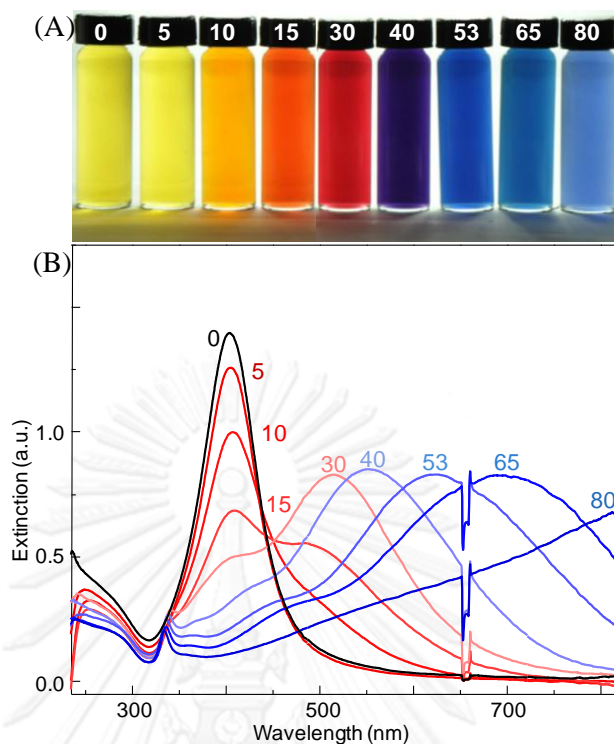


**Figure 4.4** (A) Colloidal products of AgNPs/AgNPLs synthesized by using a PVP stabilized AgNPs as a silver source under different molar ratio of  $[H_2O_2]/[AgNO_3]$ . (B) Corresponding UV-visible spectra of the as synthesized AgNPs/AgNPLs of (A).

A further increasing of  $H_2O_2$  with the molar ratio  $R$  of 40, 53, and 65, respectively, induce the formation of larger AgNPLs as the ipDPR redshifted to 554, 625, and 700 nm while the opQPR blueshifted from 340 nm to 339, 337, and 336 nm. At the molar ratio  $R$  of 40, 53, and 65, respectively, induce the formation of larger AgNPLs as the ipDPR redshifted to 554, 625, and 700 nm while the opQPR blueshifted from 340 nm to 339, 337, and 336 nm. At the molar ratio  $R$  of 80, the ipDPR shifts into the NIR region with a resonance wavelength greater than 825 nm. When a relatively high molar ratio  $R$  is employed (i. e.,  $R = 500$  in Figure 4.5), AgNPs is oxidatively dissolved without any formation of AgNPLs. Therefore, just sufficient molar ratio of  $[H_2O_2]/[AgNO_3]$  and relatively low of

initial  $\text{H}_2\text{O}_2$  concentration are required for the shape transformation of AgNPs to AgNPLs. The appropriate range of R number in this study is 10 to 80.

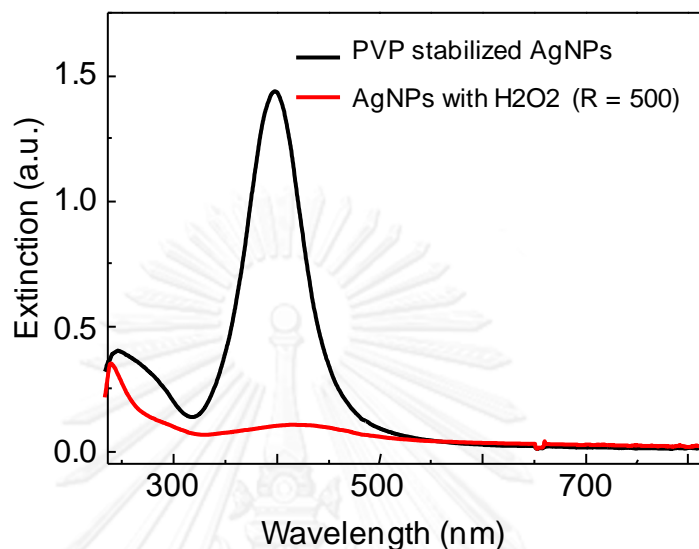


**Figure 4.5** UV-visible spectra show the over oxidatively dissolution of PVP-AgNPs when the molar ratio of R = 500 is employed.

To gain an insight understanding on the role of PVP in the shape transformation process, we have also investigated the role of PVP contents. In this study, the R number of 65 is applied through different stabilizations of PVP. In Fig. 4.6a, UV-visible spectra of the original PVP-stabilized AgNPs showed the influence of steric stabilization and PVP- $\text{Ag}^+$  complex on particles size. A prolong reduction period of PVP stabilized silver ions [25] together with the formation of non-reductive borate species in water [76] decreased the reduction efficiency of  $\text{NaBH}_4$ . Since a relatively low molar ratio  $[\text{NaBH}_4]/[\text{AgNO}_3]$  of 1.414 is employed, the stabilized silver ions may not be utterly reduced. As a result, a colloid of AgNPs of a larger particle size with greater residual silver ions is obtained at a higher concentration of PVP as indicated

by a greater redshift and a broader DPR with lower of the maximum plasmon extinction.

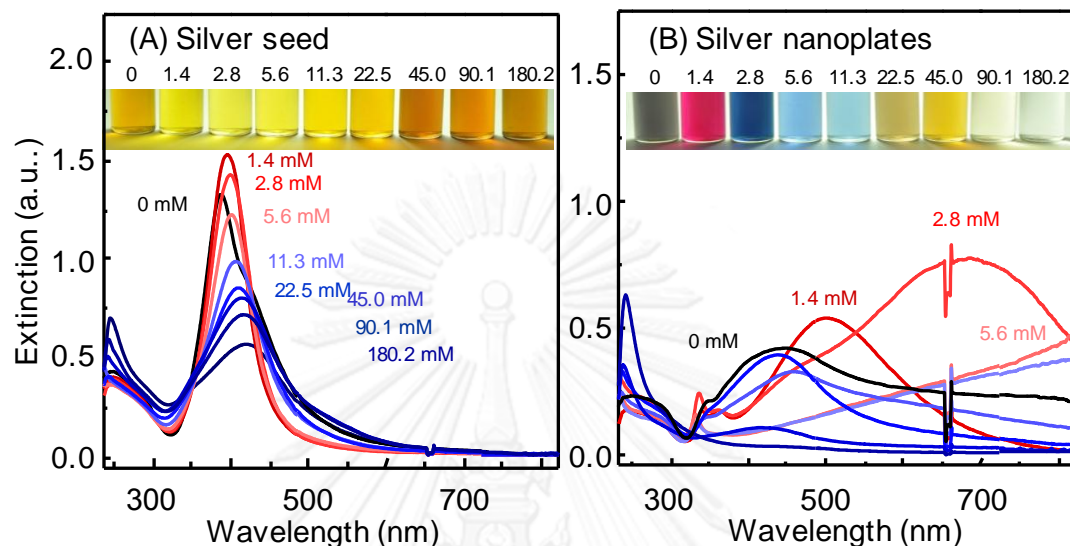


**Figure 4.6** UV-visible spectra of PVP-stabilized colloid of AgNPs (A) before and (B) after an addition of  $\text{H}_2\text{O}_2$  with a molar ratio  $R$  of 65. The colloids were stabilized by 0, 1.4, 2.8, 5.6, 11, 22, 45, 90, and 180 mM PVP.

In Figure 4.6B, AgNPs without PVP stabilization are not transformed to AgNPLs after an addition of  $\text{H}_2\text{O}_2$ . For the colloid with a low concentration of PVP (1.4 and 2.8 mM), AgNPs were converted to AgNPLs as indicated by the disappearance of the DPR at 400 nm with a concomitant development of new ipDPR at 500 and 675 nm. The structural evolutions were visually observed by the color changes from yellow to red and blue colloids. When the concentration of PVP was increased to 5.6 and 11.3 mM, large nanoplates with ipDPR in the NIR region were obtained as indicated by the resonance wavelength greater than 825 nm of the magenta colloids. The observed phenomena confirm an important role of PVP as the steric stabilizer promoting the formation and growth of AgNPLs by selectively binding on the Ag{100}

facet of the plates [35]. PVP also stabilizes  $\text{Ag}^+$  by forming inter- and intra-chain PVP- $\text{Ag}^+$  complex with lower reduction potential compared to that of  $\text{Ag}^+$ . The complex bound  $\text{Ag}^+$  at the  $\text{Ag}\{100\}$  facet was easily reduced [77].

However, a higher concentration of PVP, i.e., 22–90 mM, provided an excessive stabilization and complexation with silver ion that led to an inhibition of shape transformation process. PVP of high concentration hinders the reduction of  $\text{Ag}$  ions at the edge of the nanoplates as its abundance promotes a uniform distribution of silver ions in the solution. At the PVP concentration of 180 mM, the disappearance of the DPR at  $\sim 400$  nm without a development of a new ipDPR indicated a complete dissolution of AgNPs after the  $\text{H}_2\text{O}_2$  treatment. The oxidatively dissolved silver ions were not reduced by  $\text{H}_2\text{O}_2$  as they were efficiently stabilized and complexed by the concentrated PVP. Moreover, PVP is known to form a stable complex with  $\text{H}_2\text{O}_2$  even in the solid form [66]. As a result, reduction of the oxidatively generated silver ions by  $\text{H}_2\text{O}_2$  did not occur at high concentration of PVP.

The above phenomena indicated that PVP promoted  $\text{H}_2\text{O}_2$ -induced shape transformation of AgNPs to AgNPLs. As a result, the optical property of obtained AgNPLs can be selectively tuned by manipulating both  $\text{H}_2\text{O}_2$  and PVP contents. Further study is selectively fabrication of desired optical activity of AgNPLs by parallel adjusting of  $\text{H}_2\text{O}_2$  and PVP contents. The observed results confirm again that AgNPLs with selectively tuned surface plasmon resonance across the visible region could be selectively fabricated by controlling the concentrations of  $\text{H}_2\text{O}_2$  and PVP. As shown in Figure 4.7., larger AgNPLs with a greater redshift of the ipDPR are obtained by increasing the concentration of  $\text{H}_2\text{O}_2$ . AgNPLs with a low concentration of

PVP required a greater amount of  $\text{H}_2\text{O}_2$  to produce AgNPLs of the same ipDPR as those with a greater concentration of PVP.

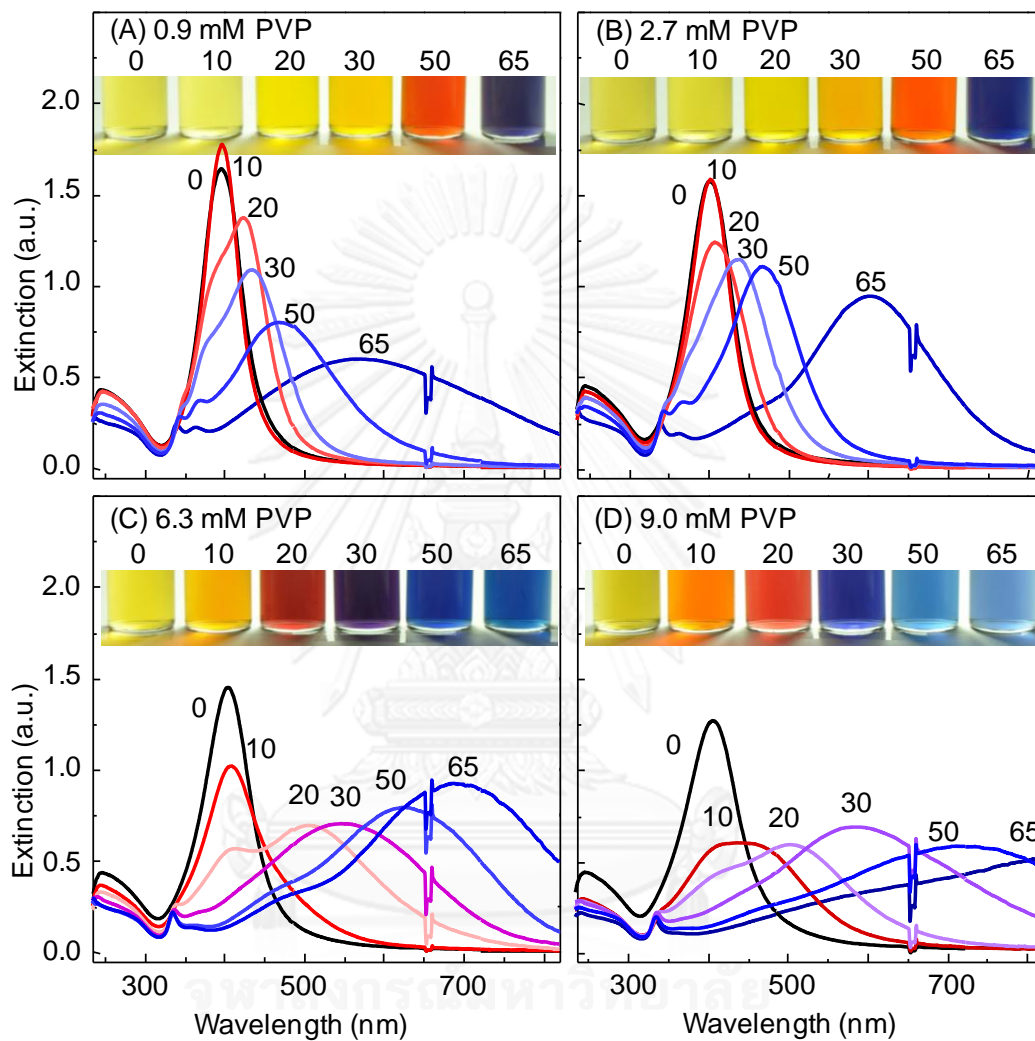


**Figure 4.7** UV-visible spectra of AgNPLs colloids obtained after a  $\text{H}_2\text{O}_2$ -induced shape transformation of AgNPs (0.232 mM) with various PVP concentrations: (A) 0.9 mM, (B) 2.7 mM, (C) 6.3 mM, and (D) 9.0 mM. The AgNPLs colloids were transformed by  $\text{H}_2\text{O}_2$  with molar ratios  $R$  of 10, 20, 30, 50, and 65. The black lines are spectra of the original colloids of AgNPs.

For example, AgNPs with 2.7 mM PVP required  $H_2O_2$  with a molar ratio R of 65 to produce AgNPs with an ipDPR at 600 nm while those with 6.3 and 9.0 mM PVP needed only  $H_2O_2$  with molar ratios R of 50 and 30, respectively. The greater concentration of  $H_2O_2$  was due to an under coverage of silver nanostructures at low concentration of PVP. The exposed area enabled the catalytic decomposition of  $H_2O_2$  without any contribution to the shape transformation. PVP facilitates the formation and growth of AgNPs by the following actions. (1) The steric stabilization of PVP prevents aggregation of newly generated nanoplates. (2) PVP stabilizes silver ions by forming inter- and intra-chain Ag-PVP complex with lower chemical reduction potential compared to that of the free ions. (3) PVP selectively binds onto the Ag{100} facets of AgNPs and promotes lateral growth with an expansion of the Ag{111} facets by facilitating the reduction of Ag-PVP complex bound onto the Ag{100} facets [35, 36].

TEM images in Figure 4.8 corroborate the formation of AgNPs via an addition of  $H_2O_2$  into a colloid of PVP-stabilized AgNPs shown in Figure 4.7C. The original AgNPs with particle size of 8-14 nm were shape-transformed into nanoplates with an average size of 25, 40, 50, 80, and 100 nm, respectively, after the shape transformation with the molar ratios R of 30, 40, 53, 60, and 80. The thickness of the nanoplates was in the range of 10-15 nm. The plates become thinner with a morphological change toward a triangular disk as the molar ratio R was increased. An increment of the aspect ratio of the nanoplates induced a blueshift of the opQPR from 340 nm to 336 nm, as observed in Figure 4.7C.

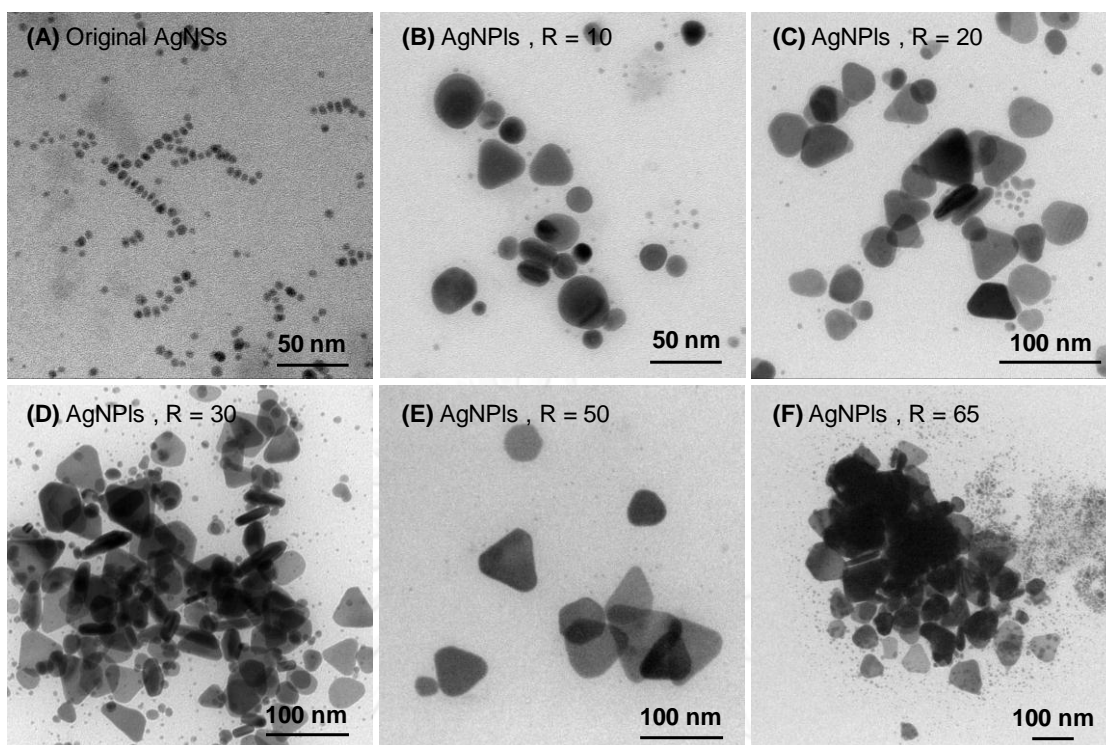


**Figure 4.8** TEM images of (A) AgNPs and AgNPLs of colloids shown in Figure 4.7C with the molar ratio  $R$  of (B) 30, (C) 40, (D) 53, (E) 65, and (F) 80. The scale bars indicate 50 nm (A, B) and 100 nm (C-F).

XRD pattern of AgNPLs in Figure 4.9A shows an intense diffraction with a weak diffraction at  $2\theta$  of  $38.02^\circ$  and  $81.46^\circ$ , respectively, correspond to the (111) and (222) lattice planes of a face-centered cubic (fcc) structure of metallic silver (JCPDS No. 4-0783) [22]. The extremely weak diffraction intensities of (200), (220), and (311) lattice planes indicate that the AgNPLs are dominated by {111} facets, which are preferentially oriented parallel to the surface of glass substrate during XRD acquisition. The six-fold symmetry of the selected area electron diffraction (SAED) spots in Figure 4.9B signifies that the atomically flat {111} facet of the nanoplates oriented normal to the electron beam. The SAED spots of the forbidden  $\frac{1}{3}\{422\}$



plane is normally observed in gold and silver nanostructures bound by atomically flat faces (i.e., nanoplates, nanosheets and nanometers-thin films) [11, 12].

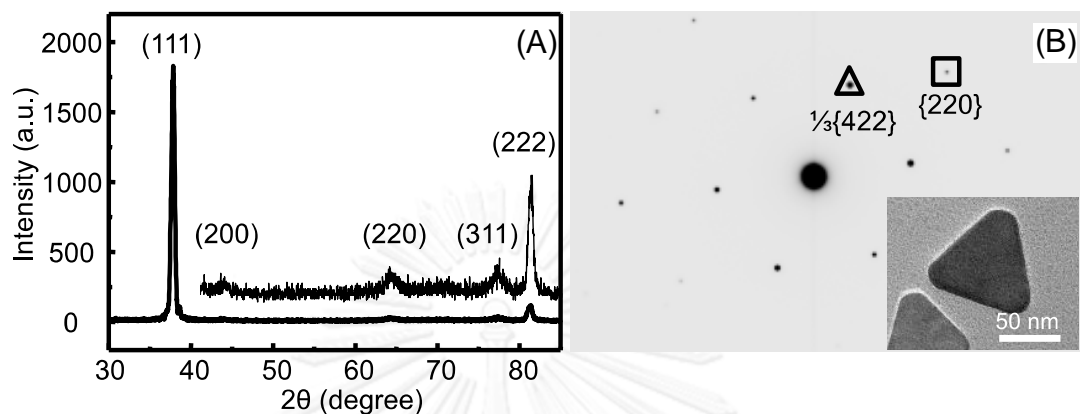


**Figure 4.9** (A) XRD pattern of AgNPLs prepared from the shape transformation of AgNPs and (B) SAED pattern of a selected AgNPLs on a TEM grid.

#### 4.4 FABRICATION OF SILVER NANOPLATES BY USING TRISODIUM CITRATE (TSC) STABILIZED SILVER NANOSPHERES

For the system with TSC stabilization, Figure 4.10, surface plasmon resonance spectrum of shows the DPR at 395 nm with a shoulder at 425 nm indicated an aggregation of small AgNPs in the original TSC-AgNPs colloid. An addition of  $H_2O_2$  induced oxidative dissolution of the TSC-AgNPs since only an extinction drop was observed. At the molar ratio R of 80, a 55% drop of the original extinction with the remaining of a single DPR at  $\sim 425$  nm signified a survival of large AgNPs. Although more than half of the original AgNPs was oxidatively dissolved to silver ions, AgNPLs were not developed as the silver ions form complex with TSC. Under the current operation, TSC inhibits the formation of AgNPLs since the Ag-citrate complex is stable and cannot be reduced by the weakly reducing  $H_2O_2$ .

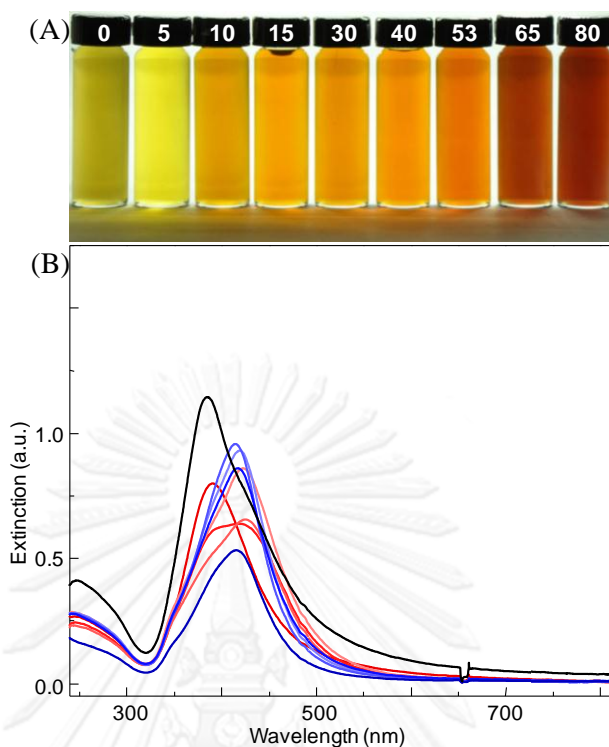


**Figure 4.10** (A) Colloidal products of AgNPs/AgNPLs synthesized by using a TSC-stabilized AgNPs as a silver source under different molar ratio of  $[H_2O_2]/[AgNO_3]$ . (B) Corresponding UV-visible spectra of the as synthesized AgNPs/AgNPLs of (A).

#### 4.5 FABRICATION OF SILVER NANOPlates BY USING PVP- COMBINED TSC-STABILIZED SILVER NANOSPHERES

For AgNPs with PVP/TSC stabilization, Figure 4.11, a development of AgNPLs was not obvious after an addition of  $H_2O_2$ . When  $H_2O_2$  with a molar ratio R of 5 was added, a 40% drop of the 400 nm DPR indicated dissolution of AgNPs without a formation of new nanostructures. There was a sign of an early development of AgNPLs (as indicated by the weak 500 nm ipDPR with a small shoulder of the 340 nm opQPR) when high molar ratios R of 53, 65, and 80 were employed. The development was similar to that with the molar ratio R of 30 in Figure 4.4. However,

the generated silver ions were not utterly reduced as they formed a stable complex with TSC.

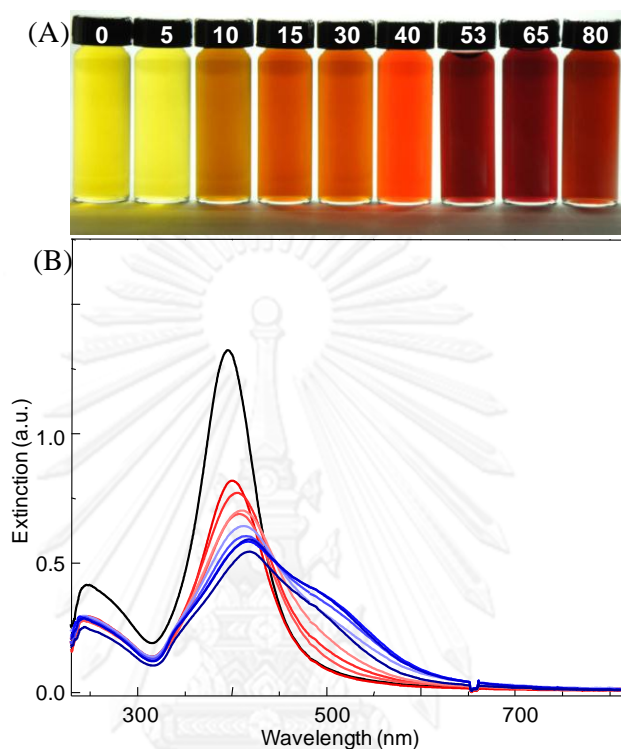


**Figure 4.11** (A) Colloidal products of AgNPs/AgNPLs synthesized by using a TSC combined PVP-stabilized AgNPs as a silver source under different molar ratio of  $[H_2O_2]/[AgNO_3]$ . (B) Corresponding UV-visible spectra of the as synthesized AgNPs/AgNPLs of (A).

#### 4.6 STRUCTURAL EVOLUTION OF SILVER NANOSPHERES TO SILVER NANOPlates UNDER DIFFERENT STABILIZATIONS

The synthetic protocol in this study exploits the concerted oxidation/reduction reactions of  $H_2O_2$  for the fabrication of AgNPLs from the existing AgNPs. By keeping the concentration of  $H_2O_2$  sufficiently low so as to minimize the catalytic decomposition of  $H_2O_2$  as well as the oxidative dissolution of AgNPs while

maintaining the reduction reaction, a kinetic growth of AgNPs could be achieved. A structural transformation of AgNPs to AgNPs upon an addition of  $\text{H}_2\text{O}_2$  was investigated through the time-dependent UV-visible spectra.

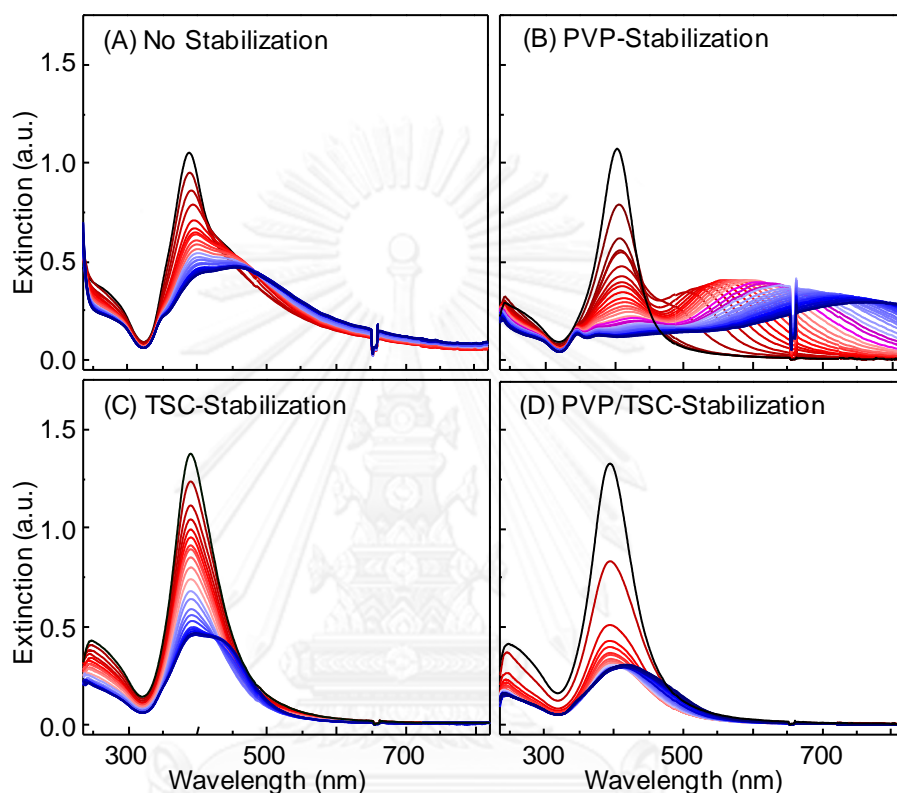


**Figure 4.12** Real-time UV-visible spectral evolution after an addition of  $\text{H}_2\text{O}_2$  into (A) non-stabilized, (B) PVP-stabilized, (C) TSC-stabilized, and (D) TSC/PVP-stabilized colloid of AgNPs. The spectra were recorded for a period of 2 min with a 10 s intervals. The experimental conditions are  $[\text{AgNO}_3] = 0.116 \text{ mM}$ ,  $[\text{H}_2\text{O}_2] = 2.94 \text{ mM}$ ,  $[\text{PVP}] = 2.72 \text{ mM}$ ,  $[\text{TSC}] = 0.05 \text{ mM}$ . The black lines are spectra of the original colloids of AgNPs.

In a system without a stabilizer, Figure 4.12A, a minor structural transformation was attained. Due to an employment of a low mole ration R of 25, an early development of plate structure is noticed by a shoulder at 340 nm of opQPR

and the 470 nm ipDPR. The shape transformation in the PVP-stabilized colloid, Figure 4.12B, is realized by the development of the unique plasmon resonances associated with the nanoplates. The following phenomena confirm the formation and growth of AgNPs. (1) A rapid disappearance of the 400 nm DPR of AgNPs with a concomitant development of the 500 nm with a 275 nm redshift of the ipDPR of AgNPs was spectroscopically detected. (2) A development of the 340 nm opQPR indicates a formation of nanometer thin plates [3, 12]. For the colloids with TSC- and PVP/TSC-stabilizations, Figures 4.12C and 4.12D, respectively, only dissolutions of AgNPs occurred as indicated by a gradual fading of the bright yellow color after an addition of  $H_2O_2$ . A development of AgNPs did not occur as the oxidatively dissolved silver ions rapidly formed a stable Ag-citrate complex.

#### 4.7 FABRICATION OF SILVER NANOPATES/NANOSHEETS FROM SILVER OXIDE

This AgNPs synthetic route was performed in order to confirm the concerted oxidation/reduction of  $H_2O_2$ . As mentioned firstly that the main idea of this research is trying to exploits the dual function of  $H_2O_2$ . In order to explore the unique concertedly  $H_2O_2$  reaction, using  $Ag_2O$  as silver source is capable to describe this hypothesis.

This synthetic route,  $Ag_2O$  was used as a silver source. The role of  $H_2O_2$  was observed under two main parameters, molar ratio of  $[H_2O_2]/[AgNO_3]$  and initial concentration of used  $H_2O_2$ . Figure 4.13, illustrates the UV-visible spectra and SEM micrographs of  $Ag_2O$  and the mixed AgNPs synthesized by employing the 0.0979 M of initial  $H_2O_2$ . The sign of two dimensional Ag nanostructures does not occur in this range of R value. Figure 4.13A shows characteristic peak of  $Ag_2O$  around 250-300 nm.

SEM images illustrate aggregated particles of average size around 100 nm. By varying the molar ratio of  $[\text{H}_2\text{O}_2]/[\text{AgNO}_3]$  from 0 to 1, the results indicate the formation of AgNPs. Figure 4.13B1 shows the shoulder of  $\text{Ag}_2\text{O}$  characteristic peak around 300 to 700 nm. Figure 4.13B2 and 4.13B3 confirm the development of Ag nanosheets with diameter around 200-800 nm. This result demonstrates the formation of large AgNPs at the initial of reaction.

Figure 4.13C demonstrates the formation of AgNPs clearly. The intra-band of UV-visible spectrum at 320 nm confirms the occurring of AgNPs [42]. The broad ipDPR peak about 350-750 indicates the wildly size distribution of AgNPs. When the molar ratios of  $[\text{H}_2\text{O}_2]/[\text{AgNO}_3]$  was increased to 0.5 as shown in Figure 4.13D, the blueshift and narrow of ipDPR peak around 450 represents a disaggregated of small AgNPs. SEM micrographs display average size of AgNPs about 50 nm. Figure 4.13E indicates growth of AgNPs in to a longer wavelength, with broadly ipDPR around 500 nm and SEM micrographs show average size of AgNPs about 80 nm.

By employing the 0.979 M of initial  $\text{H}_2\text{O}_2$  and varying the molar ratio of  $[\text{H}_2\text{O}_2]/[\text{Ag}_2\text{O}]$  from 2 to 10. Figure 4.14A represents the results of R molar ratio of 2. The SPR spectrum of AgNPs with the iPDR at 460 nm and SEM micrographs of average diameter of AgNPs about 50 nm were observed. Similarly with Figure 4.14B, the  $[\text{H}_2\text{O}_2]/[\text{AgNO}_3]$  molar ratio of 3 shows the unchanged SPR spectrum with the iPDR at 460 nm, occurrences of baseline shift from 700 nm in the longer wavelength indicates an increasing of colloidal turbidity. SEM micrographs in Figure 4.14B2 and 4.14B3 show the signature of Ag plate-liked nanostructure. The obtained two

dimensional Ag nanostructures is truncated and irregular shape with diameter around 200-400 nm.

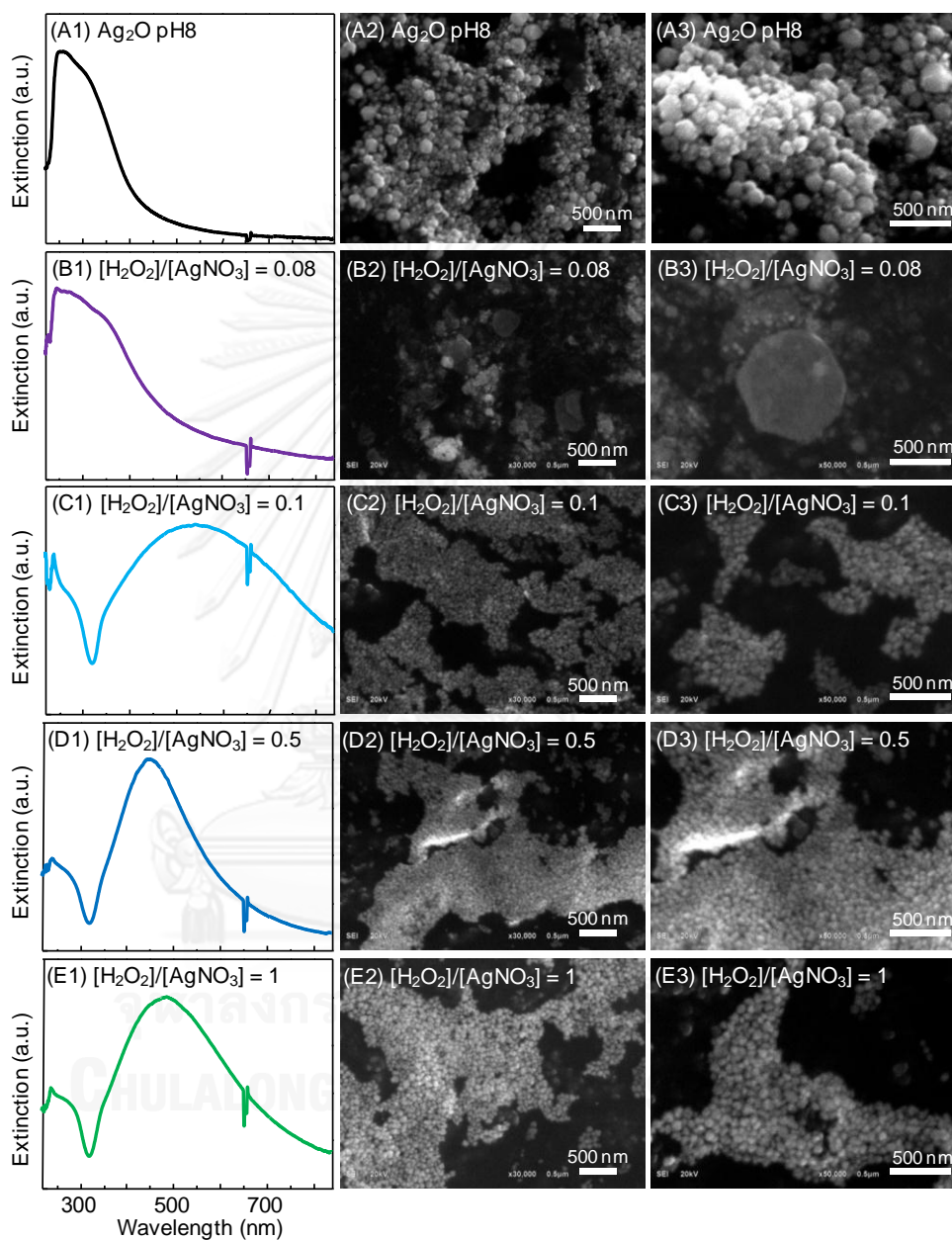


**Figure 4.13** UV-visible spectra and SEM micrographs of (A) 4.5 mM PVP stabilized  $\text{Ag}_2\text{O}$  (PVP- $\text{Ag}_2\text{O}$ ) of pH8, and (B-E) AgNPs synthesized by using PVP- $\text{Ag}_2\text{O}$  of (A) as a silver source, initial concentration of  $\text{H}_2\text{O}_2$  equal to 0.0979 M, and vary molar ratios  $[\text{H}_2\text{O}_2]/[\text{AgNO}_3]$  in the range of 0.08-1.

According to the most population of obtained colloid is AgNPs with average size 50 nm, lead to disappear of characteristic of plate-like Ag nanostructure in the UV-visible spectrum.

When the molar ratio of  $[\text{H}_2\text{O}_2]/[\text{AgNO}_3]$  was increased to 4 as shown in Figure 4.14C, the characteristic opQPR at 335 nm of Ag plate-like nanostructures appears obviously. The decreasing of ipDPR of 50-nm AgNPs at 460 nm concomitant with base line shift in the longer wavelength indicates the formation of larger Ag nanoplates were expanded by smaller AgNPs. SEM micrographs as shown in Figure 4.14C2 and 4.14C3 confirm the occurrence of truncated triangular, hexagonal, and mixed irregular shape Ag nanoplates with edge length around 200-500 nm. Small amount of AgNPs still appears in this sample contribute to the ipDPR at 460 nm in as shown Figure 4.14C1.

From Figure 4.14D, when the molar ratio of  $[\text{H}_2\text{O}_2]/[\text{AgNO}_3]$  was increased to 6, appearance of strongly opQPR at 335 nm and base line shift in to the NIR region indicate the formation of large plate-like Ag nanostructures. SEM micrographs as shown in Figure 4.14D2 and 4.14D3 illustrate complete triangular, hexagonal, and mixed irregular shape of Ag nanoplates with edge length around 200-1,000 nm. For increasing the molar ratio of  $[\text{H}_2\text{O}_2]/[\text{AgNO}_3]$  to 10 as shown in Figure 4.14E, the decreasing of opQPR at 335 nm indicates a drop of AgNPs aspect ratio. This phenomenon may be caused by the increasing of growth rate on (111) facets is more than those of (100) facets when the concerted oxidation/reduction period of  $\text{H}_2\text{O}_2$  was extended.



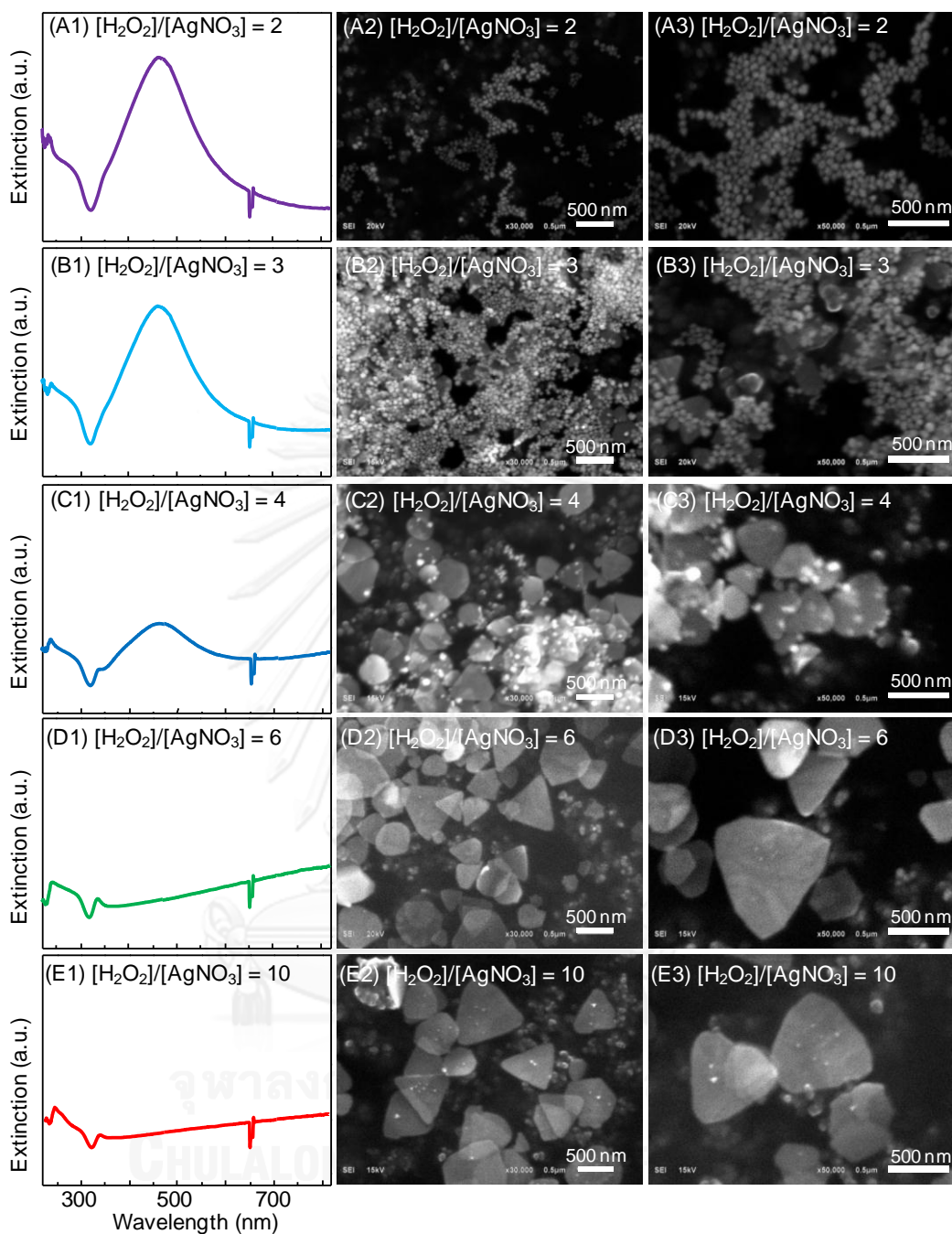


**Figure 4.14** UV-visible spectra and SEM micrographs of (A) 4.5 mM PVP stabilized  $\text{Ag}_2\text{O}$  (PVP- $\text{Ag}_2\text{O}$ ) of pH8, and (B-E) AgNPs synthesized by using PVP- $\text{Ag}_2\text{O}$  of (A) as a silver source, initial concentration of  $\text{H}_2\text{O}_2$  equal to 0.979 M, and vary molar ratios of  $[\text{H}_2\text{O}_2]/[\text{AgNO}_3]$  in the range of 2-10.

By employing the 9.79 M of initial  $\text{H}_2\text{O}_2$  and varying the molar ratios of  $[\text{H}_2\text{O}_2]/[\text{AgNO}_3]$  from 20 to 100, results were shown in Figure 4.15. The utilization of high  $\text{H}_2\text{O}_2$  amounts show the small sharp peak at 220 nm presents the nature of remained  $\text{H}_2\text{O}_2$  in the system [18, 19]. When the molar ratio  $[\text{H}_2\text{O}_2]/[\text{AgNO}_3]$  of 20 was applied, Figure 4.15A1 shows the broadly and small opQPR at 340 nm represents a mixture of low aspect ratio of AgNPLs. SEM micrographs in Figure 4.15A2 and 4.15A3 illustrate the uncompleted AgNPLs. A grain boundary on the large AgNPLs surface implies plates growth was involved by self-assembly of small 200-nm AgNPLs. The size distribution is very broad in the range of 200-1,000 nm. When the molar ratio of  $[\text{H}_2\text{O}_2]/[\text{AgNO}_3]$  was reached to 40, in Figure 4.15B, the opQPR at 340 nm almost disappears. This result indicates the small aspect ratio, increasing in thickness when lateral size still unchanged. This phenomenon could be caused by rapidly increasing of growth rate on (111) facets while the growth on (100) is limited. SEM micrographs illustrate the destructive of large AgNPLs generates the small AgNPs and the thick hexagonal AgNPLs. The obtained hexagonal AgNPLs contains edge length in the range of 200-500 nm. When the molar ratio  $[\text{H}_2\text{O}_2]/[\text{AgNO}_3]$  of 50 was applied, Figure 4.15C, almost disappear of opQPR at 335 nm concomitant with occurring of broadly ipDPR from 400 to 800 nm indicate the formation of thick and broad size distribution of AgNPLs. As shown in Figure 4.15C2 and 4.15C3, the obtained Ag nanostructures are mixture of hexagonal AgNPLs with broadly edge length from 100 to 500 nm and the 100-nm AgNPs. Figure 4.15D and 4.15E, when the  $[\text{H}_2\text{O}_2]/[\text{AgNO}_3]$  molar ratios of 70 and 100, respectively, were applied, UV-visible spectra indicate the formation of small AgNPLs.

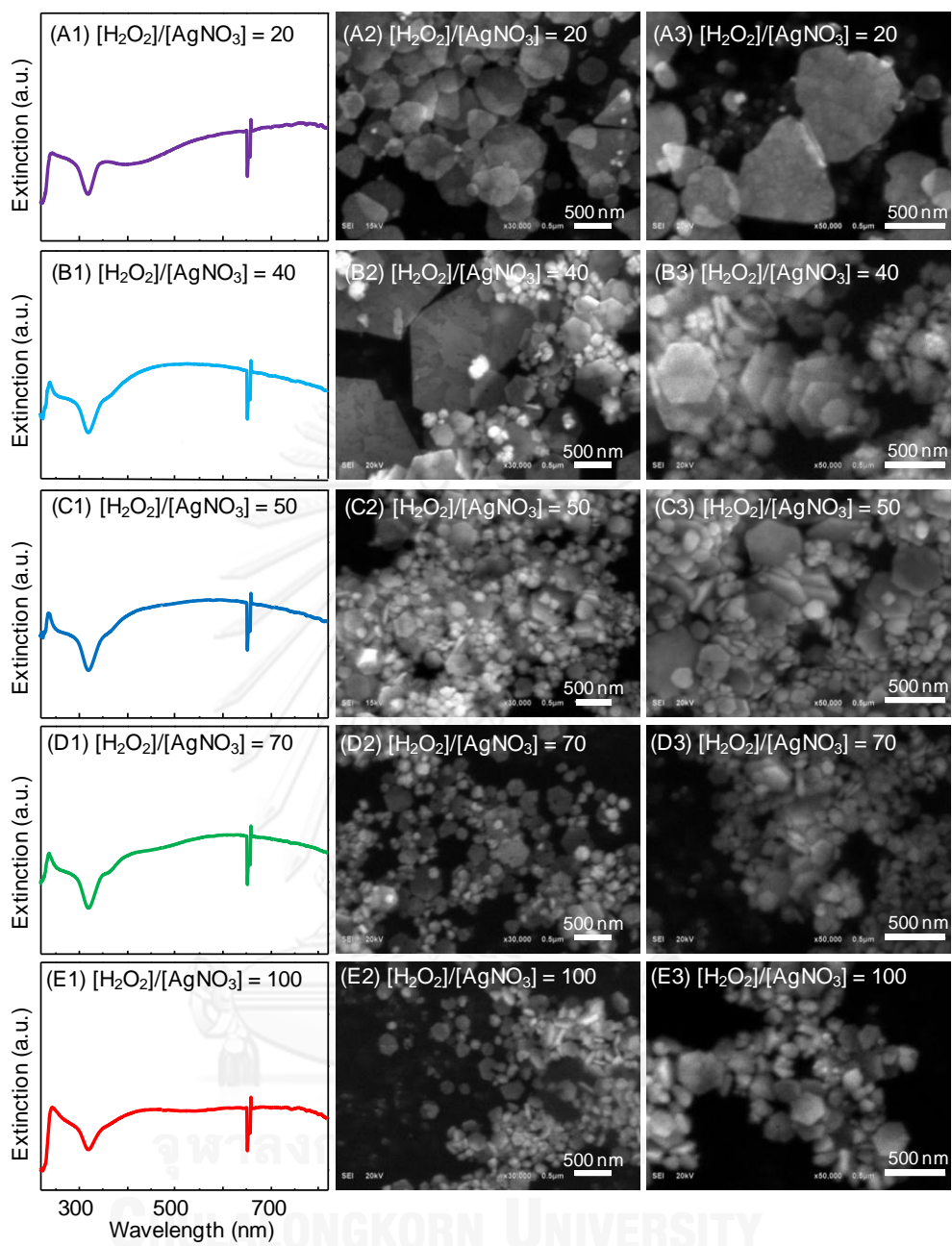


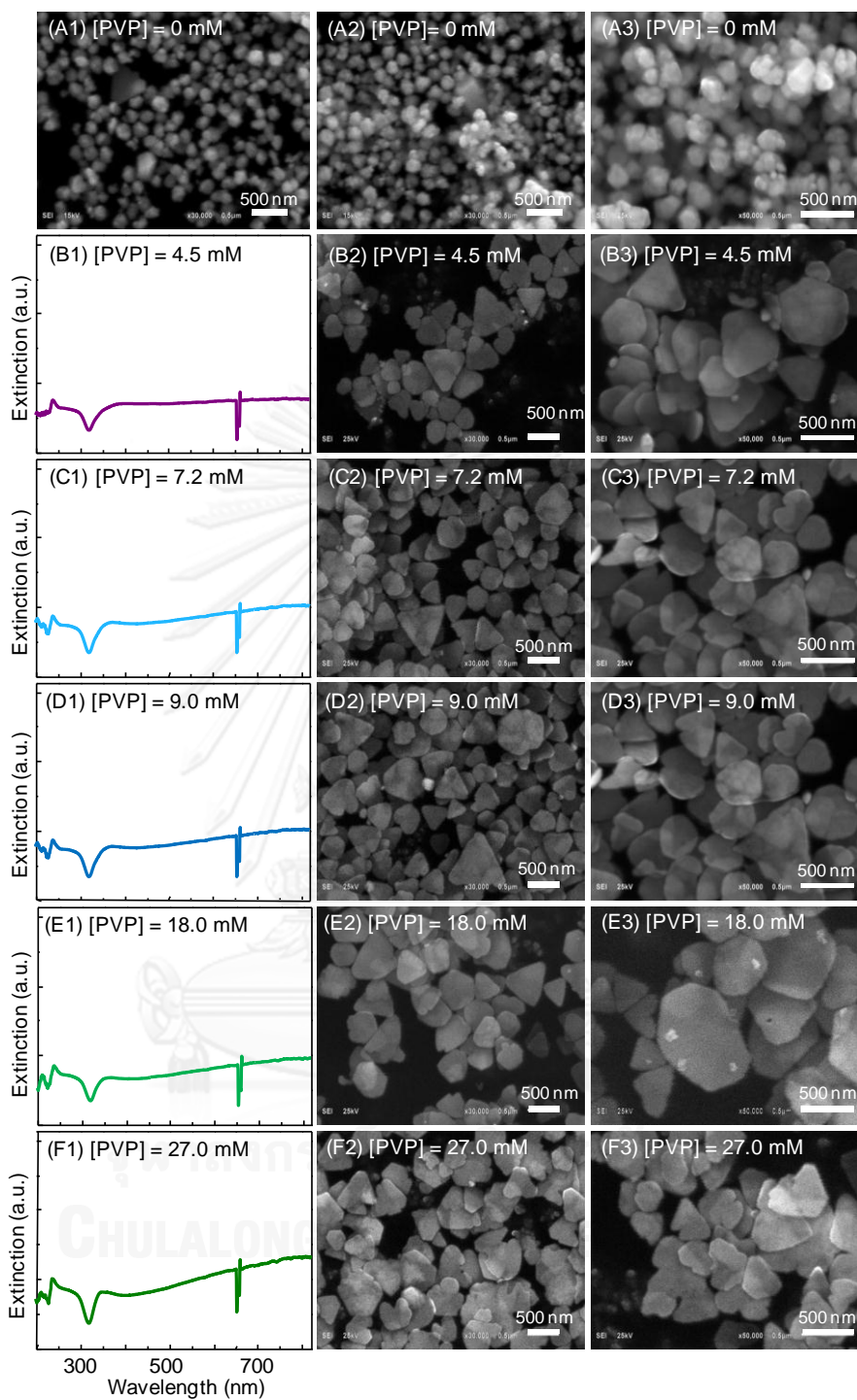
**Figure 4.15** UV-visible spectra and SEM micrographs of (A) 4.5 mM PVP stabilized  $\text{Ag}_2\text{O}$  (PVP- $\text{Ag}_2\text{O}$ ) of pH8, and (B-E) AgNPs synthesized by using PVP- $\text{Ag}_2\text{O}$  of (A) as a silver source, initial concentration of  $\text{H}_2\text{O}_2$  equal to 9.79 M, and vary molar ratios of  $[\text{H}_2\text{O}_2]/[\text{AgNO}_3]$  in the range of 20-100.

The utilization of high  $H_2O_2$  amounts involve oxidatively dissolve of large AgNPLs in the initial stage of reaction, since large AgNPLs were not appeared. SEM micrographs show obtained AgNPLs are almost hexagonal shape, the average lateral size is in the range of 100-200 nm. In summary,  $H_2O_2$  plays a pivotal role in AgNPLs formation. At a relatively low content of  $H_2O_2$ , formation of small AgNPs is always observed. Moreover, the shape transformation of  $Ag_2O$  to large AgNPLs also appeared. When  $H_2O_2$  content was increased in the range of R 2-10, complete AgNPLs occurred obviously. The high  $H_2O_2$  concentrations, R of 20-100, involved the oxidatively dissolve of AgNPLs. The results show the decreasing in their lateral size while increasing in thickness.

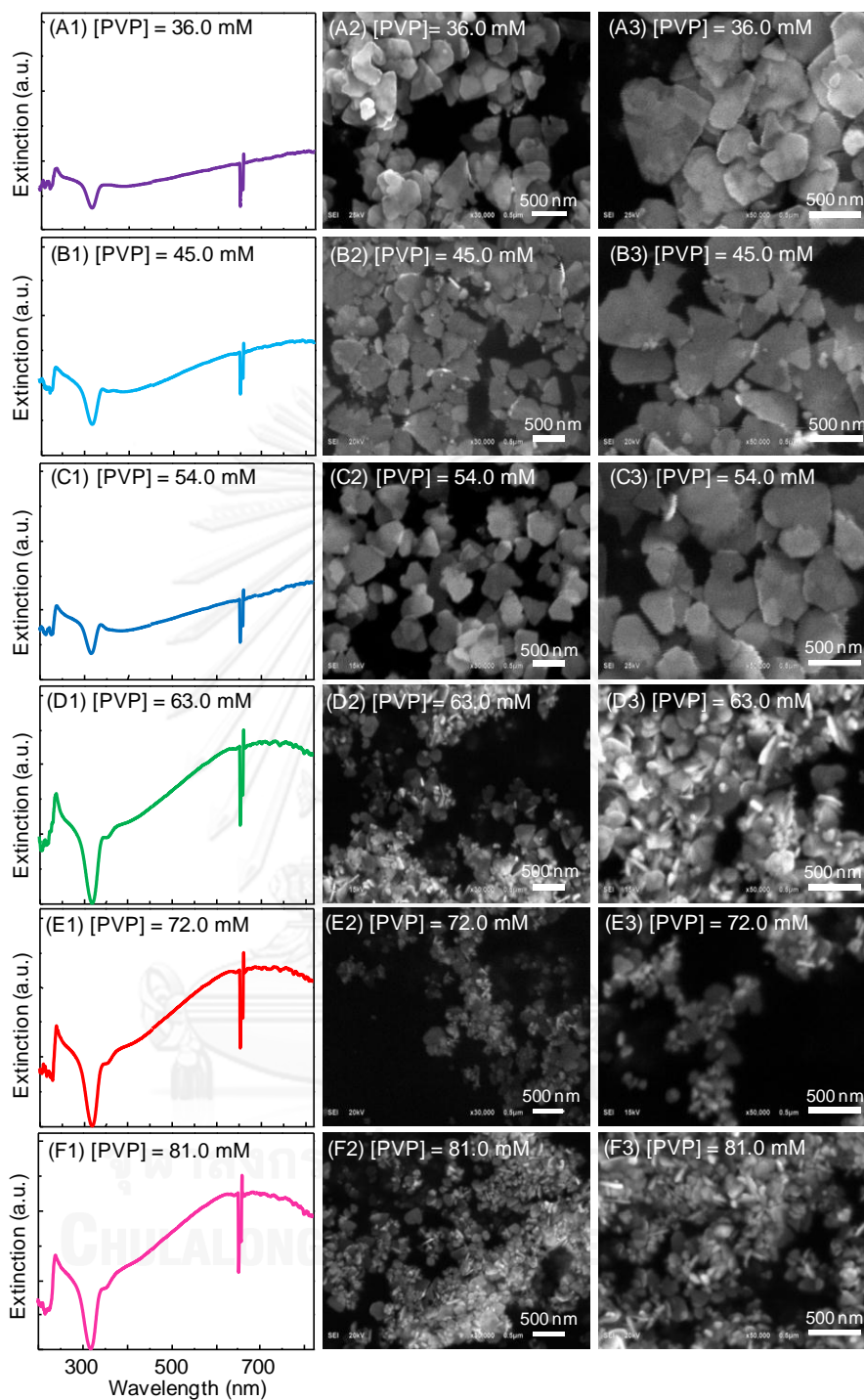
The role of PVP on AgNPLs formation is also investigated by employing the PVP concentrations in the range of 0-81 mM. Figure 4.16A, SEM micrographs of AgNPLs synthesized by without stabilization of PVP, the results illustrate aggregation of mixed irregular shape of AgNPLs. This condition, large AgNPLs and AgNPs were also observed. When 4.5, 7.2, and 9.0 mM of PVP were utilized in Figure 4.16B, 4.16C, and 4.16D, respectively. The small appearances of opQPR at 335 nm represent the low aspect ratio of AgNPLs. The base line shift in to longer wavelength implies turbidity of obtained colloidal products that may be caused by mixing of large AgNPLs. SEM micrographs show the most population of obtained AgNPLs is triangular shape. The occurrence of large irregular AgNPLs with small jag edge indicates the oriented attachment growth which was promoted by PVP [78]. The limitations of Ag supply and  $H_2O_2$  weak reducing agent involve the uncompleted AgNPLs comprise with grain boundary and small jag edge. Diameters of obtained AgNPLs were in the range of 200-1,000 nm.

Figure 4.16E and 4.16F, PVP contents were increased to 18.0 and 27.0 mM, respectively. SEM micrographs indicate jag edge of AgNPLs obviously. Although PVP can promote AgNPLs growth, high contents of PVP express a high stabilized power, able to block AgNPLs growth. The uncompleted AgNPLs were produced by the limitation of crystallization step, due to over stabilization of PVP, and weak reducing power of  $H_2O_2$  could not reduce a strong complex of PVP- $Ag^+$ .

When high contents of PVP, 36.0, 45.0, and 54 mM were applied, as shown in the Figure 4.14A, 4.17B, and 4.17C, respectively. The jag-edge AgNPLs are always observed more obviously than those of Figure 4.16. These results indicate the over successive stabilization of PVP as described above. Interesting that, when the PVP concentrations were more increased to 63.0, 72.0, and 81.0 which were shown in Figure 4.17D, 4.17E, and 4.17F, respectively. Small AgNPLs with size not over 300 nm were produced. This result may be caused by the high stabilized power of PVP in the initial stage of growth. These high PVP contents retard the formation of large AgNPLs, since only small AgNPLs were generated.



**Figure 4.16** UV-visible spectra and SEM micrographs of AgNPs synthesized by using PVP-Ag<sub>2</sub>O of pH8 ([AgNO<sub>3</sub>] = 9.28 mM) as a silver source. Using of initial H<sub>2</sub>O<sub>2</sub> concentration of 0.979 M, [H<sub>2</sub>O<sub>2</sub>]/[AgNO<sub>3</sub>] molar ratio of 10. (A-F) varying of PVP contents in the range of 0-27.0 mM.



**Figure 4.17** UV-visible spectra and SEM micrographs of AgNPs synthesized by using PVP-Ag<sub>2</sub>O of pH8 ([AgNO<sub>3</sub>] = 9.28 mM) as a silver source. Using of initial H<sub>2</sub>O<sub>2</sub> concentration of 0.979 M, [H<sub>2</sub>O<sub>2</sub>]/[AgNO<sub>3</sub>] molar ratio of 10. (A-F) varying of PVP contents in the range of 36.0-81.0 mM.

#### 4.8 IN-SITU SYNTHESIS OF SILVER NANOPlates/NANOSHEETS WITHOUT STABILIZATION

This synthesis protocol, naked silver nanoplates/nanosheets were successfully synthesized by using  $\text{NaBH}_4$  as a reducing and  $\text{H}_2\text{O}_2$  as a shape conversion agent (selective etchant) [17-19]. By applied initial 2.3 mM  $\text{AgNO}_3$  and 3.3 mM  $\text{NaBH}_4$ , as shown in Figure 4.18, SEM micrographs of silver nanoplates/nanosheets synthesized by various  $\text{H}_2\text{O}_2$  concentrations. The results indicated that shape and size of silver nanoplates/nanosheets were eluted by  $\text{H}_2\text{O}_2$ . As shown in Figure 4.18A, when  $\text{H}_2\text{O}_2$  was not applied, obtained product is aggregated particles which composed with 100 nm small particles and large particles around 1,000 nm. When 0.26 M  $\text{H}_2\text{O}_2$  was applied, silver nanoplates/nanosheets were generated, as shown in Figure 4.18B, 100 nm Ag nanoparticles and 400-1,000 nm Ag nanoplates were observed. As shown in Figure 4.18C, D, and E, when the amount of applied  $\text{H}_2\text{O}_2$  was increased ranging by 0.28, 0.33, and 0.35 M, Ag nanoplates/nanosheets with average size of 700, 1,000, and 1,200 nm were fabricated, respectively. As illustrated in Figure 4.18F, the appearance of 100 nm AgNPs, 1,000 nm AgNPLs, and 6  $\mu\text{m}$  AgNShs were observed. This result indicated the growth of Ag nanostructures induced by  $\text{H}_2\text{O}_2$  was Oswald ripening process; large particles grow by expanded other less stable particles [79].

Similarly, when the 0.35 M  $[\text{H}_2\text{O}_2]$  and 3.3 mM  $[\text{NaBH}_4]$  were applied simultaneously the role of  $[\text{AgNO}_3]$  was observed. As shown in Figure 4.19A, B, and C, SEM micrographs indicated the growth of AgNPLs/AgNShs from 300, 500, and 1,000 nm, respectively, when 0.6, 1.4, and 2.3 mM of  $[\text{AgNO}_3]$  were used. When 2.5 and 2.8 mM of  $[\text{AgNO}_3]$  were applied, AgNShs able to growth around 6  $\mu\text{m}$  (Figure 4.19D and



E). As shown in Figure 4.19F, the aggregated and large Ag crystals appear when the 3.2 mM of  $[\text{AgNO}_3]$  was applied.

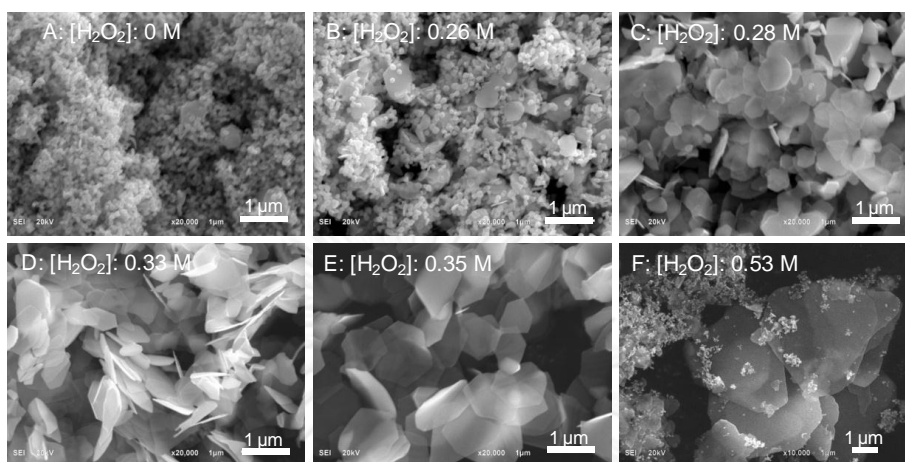


**Figure 4.18** SEM micrographs of Ag nanoplates/nanosheets synthesized by in-situ method using 2.3 mM  $[\text{AgNO}_3]$ , 3.3 mM  $[\text{NaBH}_4]$ , and  $[\text{H}_2\text{O}_2]$  of (A) 0, (B) 0.26, (C) 0.28, (D) 0.33, (E) 0.35, and (F) 0.53 M, respectively.

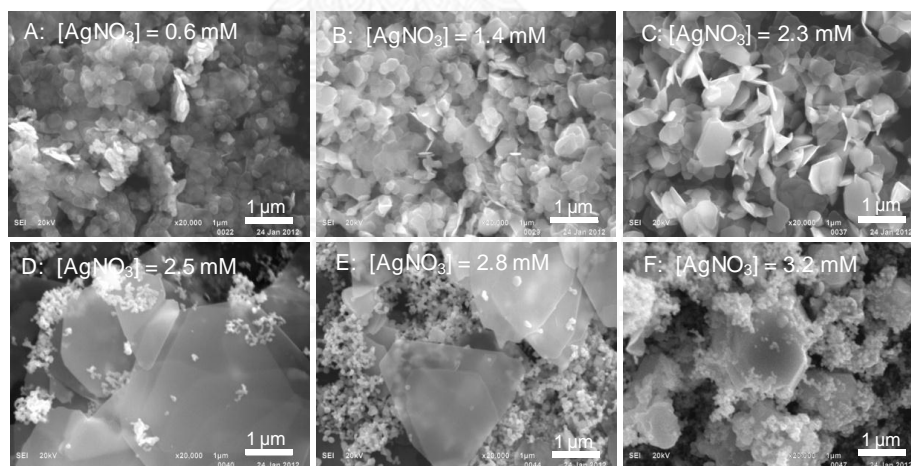


**Figure 4.19** SEM micrographs of Ag nanoplates/nanosheets synthesized by in-situ method using 0.35 M  $[\text{H}_2\text{O}_2]$ , 3.3 mM  $[\text{NaBH}_4]$ , and  $[\text{AgNO}_3]$  of (A) 0.6, (B) 1.4, (C) 2.3, (D) 2.5, (E) 2.8, and (F) 3.2 mM, respectively.

Finally, when the 0.35 M  $[H_2O_2]$  and 2.3 mM  $[AgNO_3]$  were applied simultaneously with the role of  $[NaBH_4]$  was observed. As shown in Figure 4.20A, when 2.3 mM  $[NaBH_4]$  was applied, aggregated of small AgNPs and some 400 nm AgNPLs were observed. When the  $[NaBH_4]$  was increased to 2.6, Figure 4.20B, a mixed of large AgNPLs/AgNShs with size around 500-800 nm and small AgNPs was observed. For the Figure 4.20C, when the  $[NaBH_4]$  was increased to 3.3 mM, mixed of 600-1000 nm AgNPLs/AgShs was observed. When the  $[NaBH_4]$  was increased to 3.7, 4.1, and 4.3 mM, only small AgNPs the size less than 100 nm was generated (Figure 4.20D, E, and F). These results indicated that the reducing and surface capping functions of  $NaBH_4$  [19], in addition it able to react with  $H_2O_2$ . Therefore,  $NaBH_4$  is able to withstand the AgNPLs/AgNShs growth induced by  $H_2O_2$ .

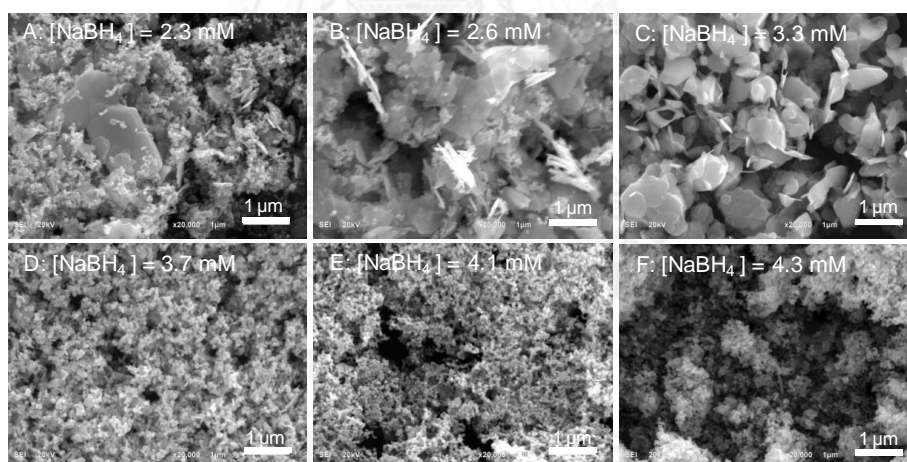
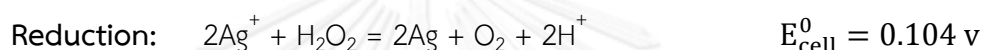
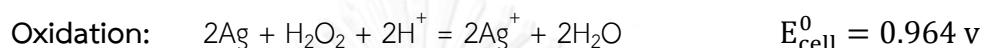


**Figure 4.20** SEM micrographs of Ag nanoplates/nanosheets synthesized by in-situ method using 0.35 M  $[H_2O_2]$ , 2.3 mM  $[AgNO_3]$ , and  $[NaBH_4]$  of (A) 2.3, (B) 2.6, (C) 3.3, (D) 3.7, (E) 4.1, and (F) 4.3 mM, respectively.

#### 4.9 OXIDATION OF METALLIC SILVER AND REDUCTION OF SILVER ION BY HYDROGEN PEROXIDE

The oxidation of metallic silver and reduction of silver ion by hydrogen peroxide in acidic medium can be adequately described by the following redox equations:



The cell potentials at various concentrations of  $\text{Ag}^+$  and  $\text{H}^+$  can be expressed by the Nernst's equations:

$$E_{\text{cell}}(\text{Ox}) = 0.964 - \frac{RT}{nF} \ln \frac{[\text{Ag}^+]^2}{[\text{H}^+]^2[\text{H}_2\text{O}_2]} = 0.964 - \frac{RT}{nF} \ln \frac{[\text{Ag}^+]}{[\text{H}^+]^2 R}$$

$$E_{\text{cell}}(\text{Red}) = 0.104 - \frac{RT}{nF} \ln \frac{[\text{H}^+]^2 p(\text{O}_2)}{[\text{Ag}^+]^2 [\text{H}_2\text{O}_2]} = 0.104 - \frac{RT}{nF} \ln \frac{[\text{H}^+]^2}{[\text{Ag}^+]^3 R}$$

$$\Delta E_{\text{cell}} = E_{\text{cell}}(\text{Ox}) - E_{\text{cell}}(\text{Red})$$

The mole ratio  $R$  is defined as  $[\text{H}_2\text{O}_2]:[\text{Ag}^+]$ . The pressure of oxygen gas evolved during the reaction is neglected and set equal to 1 atm. The difference between the oxidation and reduction cell potentials is defined as  $\Delta E_{\text{cell}}$ . Unless stated otherwise, the temperature used for the calculation is constrained at 28 °C.

As suggested by the Nernst equation, oxidation and reduction cell potentials of  $\text{H}_2\text{O}_2$  are dependent on  $\text{Ag}^+$  concentration (Figure 4.22), pH (Figure 4.23), and  $\text{H}_2\text{O}_2:\text{Ag}$  mole ratio (Figure 4.24 and 4.25). The oxidation cell potential is a decreasing, while the reduction cell potential is increasing as  $[\text{Ag}^+]$  and pH are

increased. However, both cell potentials are increasing with respect to the molar ratio R.

$\text{H}_2\text{O}_2$  can function as an oxidizing agent, reducing agent, or alternately play both roles depending on the potential gap between the oxidation and reduction reactions. The difference between the oxidation and reduction cell potentials can be effectively mediated through the adjustment of pH. The potential difference is significantly reduced when the solution pH increases from acidic (pH 2-4) to neutral or mild alkaline values (pH 7-8). This implies that the oxidizing function of  $\text{H}_2\text{O}_2$  is suppressed while its reducing function is enhanced at neutral or alkaline medium. The potential difference also decreases when  $[\text{Ag}^+]$  increases. From the observed results, AgNPs was oxidatively solubilized to  $\text{Ag}^+$  to the threshold values approximately 100  $\mu\text{M}$  before the shape transformation occurred. This suggests that the potential gap has to be narrowed down to a critical value in order to mediate the oxidizing and reducing activities of  $\text{H}_2\text{O}_2$ . The oxidizing and reducing activities were cooperated as observed in the transformation of AgNPs to AgNPLs in our experiment. The positive potential differences suggest that AgNPs are preferentially oxidized before the reduction of  $\text{Ag}^+$  by  $\text{H}_2\text{O}_2$  as the residual  $\text{Ag}^+$  was observed in the colloid after the transformation process. The potential difference is not significantly affected by  $\text{H}_2\text{O}_2$  concentration (i.e, the molar ratio of R), since the constant values of the potential are observed at all range of pH and  $\text{Ag}^+$  concentration investigated. Therefore, the neutral or mild alkaline condition of the reaction medium has to be employed in order to utilize  $\text{H}_2\text{O}_2$  simultaneously as the oxidizing and reducing agents.

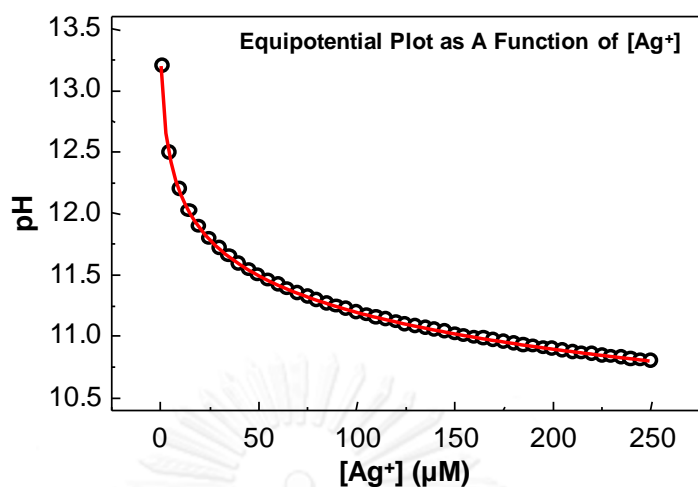


Figure 4.21 Equipotential points where  $E_{\text{cell}}(\text{Ox}) = E_{\text{cell}}(\text{Red})$  as a function of  $[Ag^+]$ .

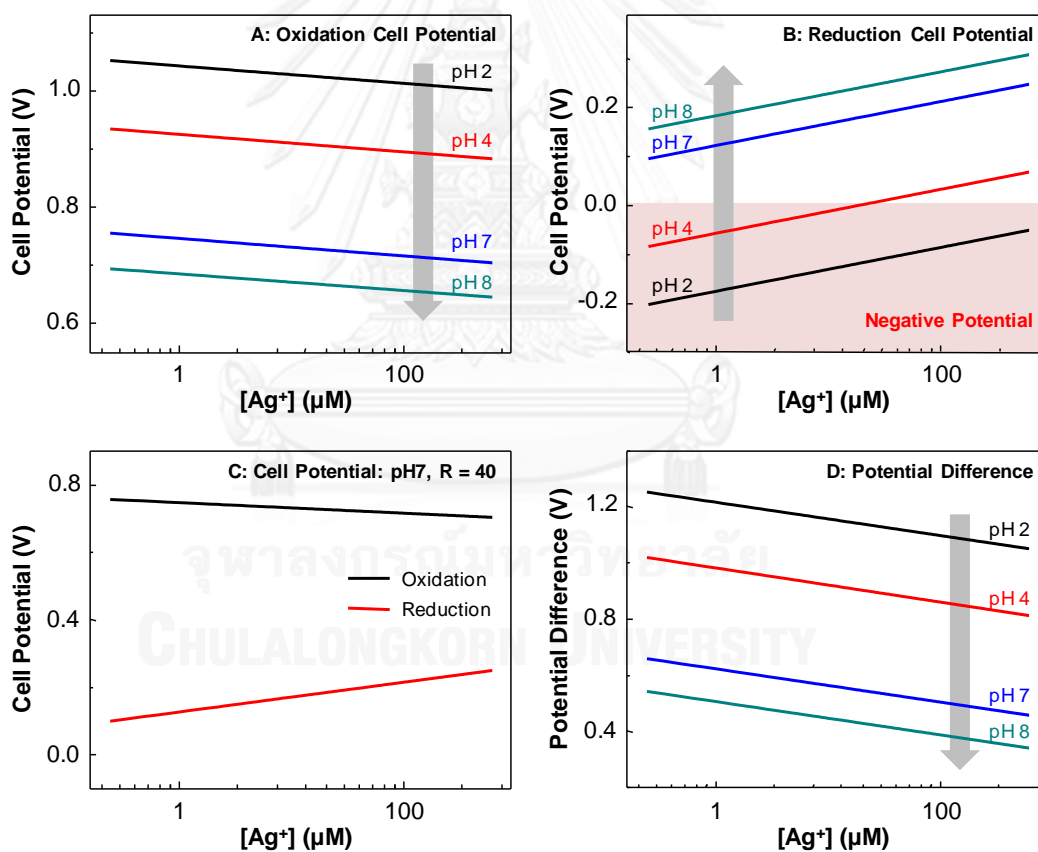


Figure 4.22  $E_{\text{cell}}(\text{Ox})$  (A),  $E_{\text{cell}}(\text{Red})$  (B), and  $\Delta E_{\text{cell}}$  (D) as a function of  $[Ag^+]$  at pH 2, 4, 7, and 8. The R molar ratio was fixed at 40.  $E_{\text{cell}}(\text{Ox})$  and  $E_{\text{cell}}(\text{Red})$  at pH 7 are compared in (C).

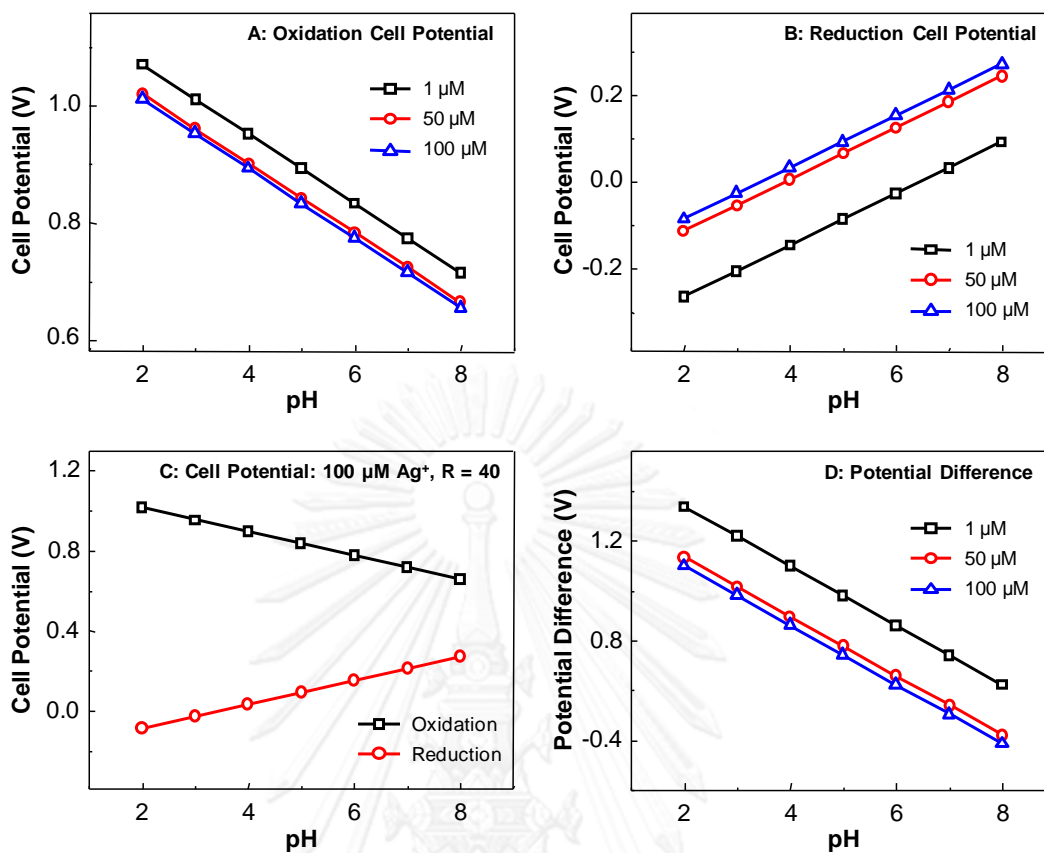


Figure 4.23  $E_{\text{cell}}(\text{Ox})$  (A),  $E_{\text{cell}}(\text{Red})$  (B), and  $\Delta E_{\text{cell}}$  (D) as a function of pH at 1, 50, and 100  $\mu\text{M}$   $\text{Ag}^+$ . The R molar ratio was fixed at 40.  $E_{\text{cell}}(\text{Ox})$  and  $E_{\text{cell}}(\text{Red})$  at 100  $\mu\text{M}$   $\text{Ag}^+$  are compared in (C).

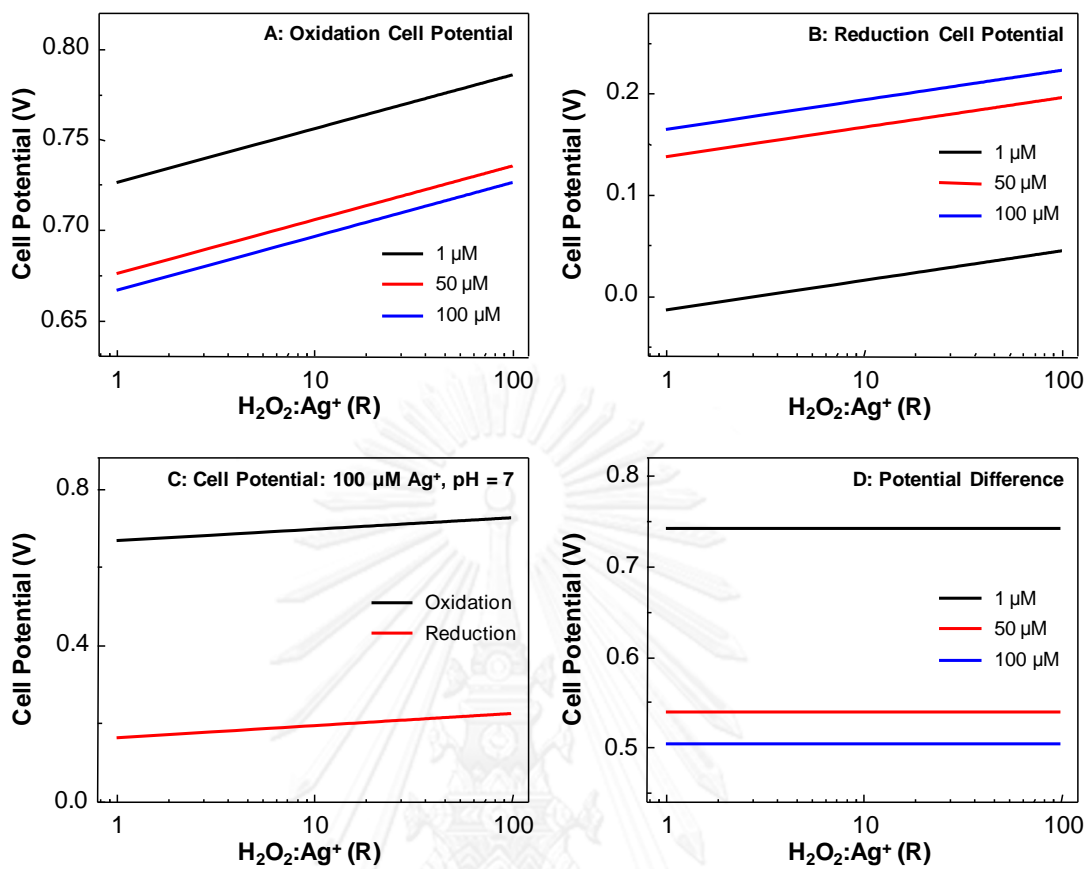


Figure 4.24  $E_{cell}(Ox)$  (A),  $E_{cell}(Red)$  (B), and  $\Delta E_{cell}$  (D) as a function of R at 1, 50, and 100  $\mu M$   $Ag^+$ . pH was fixed at 7.  $E_{cell}(Ox)$  and  $E_{cell}(Red)$  at 100  $\mu M$   $Ag^+$  are compared in (C).

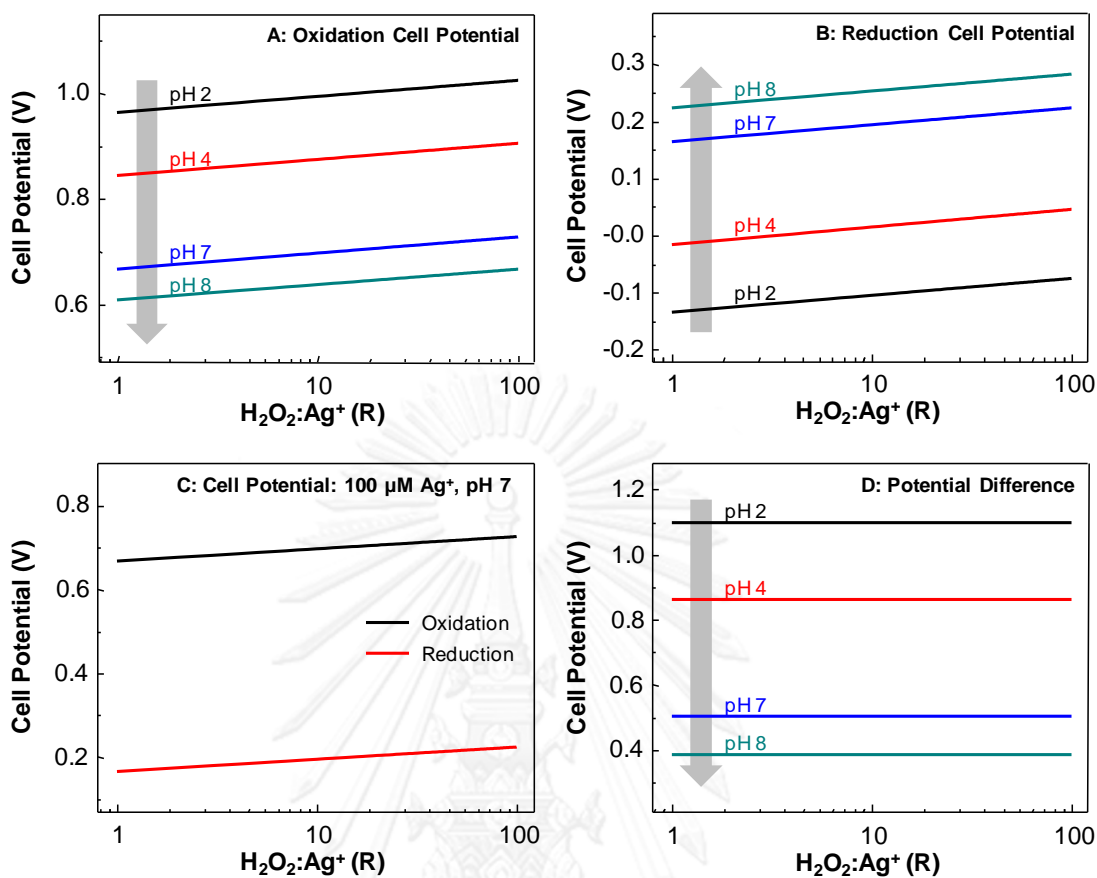


Figure 4.25  $E_{cell}(Ox)$  (A),  $E_{cell}(Red)$  (B), and  $\Delta E_{cell}$  (D) as a function of R at pH 2, 4, 7, and 8.  $[Ag^+]$  was fixed at  $100 \mu M$ .  $E_{cell}(Ox)$  and  $E_{cell}(Red)$  at pH 7 are compared in (C).

#### 4.10 PROPOSED MECHANISM OF SILVER NANOPlates FORMATION

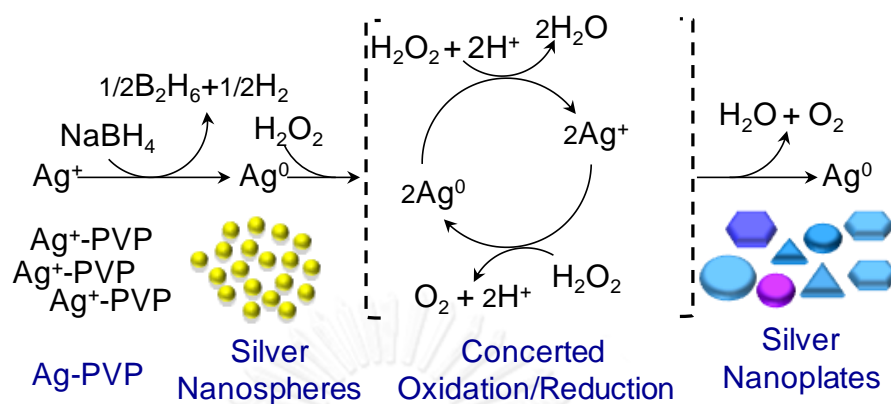
Based on the observed phenomena, we proposed a mechanism involving structural transformation of AgNPs to AgNPLs under the concerted oxidation/reduction of  $H_2O_2$  as shown in Scheme 4.1A. Generally,  $H_2O_2$  does not reduce silver ion into silver metal under the acidic environment even after a prolong incubation [19]. However, for PVP stabilized system, the  $NaBH_4$ -reduced AgNPs colloid is slightly basic (pH 7-8) and turns weakly acidic (pH 6-7) after an addition of  $H_2O_2$ . When  $H_2O_2$  is added into the colloid,  $H_2O_2$  oxidatively dissolves AgNPs as noticed by



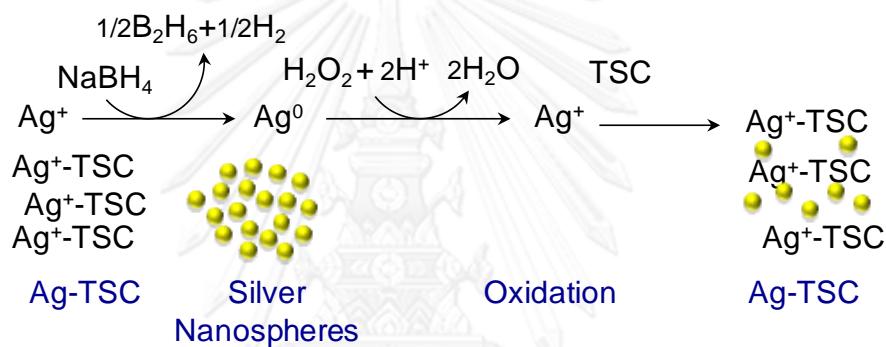
a slight fading of the yellow color during the first 30 s. Under a nearly neutral environment, the  $\text{H}_2\text{O}_2$ -reduced silver atoms nucleate and aggregate into seeds necessary for the formation of AgNPLs. As small seeds and fluctuating particles are formed,  $\text{H}_2\text{O}_2$  oxidatively dissolve unstable seeds while preserving those with twin defects and/or stacking faults [17, 19, 25]. The AgNPLs growing out of the survival seeds are noticed by a gradual development of the  $\sim 500$  nm ipDPR (Figures 1B and 3B). The more stable AgNPLs surviving the oxidative environment imposed by  $\text{H}_2\text{O}_2$  grow with the expense of AgNPs. A 275-nm redshift of the ipDPR from 500 nm to 775 nm (Figure 3B) indicates a continuous growth of AgNPLs after the disappearance of AgNPs. The successive growth of AgNPLs until  $\text{H}_2\text{O}_2$  is exhausted indicates that big nanoplates grow with the expense of small nanoplates.

The developed protocol could serve as a novel platform for a rapid fabrication of tunable AgNPLs as it is (i) simple (just a mixing of a colloid of AgNPs and  $\text{H}_2\text{O}_2$  solution), (ii) rapid (the reaction is complete within 2 min), (iii) economy (only necessary chemicals with low concentration are employed), (iv) clean (the strategic experimental design exploiting the oxidation/reduction of  $\text{H}_2\text{O}_2$  without a surface binding ligand), (v) efficient (nearly all AgNPs are converted to AgNPLs without a generation of byproducts), and (vi) greater control of product quality (AgNPLs with desired surface plasmon resonance could be selectively prepared). The obtained AgNPLs can be employed as functional nanostructures as well as building blocks for complex nanostructure fabrications.

A: Shape transformation by concerted oxidation/reduction



B: Oxidative dissolution produces silver citrate complex



**Schematic 4.1** Proposed mechanisms for the shape transformation of AgNPs to AgNPLs induced by  $\text{H}_2\text{O}_2$ ; (A) with PVP stabilization and (B) with TSC stabilization.

## CHAPTER V

### CONCLUSIONS

In conclusion, an efficient approach for the fabrication of AgNPLs/AgNShs from AgNPs and Ag<sub>2</sub>O using H<sub>2</sub>O<sub>2</sub> as the selectively oxidative etchant, reducing agent, and shape-controlling agent was developed. The shape transformation exploits the cyclic oxidation/reduction of Ag/Ag<sup>+</sup> under an oxidative environment of H<sub>2</sub>O<sub>2</sub>. H<sub>2</sub>O<sub>2</sub> oxidizes AgNPs to Ag ions simultaneously concertedly reduces Ag ions to Ag atoms necessary for the formation and growth of AgNPLs/AgNShs. This post-treatment approach is simple and rapid with high degree of controllability over the obtained anisotropic nanostructures. We have demonstrated, for the first time, that the strong oxidative and weak reductive nature of H<sub>2</sub>O<sub>2</sub> could be tuned and concertedly employed at the same time in the same colloid for the fabrication of anisotropic AgNPLs/AgNShs. An employment of a relatively low concentration of H<sub>2</sub>O<sub>2</sub> is necessary for the suppression of the catalytic decomposition of H<sub>2</sub>O<sub>2</sub> and decreasing the oxidative dissolution of silver nanostructures while maintaining the reduction reaction. Additional silver ions were not required for the growth of large nanoplates as the oxidative H<sub>2</sub>O<sub>2</sub> produces silver ions from existing AgNPs and less stable small nanoplates. AgNPLs/AgNShs with desired surface plasmon resonance could be selectively prepared by tuning the concentrations of H<sub>2</sub>O<sub>2</sub> and PVP. Although the growth process does not require a facet selective capping agent, a small amount of steric stabilizer such as PVP facilitates a formation of uniform AgNPLs/AgNShs. Under the currently employed condition, TSC inhibits the formation of nanoplates as it forms a stable Ag-citrate complex capable of withstanding the weakly reducing power of H<sub>2</sub>O<sub>2</sub>.

## REFERENCES

- [1] Lu, X.; Rycenga, M.; Skrabalak, S. E.; Wiley, B.; Xia, Y. Chemical synthesis of novel plasmonic nanoparticles. Annu. Rev. of Phys. Chem. 60 (2009): 167-192.
- [2] Rycenga, M.; Cobley, C. M.; Zeng, J.; Li, W.; Moran, C. H.; Zhang, Q.; Qin, D.; Xia, Y. Controlling the synthesis and assembly of silver nanostructures for plasmonic applications. Chem. Rev. 111 (2011): 3669-3712.
- [3] Kelly, K. L.; Coronado, E.; Zhao, L. L.; Schatz, G. C. The optical properties of metal nanoparticles: The influence of size, shape, and dielectric environment. J. Phys. Chem. B 107 (2002): 668-677.
- [4] McFarland, A. D.; Young, M. A.; Dieringer, J. A.; Van Duyne, R. P. Wavelength-scanned surface-enhanced Raman excitation spectroscopy. J. Phys. Chem. B 109 (2005): 11279-11285.
- [5] Alivisatos, P. The use of nanocrystals in biological detection. Nat. Biotech. 22 (2004): 47-52.
- [6] Thompson, D. G.; Enright, A.; Faulds, K.; Smith, W. E.; Graham, D. Ultrasensitive DNA detection using oligonucleotide-silver nanoparticle conjugates. Anal. Chem. 80 (2008): 2805-2810.
- [7] Christopher, P.; Linic, S. Engineering selectivity in heterogeneous catalysis: Ag nanowires as selective ethylene epoxidation catalysts. J. Am. Chem. Soc. 130 (2008): 11264-11265.
- [8] Jiang, Z. J.; Liu, C. Y.; Sun, L. W. Catalytic properties of silver nanoparticles supported on silica spheres. J. Phys. Chem. B 109 (2005): 1730-1735.
- [9] Aslan, K.; Wu, M.; Lakowicz, J. R.; Geddes, C. D. Fluorescent core-shell Ag@SiO<sub>2</sub> nanocomposites for metal-enhanced fluorescence and single nanoparticle sensing platforms. J. Am. Chem. Soc. 129 (2007): 1524-1525.
- [10] Yang, C.; Gu, H.; Lin, W.; Yuen, M. M.; Wong, C. P.; Xiong, M.; Gao, B. Silver nanowires: From scalable synthesis to recyclable foldable electronics. Adv. Mater. 23 (2011): 3052-3056.
- [11] Jin, R.; Cao, Y.; Mirkin, C. A.; Kelly, K. L.; Schatz, G. C.; Zheng, J. G. Photoinduced conversion of silver nanospheres to nanoprisms. Science 294 (2001): 1901-1903.
- [12] Jin, R.; Charles Cao, Y.; Hao, E.; Metraux, G. S.; Schatz, G. C.; Mirkin, C. A. Controlling anisotropic nanoparticle growth through plasmon excitation. Nature 425 (2003): 487-490.

- [13] An, J.; Tang, B.; Ning, X.; Zhou, J.; Zhao, B.; Xu, W.; Corredor, C.; Lombardi, J. R. Photoinduced shape evolution: From triangular to hexagonal silver nanoplates. J. Phys. Chem. C 111 (2007): 18055-18059.
- [14] Wu, X.; Redmond, P. L.; Liu, H.; Chen, Y.; Steigerwald, M.; Brus, L. Photovoltage mechanism for room light conversion of citrate stabilized silver nanocrystal seeds to large nanoprisms. J. Am. Chem. Soc. 130 (2008): 9500-9506.
- [15] Tang, B.; Xu, S.; Hou, X.; Li, J.; Sun, L.; Xu, W.; Wang, X. Shape evolution of silver nanoplates through heating and photoinduction. ACS Appl. Mater. Interfaces 5 (2013): 646-653.
- [16] Hao, E.; Kelly, K. L.; Hupp, J. T.; Schatz, G. C. Synthesis of silver nanodisks using polystyrene mesospheres as templates. J. Am. Chem. Soc. 124 (2002): 15182-15183.
- [17] Métraux, G. S.; Mirkin, C. A. Rapid thermal synthesis of silver nanoprisms with chemically tailorable thickness. Adv. Mater. 17 (2005): 412-415.
- [18] Tsuji, M.; Gomi, S.; Maeda, Y.; Matsunaga, M.; Hikino, S.; Uto, K.; Tsuji, T.; Kawazumi, H. Rapid transformation from spherical nanoparticles, nanorods, cubes, or bipyramids to triangular prisms of silver with PVP, citrate, and H<sub>2</sub>O<sub>2</sub>. Langmuir 28 (2012): 8845-8861.
- [19] Zhang, Q.; Li, N.; Goebel, J.; Lu, Z.; Yin, Y. A systematic study of the synthesis of silver nanoplates: Is citrate a “magic” reagent? J. Am. Chem. Soc. 133 (2011): 18931-18939.
- [20] Sun, Y. Synthesis of Ag nanoplates on GaAs wafers: Evidence for growth mechanism. J. Phys. Chem. C 114 (2009): 857-863.
- [21] Jiang, L. P.; Xu, S.; Zhu, J. M.; Zhang, J. R.; Zhu, J. J.; Chen, H. Y. Ultrasonic-assisted synthesis of monodisperse single-crystalline silver nanoplates and gold nanorings. Inorg. Chem. 43 (2004): 5877-5883.
- [22] Chen, S.; Carroll, D. L. Synthesis and characterization of truncated triangular silver nanoplates. Nano Lett. 2 (2002): 1003-1007.
- [23] Horvath, H. Gustav Mie and the scattering and absorption of light by particles: Historic developments and basics. J. Quant. Spectrosc. Ra. 110 (2009): 787-799.
- [24] Le Guével, X.; Wang, F. Y.; Stranik, O.; Nooney, R.; Gubala, V.; McDonagh, C.; MacCraith, B. D. Synthesis, stabilization, and functionalization of silver nanoplates for biosensor applications. J. Phys. Chem. C 113 (2009): 16380-16386.
- [25] Li, N.; Zhang, Q.; Quinlivan, S.; Goebel, J.; Gan, Y.; Yin, Y. H<sub>2</sub>O<sub>2</sub>-Aided seed-mediated synthesis of silver nanoplates with improved yield and efficiency. ChemPhysChem 13 (2012): 2526-2530.

- [26] Millstone, J. E.; Hurst, S. J.; Métraux, G. S.; Cutler, J. I.; Mirkin, C. A. Colloidal gold and silver triangular nanoprisms. Small 5 (2009): 646-664.
- [27] Xia, X.; Zeng, J.; Zhang, Q.; Moran, C. H.; Xia, Y. Recent developments in shape-controlled synthesis of silver nanocrystals. J. Phys. Chem. C 116 (2012): 21647-21656.
- [28] Xia, Y.; Xiong, Y.; Lim, B.; Skrabalak, S. E. Shape-controlled synthesis of metal nanocrystals: Simple chemistry meets complex physics? Angew. Chem. Int. Ed. 48 (2009): 60-103.
- [29] Yi, Z.; Zhang, J.; He, H.; Xu, X.; Luo, B.; Li, X.; Li, K.; Niu, G.; Tan, X.; Luo, J.; Tang, Y.; Wu, W.; Yi, Y. Convenient synthesis of silver nanoplates with adjustable size through seed mediated growth approach. T. Nonferr. Metal. Soc. 22 (2012): 865-872.
- [30] Zhang, Q.; Hu, Y.; Guo, S.; Goebel, J.; Yin, Y. Seeded growth of uniform Ag nanoplates with high aspect ratio and widely tunable surface plasmon bands. Nano Lett. 10 (2010): 5037-5042.
- [31] Jiang, X. C.; Chen, C. Y.; Chen, W. M.; Yu, A. B. Role of citric acid in the formation of silver nanoplates through a synergistic reduction approach. Langmuir 26 (2009): 4400-4408.
- [32] Kilin, D. S.; Prezhdo, O. V.; Xia, Y. Shape-controlled synthesis of silver nanoparticles: Ab initio study of preferential surface coordination with citric acid. Chem. Phys. Lett. 458 (2008): 113-116.
- [33] Pillai, Z. S.; Kamat, P. V. What factors control the size and shape of silver nanoparticles in the citrate ion reduction method? J. Phys. Chem. B 108 (2003): 945-951.
- [34] Goebel, J.; Zhang, Q.; He, L.; Yin, Y. Monitoring the shape evolution of silver nanoplates: A marker study. Angew. Chem. Int. Ed. 51 (2012): 552-555.
- [35] Zeng, J.; Xia, X.; Rycenga, M.; Henneghan, P.; Li, Q.; Xia, Y. Successive deposition of silver on silver nanoplates: Lateral versus vertical growth. Angew. Chem. Int. Ed. 50 (2011): 244-249.
- [36] Zhang, Q.; Cobley, C. M.; Zeng, J.; Wen, L. P.; Chen, J.; Xia, Y. Dissolving Ag from Au-Ag alloy nanoboxes with H<sub>2</sub>O<sub>2</sub>: A method for both tailoring the optical properties and measuring the H<sub>2</sub>O<sub>2</sub> concentration. J. Phys. Chem. C 114 (2010): 6396-6400.
- [37] Zhao, T.; Sun, R.; Yu, S.; Zhang, Z.; Zhou, L.; Huang, H.; Du, R. Size-controlled preparation of silver nanoparticles by a modified polyol method. Colloid. Surface. A 366 (2010): 197-202.
- [38] Jones, M. R.; Osberg, K. D.; Macfarlane, R. J.; Langille, M. R.; Mirkin, C. A. Templated techniques for the synthesis and assembly of plasmonic nanostructures. Chem. Rev. 111 (2011): 3736-3827.

- [39] Mayer, K. M.; Hafner, J. H. Localized surface plasmon resonance sensors. Chem. Rev. 111 (2011): 3828-3857.
- [40] Pastoriza-Santos, I.; Liz-Marzan, L. M. Colloidal silver nanoplates. State of the art and future challenges. J. Mater. Chem. 18 (2008): 1724-1737.
- [41] Craig, F. B.; Donald, R. H. Absorption and scattering of light by small particles. Weinheim: Wiley-VCH Verlag GmbH; (2007): 12-56.
- [42] Sosa, I. O.; Noguez, C.; Barrera, R. G. Optical properties of metal nanoparticles with arbitrary shapes. J. Phys. Chem. B 107 (2003): 6269-6275.
- [43] Chen, X.; Schluesener, H. J. Nanosilver: A nanoproduct in medical application. Toxicol. Lett. 176 (2008): 1-12.
- [44] Faunce, T.; Watal, A. Nanosilver and global public health: International regulatory issues. Nanomedicine 5 (2010): 617-632.
- [45] Kim, J. S.; Kuk, E.; Yu, K. N.; Kim, J. H.; Park, S. J.; Lee, H. J.; Kim, S. H.; Park, Y. K.; Park, Y. H.; Hwang, C. Y.; Kim, Y. K.; Lee, Y. S.; Jeong, D. H.; Cho, M. H. Antimicrobial effects of silver nanoparticles. Nanomedicine: Nanotechnology, Biology and Medicine 3 (2007): 95-101.
- [46] Quadros, M. E.; Marr, L. C. Silver nanoparticles and total aerosols emitted by nanotechnology-related consumer spray products. Environ. Sci. Technol. 45 (2011): 10713-10719.
- [47] Tang, B.; Zhang, M.; Hou, X.; Li, J.; Sun, L.; Wang, X. Coloration of cotton fibers with anisotropic silver nanoparticles. Ind. Eng. Chem. Res. 51 (2012): 12807-12813.
- [48] Xiu, Z.; Zhang, Q.; Puppala, H. L.; Colvin, V. L.; Alvarez, P. J. J. Negligible particle-specific antibacterial activity of silver nanoparticles. Nano Lett. 12 (2012): 4271-4275.
- [49] Zou, X.; Dong, S. Surface-enhanced Raman scattering studies on aggregated silver nanoplates in aqueous solution. J. Phys. Chem. B 110 (2006): 21545-21550.
- [50] Lu, L.; Kobayashi, A.; Tawa, K.; Ozaki, Y. Silver nanoplates with special shapes: Controlled synthesis and their surface plasmon resonance and surface-enhanced Raman scattering properties. Chem. Mater. 18 (2006): 4894-4901.
- [51] George, S.; Lin, S.; Ji, Z.; Thomas, C. R.; Li, L.; Mecklenburg, M.; Meng, H.; Wang, X.; Zhang, H.; Xia, T.; Hohman, J. N.; Lin, S.; Zink, J. I.; Weiss, P. S.; Nel, A. E. Surface defects on plate-shaped silver nanoparticles contribute to its hazard potential in a fish gill cell line and zebrafish embryos. ACS Nano 6 (2012): 3745-3759.
- [52] Homan, K. A.; Souza, M.; Truby, R.; Luke, G. P.; Green, C.; Vreeland, E.; Emelianov, S. Silver nanoplate contrast agents for in vivo molecular photoacoustic imaging. ACS Nano 6 (2011): 641-650.

- [53] Jiang, X. C.; Yu, A. B. Silver nanoplates: A highly sensitive material toward Inorganic anions. *Langmuir* 24 (2008): 4300-4309.
- [54] Shahjamali, M. M.; Bosman, M.; Cao, S.; Huang, X.; Saadat, S.; Martinsson, E.; Aili, D.; Tay, Y. Y.; Liedberg, B.; Loo, S. C. J.; Zhang, H.; Boey, F.; Xue, C. Gold coating of silver nanoprisms. *Adv. Funct. Mater.* 22 (2012): 849-854.
- [55] Sun, Y.; Xia, Y. Shape-controlled synthesis of gold and silver nanoparticles. *Science* 298 (2002): 2176-2179.
- [56] Fritz, J. Thermodynamic properties of chloro-complexes of silver chloride in aqueous solution. *J. Solution Chem.* 14 (1985): 865-879.
- [57] Pimpinelli, A., Villain, J. Physics of crystal growth. *Cambridge University Press*; (1998):
- [58] Wang, Z. L. Transmission electron microscopy of shape-controlled nanocrystals and their assemblies. *J. Phys. Chem. B* 104 (2000): 1153-1175.
- [59] Zhang, J. M.; Ma, F.; Xu, K. W. Calculation of the surface energy of FCC metals with modified embedded-atom method. *Appl. Surf. Sci.* 229 (2004): 34-42.
- [60] Cleveland, C. L.; Landman, U. The energetics and structure of nickel clusters: Size dependence. *J. Chem. Phys.* 94 (1991): 7376-7396.
- [61] Baletto, F.; Ferrando, R.; Fortunelli, A.; Montalenti, F.; Mottet, C. Crossover among structural motifs in transition and noble-metal clusters. *J. Chem. Phys.* 116 (2002): 3856-3863.
- [62] Baletto, F.; Mottet, C.; Ferrando, R. Microscopic mechanisms of the growth of metastable silver icosahedra. *Phys. Rev. B* 63 (2001): 155408.
- [63] Germain, V.; Li, J.; Inger, D.; Wang, Z. L.; Pileni, M. P. Stacking faults in formation of silver nanodisks. *J. Phys. Chem. B* 107 (2003): 8717-8720.
- [64] Pei-Feng, H.; Kai-Ming, C. Size-controlled synthesis of Pd nanoparticles from  $\beta$ -diketonato complexes of palladium. *Nanotechnology* 15 (2004): 1059.
- [65] Xiong, Y.; Siekkinen, A. R.; Wang, J.; Yin, Y.; Kim, M. J.; Xia, Y. Synthesis of silver nanoplates at high yields by slowing down the polyol reduction of silver nitrate with polyacrylamide. *J. Mater. Chem.* 17 (2007): 2600-2602.
- [66] Washio, I.; Xiong, Y.; Yin, Y.; Xia, Y. Reduction by the end groups of poly(vinyl pyrrolidone): A new and versatile route to the kinetically controlled synthesis of Ag triangular nanoplates. *Adv. Mater.* 18 (2006): 1745-1749.
- [67] Xiong, Y.; McLellan, J. M.; Chen, J.; Yin, Y.; Li, Z. Y.; Xia, Y. Kinetically controlled synthesis of triangular and hexagonal nanoplates of palladium and their SPR/SERS properties. *J. Am. Chem. Soc.* 127 (2005): 17118-17127.
- [68] Sun, Y.; Mayers, B.; Xia, Y. Transformation of silver nanospheres into nanobelts and triangular nanoplates through a thermal process. *Nano Lett.* 3 (2003): 675-679.



- [69] Sun, Y.; Xia, Y. Triangular nanoplates of silver: Synthesis, characterization, and use as sacrificial templates for generating triangular nanorings of gold. Adv. Mater. 15 (2003): 695-699.
- [70] Wiley, B.; Herricks, T.; Sun, Y.; Xia, Y. Polyol synthesis of silver nanoparticles: Use of chloride and oxygen to promote the formation of single-crystal, truncated cubes and tetrahedrons. Nano Lett. 4 (2004): 1733-1739.
- [71] Wiley, B.; Sun, Y.; Xia, Y. Polyol synthesis of silver nanostructures: Control of product morphology with Fe(II) or Fe(III) species. Langmuir 21 (2005): 8077-8080.
- [72] Xiong, Y.; McLellan, J. M.; Yin, Y.; Xia, Y. Synthesis of palladium icosahedra with twinned structure by blocking oxidative etching with citric acid or citrate ions. Angew. Chem. Int. Ed. 119 (2007): 804-808.
- [73] Zhang, J. H.; Liu, H. Y.; Zhan, P.; Wang, Z. L.; Ming, N. B. Controlling the growth and assembly of silver nanoprisms. Adv. Funct. Mater. 17 (2007): 1558-1566.
- [74] Luo, X.; Li, Z.; Yuan, C.; Chen, Y. Polyol synthesis of silver nanoplates: The crystal growth mechanism based on a rivalrous adsorption. Mater. Chem. Phys. 128 (2011): 77-82.
- [75] David, R. L. CRC Handbook of Chemistry and Physics. 90<sup>th</sup> ed. Boca Raton: CRC Press; (2010): 1213-1222.
- [76] Van Hying, D. L.; Zukoski, C. F. Formation mechanisms and aggregation behavior of borohydride reduced silver particles. Langmuir 14 (1998): 7034-7046.
- [77] Jiang, P.; Li, S. Y.; Xie, S. S.; Gao, Y.; Song, L. Machinable long PVP-stabilized silver nanowires. Chem. Eur. J. 10 (2004): 4817-4821.
- [78] Liu, Z.; Zhou, H.; Lim, Y. S.; Song, J. H.; Piao, L.; Kim, S. H. Synthesis of silver nanoplates by two-dimensional oriented attachment. Langmuir 28 (2012): 9244-9249.
- [79] Jang, E.; Lim, E. K.; Choi, J.; Park, J.; Huh, Y. J.; Suh, J. S.; Huh, Y. M.; Haam, S. Br-Assisted Ostwald ripening of Au nanoparticles under H<sub>2</sub>O<sub>2</sub> redox. Cryst. Growth Des. 12 (2011): 37-39.

## VITA

Name: Mr. Banjongsak Lamlua

Date of Birth: May 19, 1986

Birth place: Surin Province, Thailand

Address: 173 Moo 11 Tambol Kang-aln, Prasat District, Surin  
Province, Thailand, 32140

E-mail address: banjongsak.lamlua@gmail.com

Education:

2009 Bachelor of Science in Chemistry  
Department of Chemistry, Faculty of Science,  
Chulalongkorn University, Thailand

2013 Master of Science in Chemistry  
Department of Chemistry, Faculty of Science,  
Chulalongkorn University, Thailand

Conferences:

30 January - 1 February 2012 29th Annual Conference of the  
Microscopy Society of Thailand

10-13 December 2012 Small Science Symposium, Singapore

10-15 January 2013 Niigata Graduate Conference, Japan

23-25 January 2013 30th Annual Conference of the Microscopy Society of  
Thailand

Achievement:

2013 Best Presentation Award, Science Forum 2013, 14-15 March 2013,  
Faculty of Science, Chulalongkorn University, Bangkok 10330, Thailand